Centro de Estudios de Postgrado

Máster en Ingeniería Geodésica y Geofísica Aplicada

UNIVERSIDAD DE JAÉN

Centro de Estudios de Postgrado

Master's thesis

ANALYSIS OF THE VELOCITY FIELD IN THE EASTERN SECTOR OF THE CORDILLERA BÉTICA USING DISCONTINUOUS TIME SERIES OF GPS STATIONS POSITIONS IN THE PERIOD 2009-2018

Student: Mnishenko Taisiia

Tutor: Prof. Antonio José Gil Cruz

Dept: Cartographic Engineering, Geodesy and Photogrammetry

December, 2020

CONTENT

1. GENERAL CONCEPTS

1.1. Introduction

After successful accomplishment of all the subjects inside the Master program in Geodetic Engineering and Applied Geophysics, I am ready to accomplish Master's thesis. While doing the work the knowledge gained during aforementioned Master degree and previously completed Bachelor degree in Geodesy and Land management was used. Especially the lore of GPS data processing techniques and time series plays significant role.

The Master's thesis appear as a part of the study plan of the Master program mentioned above in University of Jaen, Spain. It is obligatory work to do which includes 6 credits and takes place in the first part of second year of study.

The main objective of the thesis is estimation of deformation velocities in network stations and their interpretation in relation to tectonics. The student of Master program in Geodetic Engineering and Applied Geophysics Taisiia Mnishenko will do the following tasks, calculations, descriptions and conclusions under the direction of Professor Antonio José Gil Cruz from the Department of Cartographic Engineering, Geodesy and Photogrammetry, from the Higher Polytechnic School of Jaen.

Selected topic consists fundamental operations, which gives the opportunity to gain experience in processing of the observations, their analysis and transformation. To process the results of the survey was completed by the Automatic Precise Positioning Service of the Global Differential GPS System, which is which belongs to Jet Propulsion Laboratory (NASA). Also the functional of the software MATLAB was used to organize and sestimize information in order to make the calculation and transformations more precisely and faster. Furthermore, to visualize and analize the results the online program SARI and sowtware AutoCAD2020 were applied.

1.2. Contents

In order to develop the theme of the Master's thesis, the following paragraphs were described:

Paragraph 1: contains the introduction and general concepts of the thesis, explains the main aim of the work.

Paragraph 2: describes the geography and geology of the field of study, the specialties of its relief.

Paragraph 3: define conception of reference system, frame of reference and coordinate system and characterize the main types of them.

Paragraph 4: concentrates on GNSS methods, their differences and modes of use; indicate GPS segments.

Paragraph 5: describes the Topo-Iberia project

Paragraph 6: includes the explication of the data processing, and coordinates transformation.

Paragraph 7: expounds the process of the absolute and residual velocities analysis, creation of the velocity maps.

Paragraph 8: general conclusions

1.3. Main target

The magisterial objective of this work is to make the estimation of the velocity field in the eastern sector of the Cordillera Bética. During the investigation and analysis, the discontinuous time series of positions of GPS stations in the period 2009-2018 were used.

In order to collect the data during the period of 9 years, five stations were selected as permanent points to make a comparison. The locations of the stations are focused in the central part of the mountain range, but rather widespread to make conclusions about general movement of the studied sector. In order to choose the situations of the stations, the geological situation and environment were taken in consideration.

To perform the post process the method PPP was used. This method bases the online application APPS (Automatic Precise Positioning Service) which was utilized to work with obtained data.

Processed information need to be converted to the Local Geodesy System. Such a type of the coordinates gives the opportunity to take out the velocities with the help of online platform SARI. The figures obtained will be represented graphically and will be used for further estimation.

The result of the work is supposed to be a conclusion about the velocity field and the movement of the mounting sector.

2. STUDY AREA STATEMENTS

2.1. Introduction

The Baetic System or Baetic Mountains is one of the biggest mountain ranges on Iberian Peninsula. Baetic System is usually being divided into Penibaetic System, Subbaetic System and Prebaetic System that together form a mountain range spreading from western Andalusia to eastern Valencia. The overall length of the Beatic Mountains is about 620 km with the highest point of 3.479 m at Mulhacen peak, which is part of the Sierra Nevada range in the Cordillera Penibética (fig 2.1).

Even though in a geographical sense, this group of mountains extends from the Gulf of Cádiz to the southern coasts of the Valencian Community and the Balearic Islands. However, as with the Pyrenees, in a geological sense, it extends beyond the geographical limits, extending to the South below the Alboran Sea and towards the Northeast part of its structures is continued without interruption by the bottom of Mediterranean and part of the Balearic promontory to the island of Mallorca.

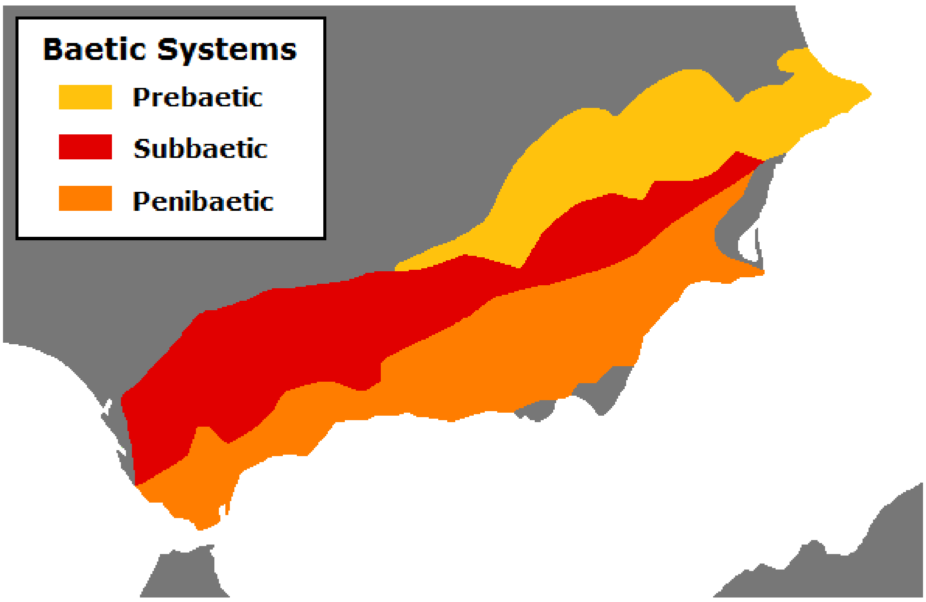

Fig. 2.1. Schematic representation of the Baetic System of mountain ranges

Image taken from https://en.wikipedia.org/wiki/Baetic_System

2.2. Geological description

Together with the Rif Mountains in North Africa, the Baetic Mountains form the most western segment of the Mediterranean alpine orogen. Geologically the Rif Mountains and the Serra de Tramuntana in the island of Majorca are extensions of the Baetic System. These two mountain ranges are separated by the Neogene Alboran basin and form the most closed orogenic arch (Gibraltar arch) of the Alpine orogens. [2]

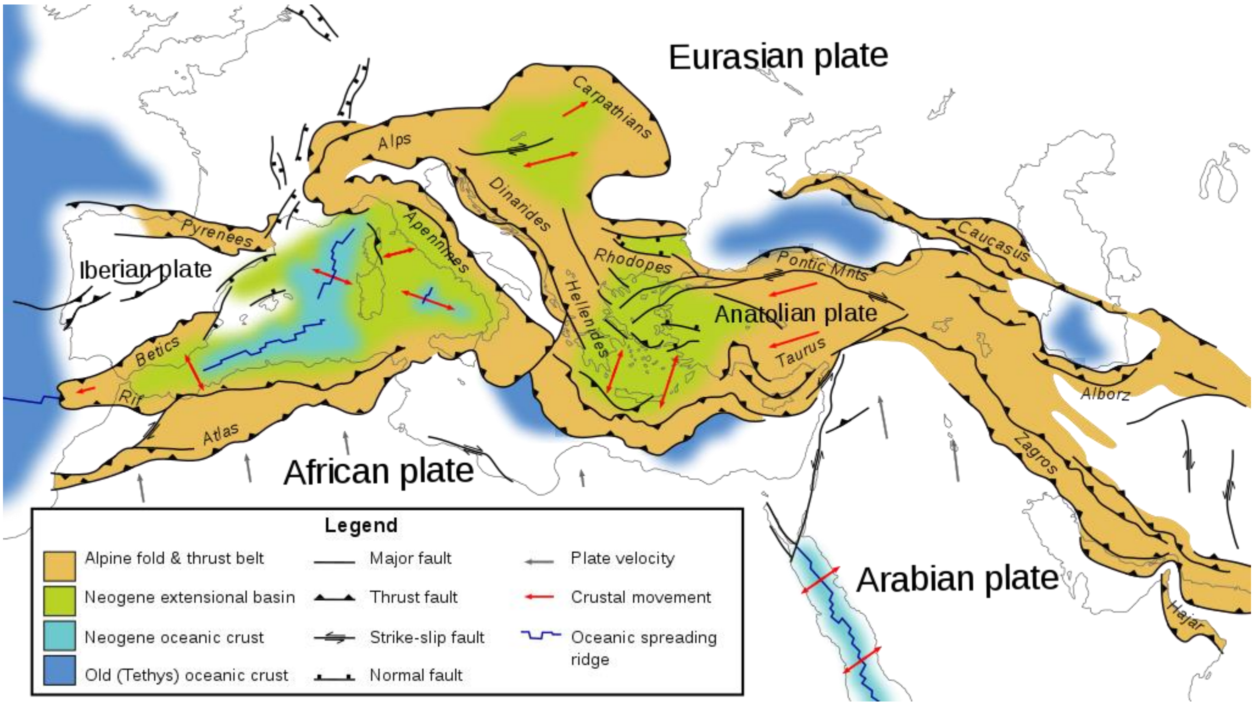

Fig. 2.2. Alpine mountain orogeny

Image taken from https://en.wikipedia.org/wiki/Alpine_orogeny#/media/File:Tectonic_map_Mediterranean_EN.svg

This mountain range was formed as a consequence of the compressive regime that began at the end of the Cretaceous, about 100 million years ago, and which mainly affected the North and South edges of the Iberian plate (fig.2.2). Its structure and subsequent evolution is complex, since it results from the interaction of two large plates and a continental block, the Alboran microplate that today constitutes the Internal Zones of this mountain range, which moved towards the West and finally collided with the Mesozoic margins of Iberia and Northwest Africa, forming the Betic-Rifeña Mountain Range.

At the cortical level, the most remarkable fact is that a notable root is not detected under the mountain range as is the case with other alpine orogens, since although some thickening of the crust is observed, in no case it exceeds more than 40 km. The lack of a clear cortical and lithospheric root can be explained if it is assumed that what we observe today is only a part of a large orogen that was located further to the east and that was partially dismembered by a series of geodynamic processes, so that part of this orogen would be submerged under the Mediterranean Sea. Another notable fact is the rapid thinning that is observed towards the coastal zone where the thickness of the crust is around 20-22 km, continuing the thinning towards the interior of the Alboran basin, where minimum values are reached around at 15 km.

Subbetic and Penibetic range occupies an intermediate position that reaches its greatest development towards the West, while towards the East it loses importance, since it is covered by the mantles of the Internal Zones and the Neogene of the Murcia Basin.

The Paleozoic structures do not outcrop throughout this area and the Mesozoic is represented from the lower Jurassic by sediments, generally of deep pelagic origin, from the marine basin of the Sea of Tethys, which would constitute the westernmost end. They are generally marine sediments far from the coast, with little or no continental detritic influence, represented for the most part by margocalizas and marls, in many cases constituted mainly by a multitude of microorganisms -foraminifera and radiolaria-, with sporadic intercalations of basic volcanic rocks from underwater eruptions. A stratigraphic and paleogeographic evolution equivalent to that of the passive continental margins is detected here.

Prebetic range on the other hand is the northernmost, located immediately south of the Sierra Morena Paleozoic. Its greatest development reaches the East, between Jaén and Alicante -sierras de Cazorla, Segura y las Villas, Alcaraz, Hellín and in the Balearic Islands (Mallorca and Ibiza). Towards the west, between Jaén and Cádiz, it is poorly developed, being covered by the subbetic mantles and by the Miocene of the Guadalquivir Valley. Its Mesozoic rocks present in some areas common stratigraphic characteristics with those of the Iberian System, establishing their limit by the dominant direction of the axis of the folds.

During most of its geological history, Jurassic and Cretaceous, it constituted a shallow marine platform domain adjacent to the continent, with a predominant deposit of carbonate sediments [3].

3. REFERENCE SYSTEM, REFERENCE FRAME, COORDINATE SYSTEM

3.1. Introduction

Reference systems are considered in the framework of the general theory of relativity. They form a conceptual basis for determining the position and movement of objects in space and time. Their practical implementation are *reference frames* - catalogs of coordinates of positions and parameters of movements of physically fixed points; on the earth's surface, these points correspond to points of geodetic control networks.

Therefore, reference system is a theoretical concept containing ideas about the systems of counting coordinates and time, about the parameters of the Earth, necessary for their introduction, and considerations for establishing these systems in the space under consideration.

The result of the practical implementation of this concept is a reference frame fixed in space. In the case of ground measurements, this is a *reference geodetic network*, the points of which are determined in the selected coordinate system, coordinate catalogs are created for the epoch t_0, and the rates of change of coordinates are also determined.

3.2. Reference system

The network of stations of the IGS (International GNSS Service) makes a large contribution to the study of the Earth and the development of coordinate reference systems. Its active work began in 1994. Over 200 organizations worldwide support the IGS work on a voluntary basis.

The IGS service includes continuous tracking stations, as well as data collection and analysis centers. At tracking stations, GPS / GLONASS receivers collect "raw" data. They are transferred to operations centers for conversion to the

RINEX exchange format. After that, they are sent to the regional centers, and then to global centers. Operation centers are located in Europe (Germany, Italy, Netherlands, and France), America (USA, Canada), Asia (Japan), and Africa (South Africa), Australia.

The IGS service collects, archives and distributes updated ephemeris of GPS and GLONASS satellites, parameters of the Earth's rotation, coordinates and displacement rates of IGS stations, corrections to the time scales of satellite stations, estimates of signal delays in the atmosphere, etc. IGS data is also used to build geodetic reference networks, a special SINEX format is used for data exchange.

In 2011, IGS created its own new reference frame, IGS-08, based exclusively on revised GNSS observations and ITRF-2008.

Terrestrial coordinate reference systems are of particular interest: after all, the measurement process is performed in the frame of reference established on Earth. Terrestrial reference systems are classified by territorial coverage, distinguishing global (terrestrial), regional (uniting several states), national (state) and local. They are implemented in the course of cooperation of many countries (international), countries of a separate region (regional), by the forces of one state (global, national), or by the forces of individual organizations (local). An example of a terrestrial international system is the ITRS and its reference frame ITRF.

3.2.1. GRS80

The ellipsoid GRS80 (Geodetic Reference System) was adopted by the XVII General Assembly of the International Union of Geodesy and Geophysics in Canberra in December 1979 as a general terrestrial reference ellipsoid. The defining parameters of the GRS80 and other data are given in the table. 3.1. GRS80 parameters are used to construct other coordinate systems.

Table 3.1. Ellipsoid parameters

	GRS-80	WGS-84
a	6378137	6378137
b	635752.3141	635752.314
c	6399593.6259	6399593.626
α	1/298.257222101	1/298.257223563
e^2	0.00669438002290	0.006694379990
e'^2	0.00673949677548	0.006739496742

Concepts in the table:

- equatorial semi-major axes *a*
- flattening *α*
- semi-minor axis *b*
- polar radius *c*
- first *e* and second e' ellipse eccentricities

The first eccentricity is determined by the ratio of the linear eccentricity, the segment from the center of the ellipse to each of its foci to the semiaxis *a*, the second - by the ratio of the same segment to the semiaxis *b* (fig.3.1).

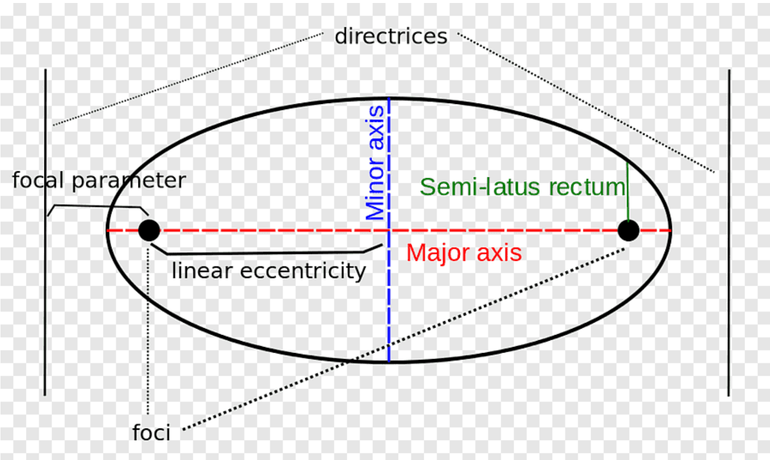

Fig. 3.1 – The main parameters of the ellipsoid

Image taken from https://www.pngegg.com/ru/png-ctsyb

The minor axis of the GRS80 is parallel to the direction to the International Origin (average position of the true pole for the period from 1900 to 1905). GRS80 is based on the theory of the equipotential (level or normal) ellipsoid. If an ellipsoid with semiaxes *a* and *b* is given, then it can be described by an equipotential surface, called the normal potential. It is such a surface, which is orthogonal at any point to the field lines.

Ellipsoid GRS80 is recommended for carrying out geodetic work and calculating the characteristics of the gravitational field on the Earth's surface and in external space.

3.2.2. WGS84

World Geodetic System WGS-84 (World Geodetic System, 1984) provides GPS work. It was preceded by earlier versions. Through the efforts of the USA Army, the WGS-60 model was created on the basis of astronomical-geodetic, gravimetric and satellite measurements, and then the WGS-66 and WGS-72 models were designed. WGS-72 has already relied on data from the World Satellite Triangulation Network. In the early 1980s, a new system of geodetic parameters GRS-80 appeared. New results of laser ranging of satellites, VLBI (very long base interferometry), satellite altimetry, etc. were also obtained. As a result, the WGS-84 model was formed.

The WGS-84 reference frame was installed in 1987. Its further improvements were made thanks to extensive GPS measurements. In 1994, improvements to the WGS-84 datum occurred at the beginning of the 730th GPS Week. It received the designation G-730. In 1996, with the beginning of the 873rd GPS week, a new improved geodetic reference G-873 was created. It has become very close to ITRF-96. In 2002, the third refinement was made - G-1150. According to the mean square criterion, the differences between the coordinates WGS-84 (G-1150) and ITRF-2000 are ~ 1 cm. At this level of accuracy, the reference bases of WGS-84 and ITRF are the same. Nowadays, ITRS and WGS-84 are almost identical in terms of their parameters.

WGS84 and GRS80 has the same distance at the equator but the GRS80 ellipsoid is a little bit more flattened.

3.2.3. ITRS

ITRS is recommended for determining the positions and parameters of the motion of objects on Earth and in near-Earth space. It is a complete international geocentric coordinate system.

ITRS is the world's premier and supported by the International Earth Rotation Service (IERS). The IERS service was established in 1987 by the International Astronomical Union (IAU) and the International Union of Geodesy and Geophysics IUGG. The beginning of its work - January 1, 1988.

The origin is the center of mass of the Earth (including the ocean and atmosphere). The system rotates with the Earth and is not inertial.

Inertial frame of reference is a frame of reference in which all free bodies move rectilinearly and uniformly, or are at the rest.

The z-axis is the mean axis of the Earth's rotation and is directed to the reference pole (IRP - IERS Reference Pole). The x-axis lies in the plane of the reference meridian (IRM - IERS Reference Meridian). The unit of length is the meter, and the time scale is the TCG (Geocentric Coordinate Time) scale.

Geocentric Coordinate Time (TCG) refers to the Earth's center of mass and linearly related to the earth time TT.

3.2.4. ETRS89

The European Terrestrial Reference System 1989 (ETRS89) is a geodesic Cartesian reference system in which the Eurasian plate as a whole is static. The coordinates and maps in Europe based on ETRS89 do not change due to continental drift.

The development of ETRS89 is associated with the global ITRS geodetic data, in which the presentation of continental drift is balanced so that the total momentum of the continental plates is about 0. ETRS89 was officially born at the 1990 Florence meeting of EUREF. ETRS89 and ITRS diverge due to continental drift at a rate of about 2.5 cm per year.

ETRS89 is the EU recommended coordinate system for geodata for Europe. This is the only geodetic data that can be used for cartographic and geodetic purposes in Europe. The ETRS89 is based on the GRS80 ellipsoid.

3.3. Reference Frame

The term reference frame means the materialization of the reference system, or in other words, the physical implementation of the geometric component of the "reference system". The reference frame is a certain limited set of physical carriers of coordinates and a mathematical model of the movement of carriers inrelatively to the adopted coordinate system.

The physical carriers of the earth's reference frame can be the centers of geodetic points, rigidly connected with the earth's body. In turn, the mathematical model of the movement of coordinate carriers includes a description of the coordinate system in which the model is created, a mathematical description of the model and the numerical values of the parameters of this model.

3.3.1. ITRF

International Terrestrial Reference Frame (ITRF). Practical implementation of ITRS. The reference frame is formed and refined annually with the latest methods of space geodesy. Technologies used:

1) Observation of extragalactic point radio sources by the method of radio interferometry with a very long baseline - VLBI (Very Long Baseline Interferometry)
2) Positioning by GLONASS and GPS systems
3) Laser ranging of the moon (LLR Lunar Laser Ranging)
4) Laser ranging of artificial earth satellites (SLR - Satellite Laser Ranging)
5) Measurements by the Doppler satellite system DORIS (DORIS - Doppler Orbitography and Radiopositioning Integrated by Satellite).

Due to geodynamic processes, the coordinates of points change on average at a rate of ~ 2–4 cm / year, even faster in some regions. Therefore, the coordinates are constantly updated, and the catalogs indicate the year of their implementation. For example, the 1989 epoch coordinate reference frame is designated ITRF-89.

In the thesis, the latest version of this frame, ITRF2014, was used in the case of absolute velocities.

ITRF2014 uses as input data time series of station positions and Earth Orientation Parameters (EOPs) provided by the Technique Centers of the four space geodetic techniques (VLBI, SLR, GNSS and DORIS). Based on completely reprocessed solutions of the four techniques, the ITRF2014 is expected to be an improved solution compared to ITF2008 [1].

3.3.2. ETRF

The EUREF Permanent Network (EPN) is a European network of more than 300 continuously operating GNSS base stations with precisely known coordinates anchored to ETRS89. EPN is a key tool in maintaining the ETRS89 geodetic coordinate system. EPN stations continuously collect observation data from high-precision multi-GNSS receivers. Data is processed centrally in multiple data centers. EPN is created and maintained on the basis of a voluntary agreement of about 100 European agencies and universities. EPN activities are coordinated by EUREF.

EPN consists of the following components:

- Tracking stations include GNSS tracking receivers and antennas on suitable survey markers.
- Operations centers perform data validation, converting raw data to RINEX format, compressing data, and uploading to local data centers.
- Local data centers store tracking station data and distribute it over the Internet.
- Local analytical center process the subnet of EPN stations and deliver subnet solutions to combined centers weekly.
- Combined centers combine subnet solutions into one formal EPN solution that is sent weekly to IGS for integration into a global GNSS network solution.
- The Central Office manages the day-to-day operations of EPN. It is located at the Royal Observatory of Belgium in Brussels.

In the thesis, the latest version of this frame, ETRF2014, was used in the case of residual velocities.

3.4. Systems of coordinates

All coordinate systems can be distinguished from each other by type, location of the origin, choice of the main coordinate plane, orientation of the abscissa axis, type. The spatial position of a ground point is most conveniently determined in coordinate systems rigidly connected with the rotating Earth. These are the so-called terrestrial coordinate systems.

3.4.1. Geodetic coordinate system

In order to pass geocentric Cartesian coordinates to geodetic coordinates the GRS80 parameters were used.

The concepts of geodetic latitude, longitude and altitude are associated with a geodetic coordinate system (fig.3.2).

Geodetic latitude (Phi) is the angle between the equatorial plane and the normal (perpendicular) to the surface of the earth's ellipsoid passing through a given point. The normal does not pass through the center of the ellipsoid.

Geodetic latitudes are counted from 0° to 90° north and south of the equator. Geodetic latitudes of the Northern Hemisphere are called northern and have a "+" sign, and those of the Southern Hemisphere are called southern and have a "-" sign.

The geodetic latitude for points located at the equator will be 0°, and for points located at the poles ± 90°.

Geodesic longitude (Lambda) is the dihedral angle enclosed between the plane of the initial meridian and the plane of the geodesic meridian passing through a given point.

Currently, the Greenwich meridian, passing through the Astronomical Observatory in Greenwich (London), is considered the primary meridian. From this meridian, the so-called international Greenwich time is counted.

Geodetic longitude is measured either by the central angle in the plane of the equator or parallel, or by the arc of the equator from the initial (Greenwich) meridian to the meridian passing through a given point, ranging from 0° to 180° east or west.

Geodetic longitudes for points located east of the Greenwich meridian up to 180° are called east and are considered positive, and west - west and are considered negative.

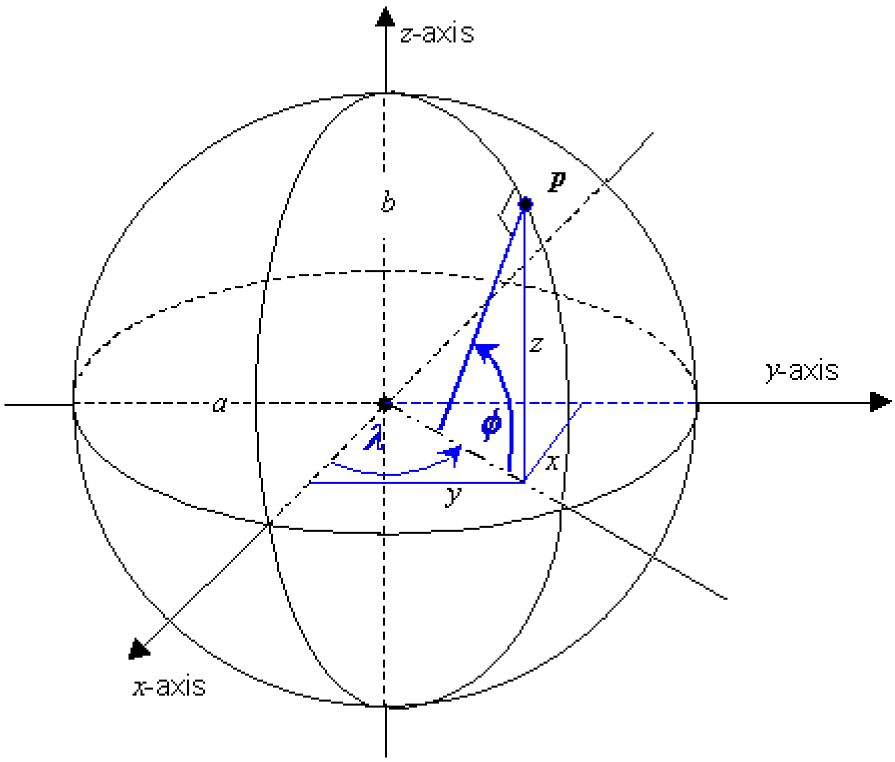

Fig. 3.2 – Geographical coordinates

Image taken from https://standards.sedris.org/18026/text/ISOIEC_18026E_CONCEPTS.HTM

3.3.2. UTM

The UTM conformal transverse cylindrical projection is the Universal Transverse Mercator. UTM is the projection of an ellipsoid onto a secant cylinder.

The UTM projection was developed in 1936 by the International Union of Geodesy and Geophysics and adopted by many national and international cartographic organizations.

In this projection, as well as in the Gauss-Kruger projection, six-degree zones are used. Unlike the Gauss-Kruger projection, the zones do not extend from the North Pole to the South Pole, but only in the strip from the parallel of 84° north latitude to the parallel of 80° south latitude. A conformal azimuthal (stereographic) projection is used for mapping circumpolar spaces (fig. 3.3).

The earth's ellipsoid is divided into 60 six-degree zones, which are numbered from 1 to 60, starting from the meridian 180° West longitude. Zone 1 is bounded by meridians with longitudes of 180° and -174 °, and zone 60 - by meridians + 174° and +180 °. Each zone has its own axial meridian.

Within each 6-degree zone, two rectangular coordinate systems are established in which the positive y and x directions are north and east, respectively.

UTM coordinates are referenced to GRS-80 ellipsoid. UTM can be set for different ellipsoids depending on φ, λ that repeats one ellipsoid to another.

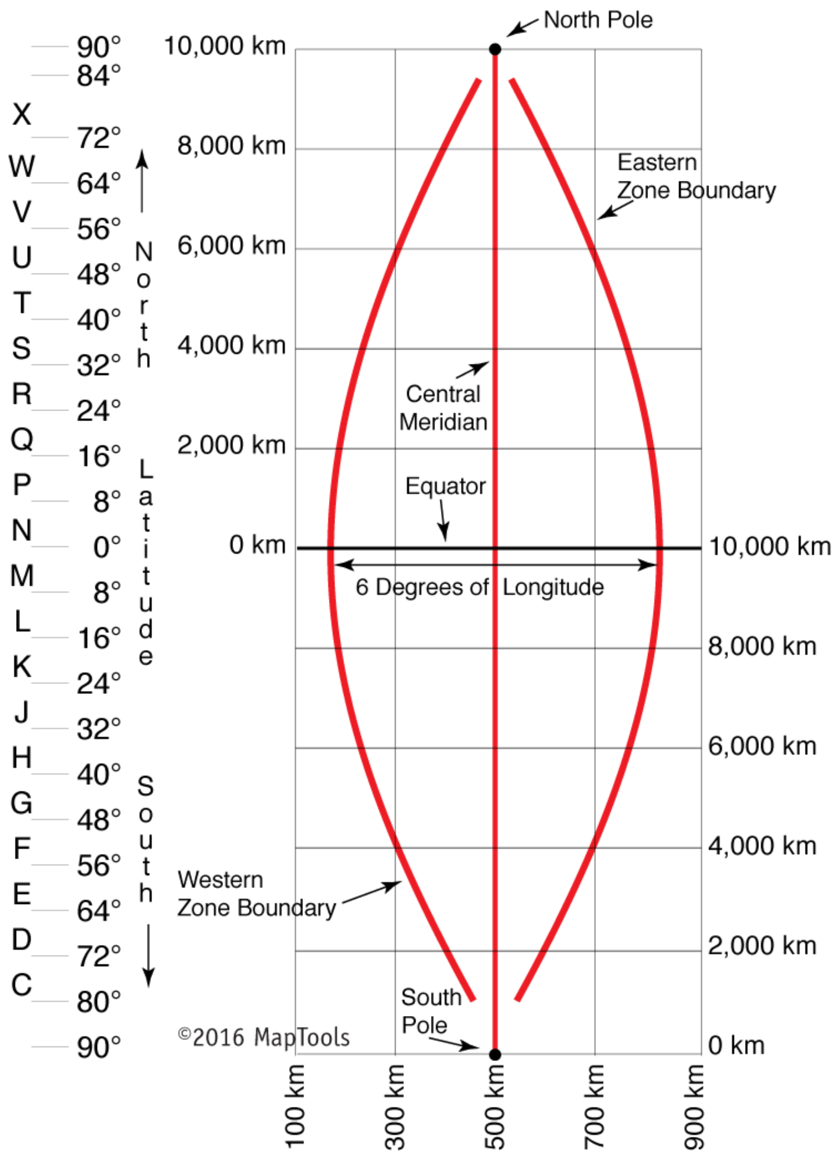

Fig. 3.3 – UTM zone

Image taken from https://www.liberaldictionary.com/easting/

4. GNSS POSITIONING

4.1. Introduction

Satellite methods for determining spatial coordinates are widely used in modern geodesy. The US has developed a GPS (Global Positioning System) system, Russia has a GLONASS (Global Navigation Satellite System) system, and Europe has a Galileo satellite system. All of these systems can be combined by the term GNSS (Global Navigation Satellite System). GNSS technologies are successfully applied in those areas where accurate information about the spatial position of objects on Earth, their size and changes in geometric parameters over time are needed.

Positioning is the implementation of possible ways of using this system in order to determine the parameters of the spatial state of objects of observation. To solve the positioning problem, it is necessary to measure the ranges, i.e. distance between receiver and transmitters. The object coordinates are the coordinates of the point of intersection of imaginary spheres with radius R1, R2 and R3 equal to the ranges. The third transmitter is needed to eliminate possible ambiguity arising from the intersection of two circles.

There are two methods of measuring exist: phase and code. Phase mode is a high-precision geodetic measurement mode. It involves at least two receivers simultaneously. In this mode, the coordinates of the base vector are obtained, that is, the difference in the coordinates of the points at which the antennas of the satellite receivers are installed.

4.2. GPS

GPS (Global Positioning System) is developed and maintained by the US Department of Defense, also known by the military under the code name NAVSTAR

(Navigation Satellite Timing and Ranging). The final GPS commissioning took place in 1995.

GPS consists of three main segments: space, control and user. GPS satellites broadcast a signal from space, and all GPS receivers use this signal to calculate their position in space in three coordinates in real time.

The space segment consists of 32 satellites orbiting the Earth's average orbit.

As of April 07, 2020, 31 spacecraft are in use for their intended purpose.

The control segment is the main control station and several additional stations, as well as terrestrial antennas and monitoring stations, some of the resources mentioned are shared with other projects.

The consumer segment is represented by GPS receivers operated by government institutions and receivers owned by ordinary users.

4.2.1. Segments of GPS

Satellite segment. Nominally, in each epoch, there are 24 working (healthy) satellites of the system. The satellites are spread over six circular orbits (table 4.1). There are thus 4 satellites in each orbit. The inclination of the orbital plane to the equatorial plane is 53°. This is the inclination angle for GPS satellites. The distance of the satellites from the Earth's surface is 20,200 km.

The GPS command changes the status of the satellites: it corrects the orbits, transfers the satellite from healthy to sick, turns off operational satellites, turns on backup satellites. There are three additional satellites in orbits, which are sometimes turned on. Often there are not 24, but 25 or more operational satellites. Several satellites ready for launch are always kept in reserve.

The control segment is a ground control system designed to control the functioning, direct control and information support of the satellite network. The main functions of the monitoring and control subsystem:

• measurement and prediction of parameters of the orbit of navigation satellites

• adding precise ephemeris and corrections on board the spacecraft

• monitoring of the navigation field (control of the navigation signal)

• control of the state of onboard equipment

• spacecraft control

The GPS control segment contains the main control station - Falcon Air Base in Colorado, five tracking stations located at US military bases in Hawaii, Ascension Islands, Diego Garcia, Quajelin and Colorado Springs and three stations: Ascension Islands, Diego Garcia, Kwajelin.

User segment. A GPS user is a person or a team that has at its disposal all necessary for operation satellite equipment and software. Consequently, a user segment is a collection of satellite receivers and other equipment in operation. Users are categorized in several ways: civil and military, navigators and surveyors who have full access to the system and have limited access. Typically, the US military has full access to the system. Such users are called authorized users. The rest of the users, usually civilians, are unauthorized users. The equipment of authorized users allows them to receive and process information with the accuracy that only the system is capable of. Until recently, the equipment of unauthorized users was only able to receive information with intentionally coarse precision. The intentional coarsening mode is now disabled.

Table 4.1 – Comparative characteristics of GPS and GLONASS

Parameter	**GPS**	**GLONASS**
Orbital planes	6	3
Orbital altitude relative to the center of mass (km)	26600	25500
Carrier frequency **L1** **L2**	 1575,4 1227,6	 1602,6-1615,5 1246,4-1256,5
Spatial coordinate system	WGS-84	PZ-90
Ephemeris type	Modified Keplerian elements	Geocentric coordinates and their derivatives

4.3. GNSS methods

The method of satellite measurements consists of the distance determination from the receiver of the navigation system to the satellite. The main methods of the surveying can be divided into the following groups:

Due to the reference system

- Absolute
- Differential (relative)

Due to the method of the observance

- Static
- Cinematic

  Stop and go

  PPP

Due to the method of the process

- Post-process
- RTK

To be more representative and clear the diagram 4.1 shows the correlation between different methods.

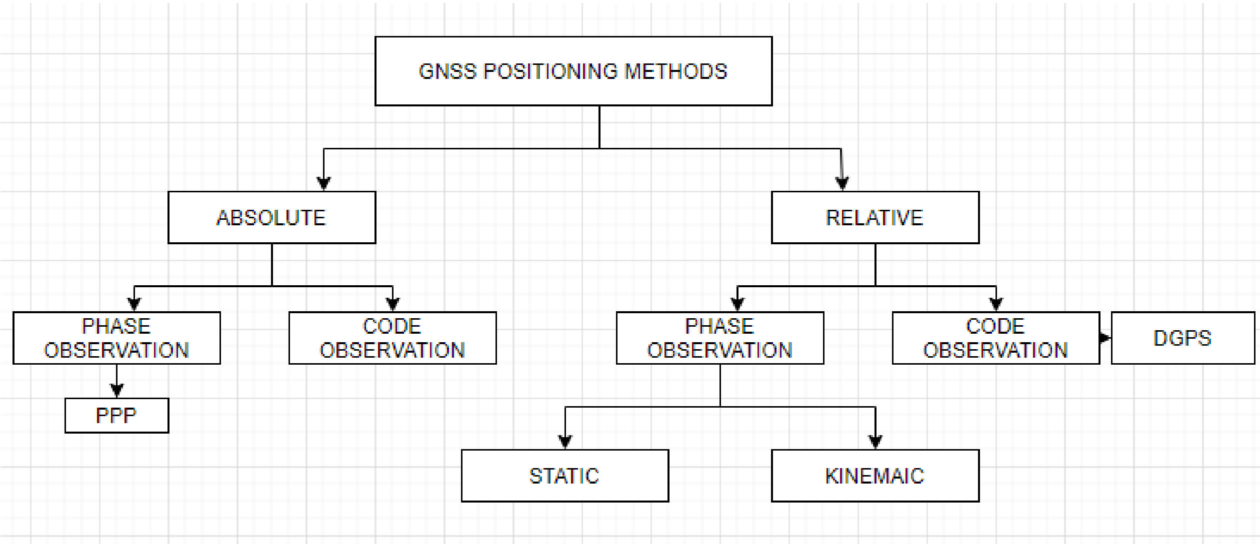

Fig. 4.1 – The correlation between GNSS methods

4.3.1. Absolute and differential (relative) methods

The **absolute method** is characterized by an independent determination of the position of the receiver using a spatial intersection. To implement it, it is necessary to know the value of the pseudo-range and the coordinates of at least 4 satellites. The pseudo-range is calculated by code or by phase, and the coordinates of the satellites are transmitted in the navigation message from each of them. Thus, the unknown coordinates X, Y, Z and the receiver clock correction are calculated (fig.4.2).

The absolute method is based on measurements by code, therefore, the accuracy depends on the quality of the quartz clock generator of the receiver and is 3-15 m. This method is used in low-current navigation (monitoring of vehicles, ships, etc.). To refine the data, various differential services using PPP (Precise Point Positioning) technology can be used. Such services (RTX, Atlas, TerraStar) transmit pre-calculated correction information (accurate ephemeris and clock drifts) so that the receiver can calculate its position with sub-decimeter accuracy. Here, geostationary satellites or the Internet can be used as a channel for delivering correction information. However, there are a number of limitations: the receiver must be multi-frequency, observations must be carried out for at least an hour, and subscription to these services is paid.

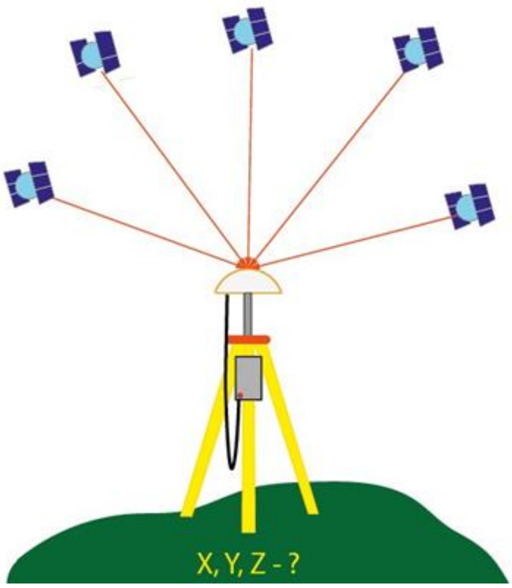

Fig. 4.2 – Configurations for the absolute method

Image taken from https://russiandrone.ru/publications/metody-gnss-nablyudeniy/

In the relative method, at least 2 receivers are involved, one of which is located at a point with known coordinates (Base), and the second at a specified one (Rover). In this case, a pseudo-range correction is calculated based on the difference between the coordinates determined by the Base receiver by satellites and the manually entered known coordinates of this point. This correction is transmitted to the Rover (at the designated point) and corrects its measured pseudo-ranges to refine the position determination (fig. 4.3).

The relative method, implemented by code measurements, is also called differential or DGPS. The accuracy of this method is sub-meter (50-80 cm).

Using the relative method to measure the carrier phase achieves centimeter accuracy. Only this method is suitable for solving geodetic problems. By the nature of the movement, it can be both statics and kinematics. Statics is realized in the measurement of a specific point, when data from satellites are collected and averaged at the point over several epochs. Kinematics is the creation of the trajectory of the receiver movement. Moreover, in accordance with the filters that determine whether the receiver is stationary or moving, the processing of this data occurs according to various algorithms. In general, the increase in accuracy is associated with the duration of measurements, as well as with the shooting conditions.

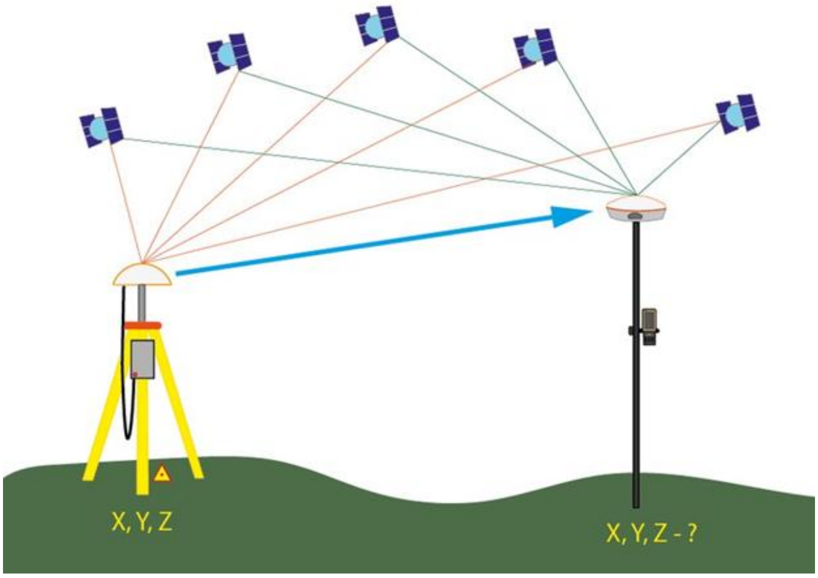

Fig. 4.3 – Configurations for the relative method

Image taken from https://russiandrone.ru/publications/metody-gnss-nablyudeniy/

4.3.2. Code and phase signals

The **coded mode** is the mode originally built into the system. The signal of each satellite contains its ephemeris - data about the location of the satellite, allowing you to calculate the coordinates of the satellite in the earth's coordinate system.

The receiver of satellite signals, like the satellite, has a frequency and time sensor; it also generates the frequencies L1 and L2 (in a single-frequency receiver, only L1). The L1 frequency is modulated by copies of the C / A and P codes, the L2 frequency is modulated only by the P code.

The time interval between the appearance on the receiver of its own code and the analogous code received from the satellite is measured.

If the clock of the receiver were precisely synchronized with the clock of the satellite, then the formation of codes on the satellite and in the receiver would occur simultaneously. In this case, the measured time interval between the appearance at the receiver of its own code and the code received from the satellite would be equal to the transit time of the signal from the satellite to the receiver, which would make it possible to calculate the distance to the satellite. However, the clock readings of the satellite and the receiver diverge by some amount equal to the difference between the satellite clock error and the receiver clock error. Therefore, the measured distance differs significantly from the correct one and is called pseudo-distance.

Information about the satellite clock is transmitted as part of the navigation message, which makes it possible to calculate the satellite clock error at the epoch t and take it into account.

The unknown quantities here are Xp, Yp, Zp, δp (t). To determine the four unknowns, it is necessary to have at least four equations, that is, in one epoch it is necessary to measure the pseudo-distances of at least four satellites.

The coordinates are determined from the results of code measurements with an accuracy of about 3 m.

The differential (relative) method is used to improve the accuracy. At the checkpoint with known coordinates, a satellite receiver is installed and, having determined its coordinates by satellites, the distances to the satellites are calculated. By comparing these distances with those calculated from known coordinates, corrections are determined and communicated to consumers by radio. The amendments correct the pseudo-distances measured by consumers, while the errors in determining the location relative to the checkpoint do not exceed 1 m.

Code measurements are used to solve navigation problems. In geodetic work, code measurements play an auxiliary role - they are used to determine the approximate coordinates of network points.

Phase mode is a high-precision geodetic measurement mode. It involves at least two receivers simultaneously. In this mode, the coordinates of the base vector are obtained, that is, the difference in the coordinates of the points at which the antennas of the satellite receivers are installed. The error in determining the base vector ranges from several millimeters to several centimeters.

Accurate geodetic measurements are performed at carrier frequencies L1 and L2 (in single-frequency receivers, only at frequency L1). In this case, the phase difference is measured between the oscillations received from the satellite and the oscillations of the same frequency generated in the receiver.

Phase differences are measured with high precision, corresponding to fractions of a millimeter. However, it is impossible to calculate the receiver coordinates with the specified accuracy by solving the system of equations, compiled from the results of phase measurements, due to orbital errors, the influence of the ionosphere, and other reasons.

The accuracy of phase measurements is realized using the method of relative determination of the position of points. The results of simultaneous observations of the same satellite at two points contain significant, but close in magnitude errors. Therefore, the differences in the measurement results are practically free from them and make it possible to determine with high accuracy the differences in the coordinates X, Y, Z of two points, that is, the three-dimensional vector DX, DY, DZ connecting them. Therefore, knowing the X, Y, Z coordinates of one point, we can, having determined the difference of the coordinates DX, DY, DZ to another, calculate its coordinates.

Phase measurements in geodetic works are the main ones, providing the ability to build high-precision geodetic networks.

4.3.3. Static and kinematic methods

There are several measurement techniques that can be used with most surveying GPS receivers.

Static is used to measure long lines, develop geodetic networks, study the movements of tectonic plates. It offers high accuracy over long distances, but relatively slow measurements.

It can be used to measure long lines (about 20 km or more). One receiver is installed at a point whose coordinates are accurately known in the WGS84 (or other) system. It is called a reference station. The other receiver at the other end of the baseline is called a rover. Data is recorded by both receivers simultaneously. It is important to record data by each receiver at the same frequency (interval in data logging). This is usually 15, 30 or 60 seconds. Receivers record data over a period of time. This period depends on the length of the link, the number of satellites observed, and the satellite geometry (DOP). It is generally assumed that static should be performed for a minimum of 1 hour on 20 km lines with five satellites and a predominant GDOP of 8. Long lines require longer observation periods.

After sufficient data accumulation, the receivers can be turned off. The rover can then move to the next target point to measure the next baseline. It is very important to perform redundant measurements on the network. For example, measure points at least twice, or measure additional vectors to avoid problems that would not otherwise be detected. The productivity increases significantly by adding more rovers.

The **kinematic method** is usually used for topographic surveying, registration of vehicle trajectories.

A moving rover, whose coordinates can be calculated relative to the base, is used. First, the rover must perform an initialization, which is essentially a fast static measurement that allows the software to resolve the ambiguity during post-processing. The base and rover turn on and remain completely stationary for 5-20 minutes while collecting data. (Actual time depends on baseline length and number of satellites observed). After the measurements, the rover can move freely. The user has the ability to choose: record coordinates with a pre-set interval in the recording, record individual coordinates or record a combination of these data

4.3.4. Point precise positioning (PPP)

Precise Point Positioning (PPP) is an absolute positioning method based on the use of satellite correcting information containing corrections to the ephemeris and time of the onboard clocks of navigation satellites and atmospheric corrections within the local area, which allows determining the spatial coordinates of objects with an accuracy of several decimeters to several centimeters.

Ephemeris-time information is calculated from the results of satellite observations performed by permanent ground stations for receiving GNSS signals with precisely known coordinates. To implement the PPP method, it is necessary to measure the phases of the carrier frequencies of the GNSS signals at the determined point.

The PPP method is implemented both in a posteriori mode and in real time. In the first case, the result can be obtained in the process of cameral processing of satellite observation data or with the help of special services on the Internet, given by providers of global high-precision satellite positioning services. In the second case, the coordinates of the position can be obtained in the process of receiving corrective information transmitted by the providers of global high-precision satellite positioning services via satellite communication channels or via the Internet online.

The PPP method differs from the relative satellite determination method in that the corrections change the parameters of the orbits and clocks, rather than in the measurements of the radio carriers of the GNSS satellites. It is similar to the absolute definition method. However, in the absolute method, the correction for the clock and ephemeris is set in advance. That is, the receiver receives the predicted correction information. In PPP, ephemeral time information is defined a posteriori, that is, the satellite has already passed over the network of base stations. Base stations and the user simultaneously observed it, and information about corrections is transmitted to the user with minimal delay.

For PPP, the location of base stations is global, so the distance between the designated and the base point does not matter.

Services for receiving corrections: RTX, Atlas, TerraStar.

5. TOPO-IBERIA PROJECT

5.1. Introduction

The Iberian Peninsula is a peninsula in southwestern Europe. It is washed by the Mediterranean Sea, the Atlantic Ocean and the Bay of Biscay. In the south, the Strait of Gibraltar separates it from Africa.

Mountains and plateaus dominate the relief of the Iberian Peninsula: lowlands are located only in places in the coastal zone and occupy a relatively small area. The average height of the peninsula is significant - about 600 m above sea level.

Along with the significant development of plateaus, a sharply dissected and rocky mountain landscape is also widely represented in the relief of the peninsula; mountains often have steep slopes, with deeply cut river valleys and gorges. Features of high-mountainous relief are also inherent in other mountain ranges (in their highest parts) - such as the Cantabrian Mountains, the Central Cordillera, the Andalusian mountains.

Taking into consideration such a varied relief, a continuous GPS network was established to monitor the kinematic movement of the Iberian Peninsula region.

5.2. Description

«Geociencias en Iberia: Estudios integrados de topografía y evolución 4D (Topo-Iberia)» is a research project which includes a continuous GPS network of 26 stations. Twenty-two stations are located on the territory of Spain, while the rest four are in Morocco (fig 5.1).

The network has a new integrated database, which includes geologic, seismic and geodetic observations. This information will produce a complete overview of interactions among deep, shallow and surface processes like tectonics, mass transport and landscape evolution.

Important geodesy contribution to the project is the possibility to avoid the placing of the antennae on the buildings.

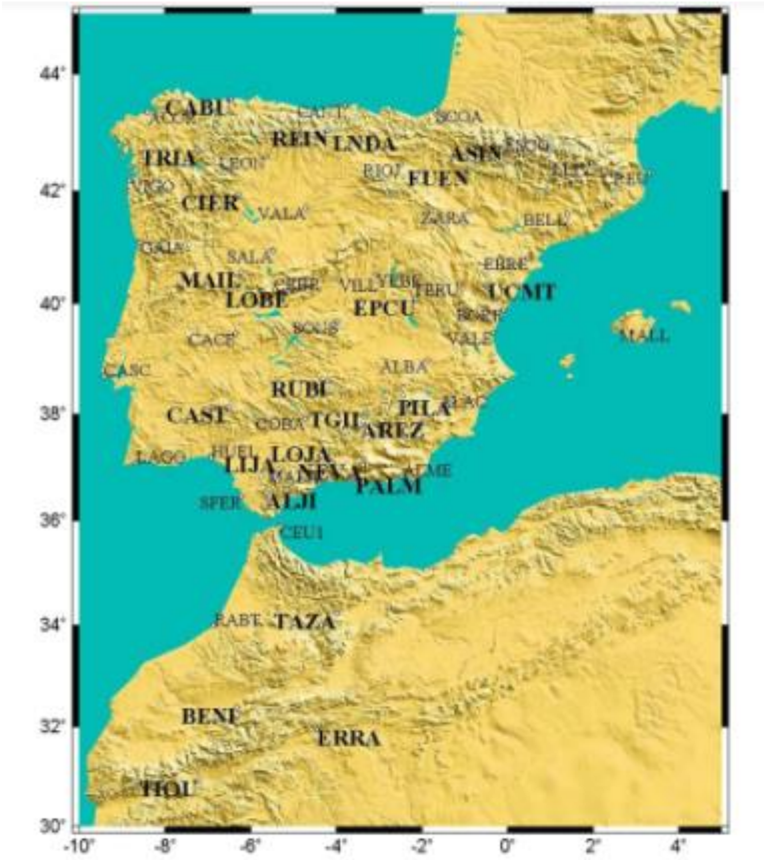

Fig. 5.1 – Location of the stations

Image taken from the article «Topo-Iberia project: CGPS crustal velocity field in the Iberian Peninsula and Morocco»

The use of GPS techniques for the control of deformations of the terrain, allows the monitoring of tectonically active areas and the detection of relative movements of small magnitude (below the centimeter), as it happens in the areas of the Iberian Peninsula. The three major research domains that have been identified are the southern and northern parts of the Iberian plate and its central part.

In the case of this thesis, the data analysis was performed for 5 stations in the eastern sector: AREZ, NEVA, PALM, PILA and TGIL (fig5.2).

Geodesy coordinates of these points are represented in the table 5.1.

Table 5.1 – Topo-Iberia Project CGPS Stations: 4-char ID, Geographic position and their location.

Station	Longitude	Latitude	Location
AREZ	-1.9405	37.8354	Sierra of Almirez, Murcia
NEVA	-3.3856	37.0626	Sierra Nevada, Granada
PALM	-3.5623	36.8090	Sierra of Guájares, Granada
PILA	-1.2894	38.2543	Sierra of Pila, Murcia
TGIL	-3.3026	38.0342	Torreperogil, Jaén

Fig. 5.2 – CGPS site TGIL (courtesy of Prof. Antonio J. Gil)

6. THE DATA PROCESSING

6.1. Introduction

The main aim of this work is to estimate the velocity field and make the conclusions about the movements of the points and their velocity. In order to fulfill this target, the observations on the stations AREZ, NEVA, PALM, PILA and TGIL were considered.

The information from the stations was gathered during 20-25th of June each year since 2009 to 2018. To make the analysis of the data the work was divided on several tasks:

1. Processing of the GNSS data on the online server APPS
2. Creation of the text files with the processed information
3. Transformation of the coordinates XYZ of Cartesian system to NEU of Local system
4. Absolute velocity field estimation in the program SARI
5. Residual velocity field estimation
6. Creation of the velocity maps

These steps will be described in the further subparagraphs and paragraphs.

6.2. Processing of the GNSS data

The meaning of the GNSS observation process is obtain true, refined coordinates by working on observations in RINEX format.

RINEX (Receiver Independent Exchange Format) is a data exchange format for source data files of satellite navigation receivers. The part of the file is used as example on the picture 6.1. The observation file consists of a header and measurement blocks for each epoch, descriptions of which can be found on International GNSS service (https://kb.igs.org/hc/en-us/articles/201096516-IGS-

Formats). It is also important to pay attention on the version of the file and depending on that select appropriate manual.

```
     2.11           OBSERVATION DATA    G (GPS)             RINEX VERSION / TYPE
teqc  2016Nov7      Juan Antonio        20170524 08:57:46UTCPGM / RUN BY / DATE
Linux 2.4.21-27.ELsmp|Opteron|gcc|Linux x86_64|=+           COMMENT
teqc  2016Nov7      Juan Antonio        20170524 08:57:45UTCCOMMENT
BIT 2 OF LLI FLAGS DATA COLLECTED UNDER A/S CONDITION       COMMENT
AREZ                                                        MARKER NAME
AREZ                                                        MARKER NUMBER
AJGIL               UJA                                     OBSERVER / AGENCY
4724134738          TRIMBLE NETRS       1.3-1               REC # / TYPE / VERS
00038148            TRM29659.00     NONE                    ANT # / TYPE
  5041661.7340  -170814.1675  3891733.1213                  APPROX POSITION XYZ
        0.0000        0.0000        0.0000                  ANTENNA: DELTA H/E/N
     1     1                                                WAVELENGTH FACT L1/2
     7    L1    L2    C1    P1    P2    S1    S2            # / TYPES OF OBSERV
    17                                                      LEAP SECONDS
 SNR is mapped to RINEX snr flag value [0-9]                COMMENT
  L1 & L2: min(max(int(snr_dBHz/6), 0), 9)                  COMMENT
  2016     6    25     0     0    0.0000000      GPS         TIME OF FIRST OBS
                                                            END OF HEADER
 16  6 25  0  0  0.0000000  0 11G30G01G06G07G17G19G09G03G02G22G23
   -850955.50156   -740066.58152  25467364.2194                   25467360.4224
        37.2504         17.7504
  -4094856.38956  -3167285.90253  24698306.3054                   24698304.6644
        38.2504         23.2504
 -19876725.93058 -15378411.65957  20979684.2194                   20979682.2234
        51.2504         43.7504
 -10957417.46857  -8317897.95855  23500208.2424                   23500202.9614
        42.0004         30.5004
 -12768452.80257  -9108533.35355  22947590.5944                   22947586.7894
        46.0004         34.0004
 -13787699.65657  -8514121.63956  22622319.2894                   22622312.8134
        46.5004         37.2504
 -27441160.85959 -21361670.41858  20159982.6254                   20159979.2194
        55.2504         49.7504
 -15119679.65657 -11712914.91955  22403392.3364                   22403390.5944
        43.5004         34.0004
  -4910641.65456  -2939653.53853  24672153.2734                   24672146.8134
        40.0004         21.7504
  -4060034.81056  -3145106.49553  24173907.3674                   24173901.6684
        39.0004         22.0004
 -24613135.61759 -18888208.97457  21020784.4614                   21020777.7974
        54.5004         44.0004
 16  6 25  0  0 30.0000000  0 11G30G01G06G07G17G19G09G03G02G22G23
```

Fig. 6.1 – RINEX file structure

The picture above shows the part of the GNSS observation file of the station AREZ. The measurements were held each 30 seconds during almost all day long.

All the observation files were used to execute the post-process, which is obligatory in order to get precise coordinates instead of approximate ones. To fulfill this object, the online application APPS was used. This web page is dedicated to process the GPS measurements, the results of which could be downloaded immediately. In order to start the work, the user need to adjust the parameters of the post-process and upload the file with raw data. The parameters, which were used for this thesis, are shown on the illustration 6.2. In order to process the information, APPS uses JPL's (Jet Propulsion Laboratory) GIPSY-OASIS (GNSS-Inferred Positioning System and Orbit Analysis Simulation Software) software.

The processed coordinates are indicated in the Supplement 1.

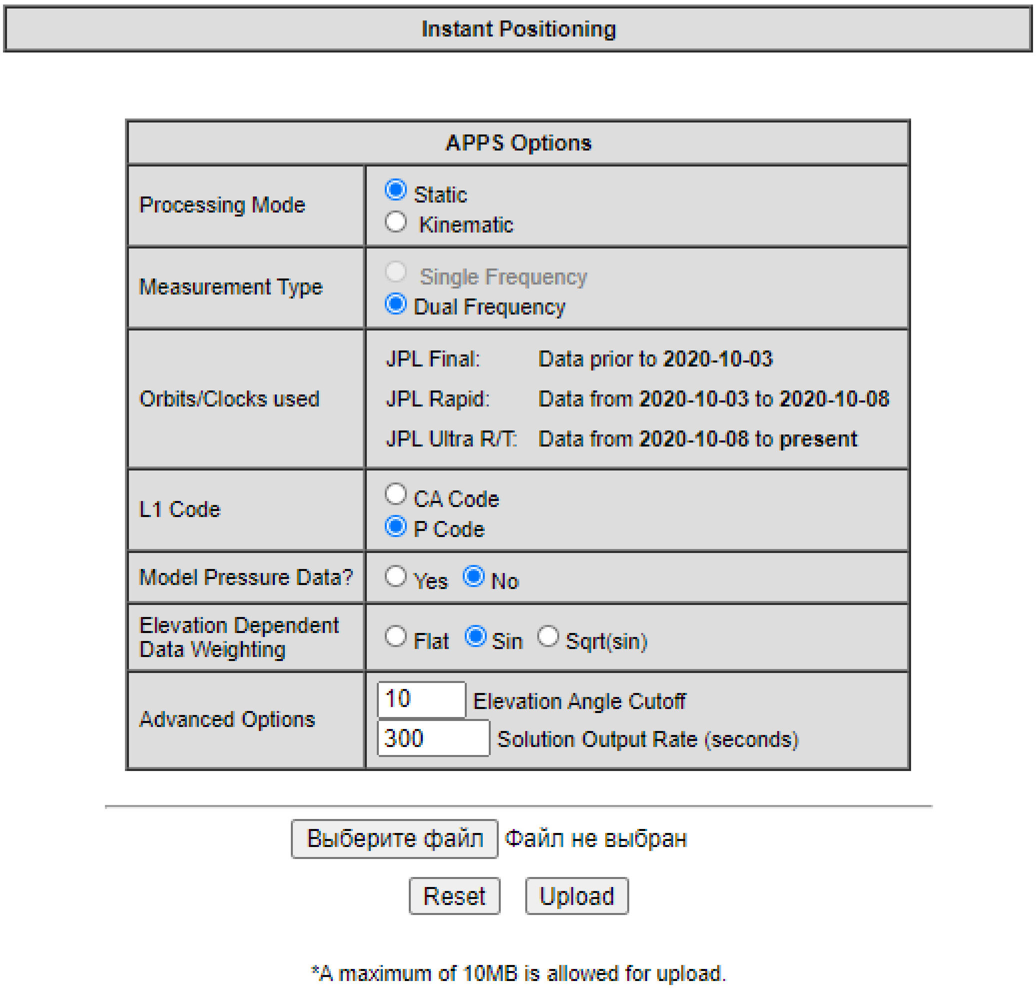

Fig. 6.2 – APPS parameters

The estimated coordinates are gathered in the file .stacov together with standard deviations and correlations (fig.6.3). Let's give an example of this file using the AREZ station from June 20, 2009.

```
     3 PARAMETERS ON 09JUN20.
     1   AREZ STA X          0.504166048421234E+07  +-   0.365080827299619E-02
     2   AREZ STA Y         -0.170813887564182E+06  +-   0.101958938881546E-02
     3   AREZ STA Z          0.389173184872366E+07  +-   0.274032792361359E-02
     2       1   -0.125363580952064E+00
     3       1    0.855760731617172E+00
     3       2   -0.887054752531664E-01
  AREZ ANTENNA LC     0.0000      0.0000      0.0000    !up north east (m)
```

Fig. 6.3 – The .stacov file

The characters marked with blue color represent coordinates XYZ ITRF2014 top down, with green – standard deviations $\sigma_{X_i}, \sigma_{Y_i}, \sigma_{Z_i}$ and with pink – correlations $\rho_{Y_iX_i}, \rho_{Z_iX_i}, \rho_{Z_iY_i}$

6.3. Coordinates transformation

The transformation from the estimated Cartesian coordinates XYZ ITRF2014 to the local coordinates NEU is important for the further velocity field analysis. All the calculations and transformations was made with help of MatLab application. Created MatLab codes are gathered in the Supplement 2.

6.3.1. Creation of the .txt file

First, in order to speed up the work we write, all the values of one station from the .stacov file should be saved in one .txt file. In order to manage it, the Code 1 was written and implemented (fig. 6.4). As the result, we got the common catalog, which contains coordinates XYZ, standard deviations $\sigma_{X_i}, \sigma_{Y_i}, \sigma_{Z_i}$ and correlations $\rho_{Y_iX_i}, \rho_{Z_iX_i}, \rho_{Z_iY_i}$. In addition, it includes the fraction of the year corresponding to the day of the GPS observation, which was calculated with online servers (http://sopac-old.ucsd.edu/convertDate.shtml).

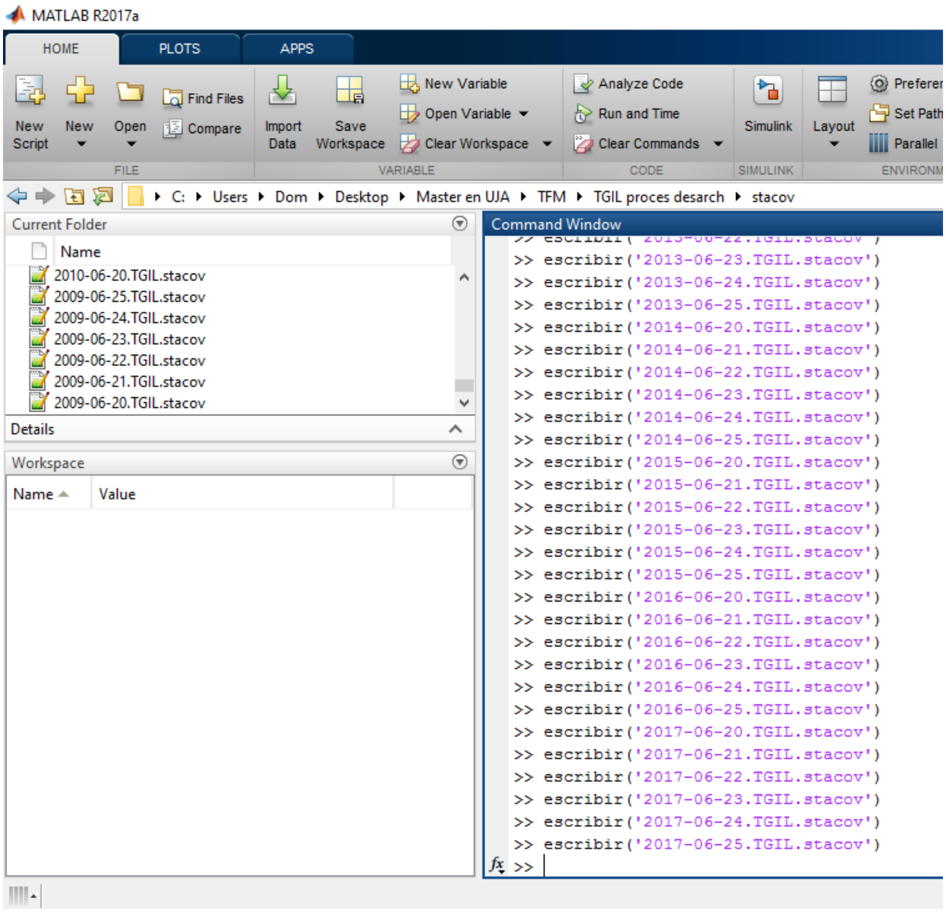

Fig. 6.4 – The implementation of the code to create the common file

6.3.2. Calculation of the matrix $\sum_{(XYZ)_i}$

The matrix has the following form:

$$\sum_{(XYZ)_i} = \begin{bmatrix} \sigma_{X_i}^2 & \sigma_{X_iY_i} & \sigma_{X_iZ_i} \\ \sigma_{X_iY_i} & \sigma_{Y_i}^2 & \sigma_{Y_iZ_i} \\ \sigma_{X_iZ_i} & \sigma_{Y_iZ_i} & \sigma_{Z_i}^2 \end{bmatrix}$$

It is symmetric and contains squared standard deviations on the diagonal and calculated deviations on the rest. They are calculated using the following formulas:

$$\rho_{Y_iX_i} = \frac{\sigma_{X_iY_i}}{\sigma_{X_i} \cdot \sigma_{Y_i}} \Rightarrow \sigma_{X_iY_i} = \sigma_{X_i} \cdot \sigma_{Y_i} \cdot \rho_{Y_iX_i}$$

$$\rho_{Z_iX_i} = \frac{\sigma_{Z_iX_i}}{\sigma_{X_i} \cdot \sigma_{Z_i}} \Rightarrow \sigma_{Z_iX_i} = \sigma_{Z_i} \cdot \sigma_{Z_i} \cdot \rho_{Z_iX_i}$$

$$\rho_{Y_iZ_i} = \frac{\sigma_{Z_iY_i}}{\sigma_{Z_i} \cdot \sigma_{Y_i}} \Rightarrow \sigma_{Z_iY_i} = \sigma_{Z_i} \cdot \sigma_{Y_i} \cdot \rho_{Y_iZ_i}$$

To calculate these equations the Codes 2 and 3 were written. The Code 2 reads the values from the opened common .txt file, which was created on the previous step, while Code 3 calculates deviations and save all necessary information to the new file (fig. 6.5). This file contains values of the matrix $\sum_{(XYZ)_i}$ (fig. 6.6).

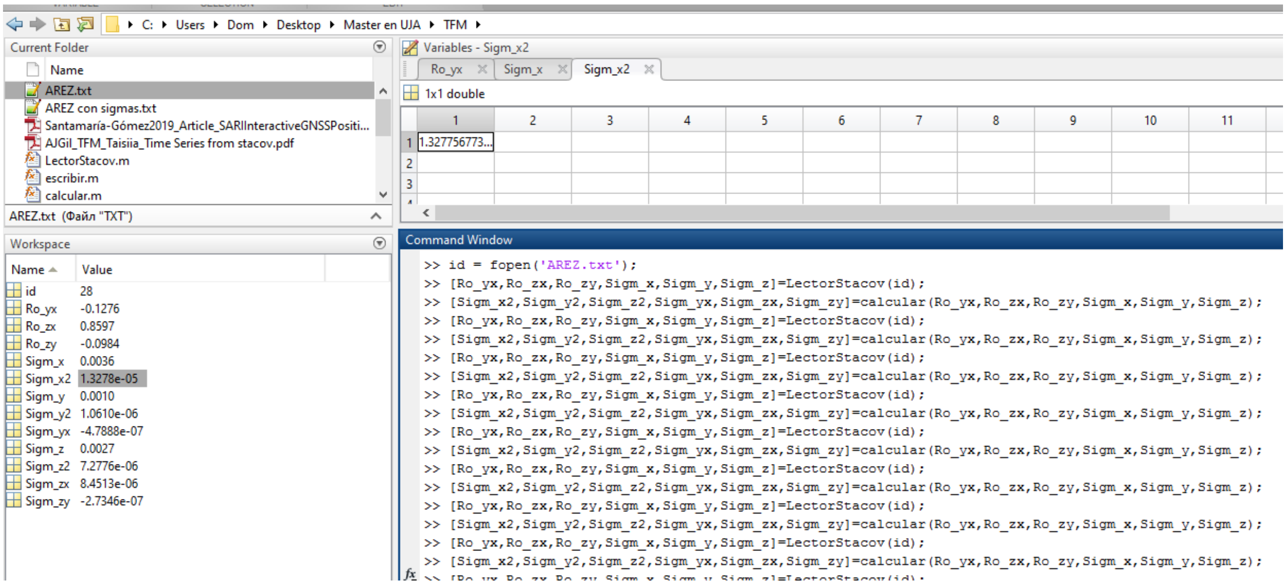

Fig. 6.5 – The implementation of the Codes 2 and 3 to save and calculate the deviations

	t	Sigm_x2	Sigm_y2	Sigm_z2	Sigm_yx	Sigm_zx	Sigm_zy
2	2009.4671	1.332840e-05	1.039563e-06	7.509397e-06	-4.666440e-07	8.561383e-06	-2.478439e-07
3	2009.4699	1.266108e-05	1.003459e-06	7.225257e-06	-3.574062e-07	8.194975e-06	-2.249672e-07
4	2009.4726	1.272500e-05	1.005368e-06	7.189856e-06	-3.835677e-07	8.194449e-06	-2.277420e-07
5	2009.4753	1.281602e-05	1.020153e-06	7.365508e-06	-3.691105e-07	8.330580e-06	-2.260346e-07
6	2009.4781	1.275481e-05	1.007040e-06	7.382898e-06	-4.146604e-07	8.304635e-06	-2.571591e-07
7	2009.4808	1.286193e-05	1.010964e-06	7.292751e-06	-4.513181e-07	8.289702e-06	-2.692202e-07
8	2010.4671	1.292088e-05	1.092001e-06	7.234057e-06	-6.477955e-07	8.294948e-06	-3.589471e-07
9	2010.4699	1.280096e-05	1.085681e-06	7.282880e-06	-6.276169e-07	8.283021e-06	-3.592183e-07
10	2010.4726	1.322152e-05	1.098626e-06	7.377282e-06	-6.546505e-07	8.489650e-06	-3.711492e-07
11	2010.4753	1.235398e-05	1.050542e-06	7.045853e-06	-5.343417e-07	7.983793e-06	-3.144917e-07

Fig. 6.6 – The part of the new file with the deviations

After that, we need to prepare the workspace in MatLab for further calculations and create the cells *a* and *b* with all sigma (σ) and coordinates respectively for each station. To accomplish this task, the Codes 4 and 5 were used. Applying the cleated cell *a* with sigma and Code 6, we form the matrixes $\sum_{(XYZ)_i}$ for each time epoch and each observation (fig. 6.7).

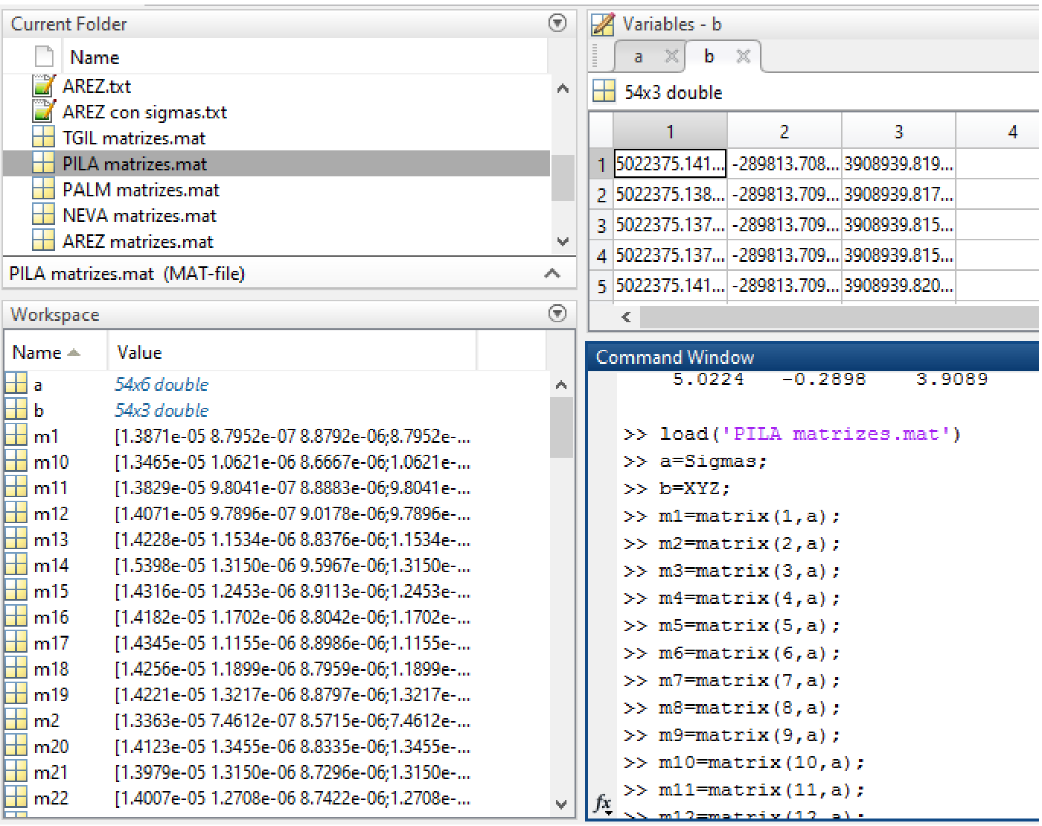

Fig. 6.7 – The part of the creating of the matrixes $\sum_{(XYZ)_i}$

Furthermore, we create similar matrixes of the coordinates XYZ for each time epoch and each observation with the help of Code 7 (fig. 6.8).

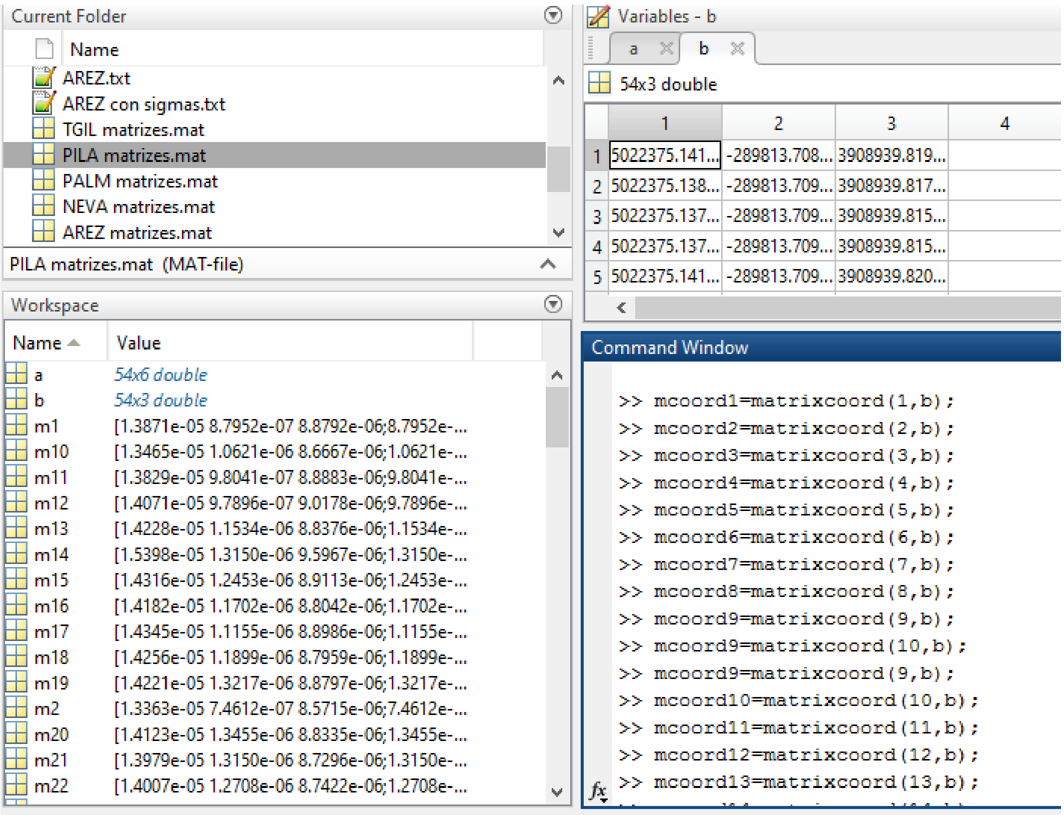

Fig. 6.8 – The part of the creating of the matrixes of the coordinates XYZ

6.3.3. Calculation of the covariance matrix $\sum_{(\Delta X \Delta Y \Delta Z)_{1n}}$

The covariance matrix has the following form:

$$\sum_{(\Delta X \Delta Y \Delta Z)_i} = \begin{bmatrix} \sigma^2_{\Delta X_{1n}} & \sigma_{\Delta X_{1n} \Delta Y_{1n}} & \sigma_{\Delta X_{1n} \Delta Z_{1n}} \\ \sigma_{\Delta X_{1n} \Delta Y_{1n}} & \sigma^2_{\Delta Y_{1n}} & \sigma_{\Delta Y_{1n} \Delta Z_{1n}} \\ \sigma_{\Delta X_{1n} \Delta Z_{1n}} & \sigma_{\Delta Y_{1n} \Delta Z_{1n}} & \sigma^2_{\Delta Z_{1n}} \end{bmatrix}$$

To calculate the matrix several steps were fulfilled for each station.

– Difference of the coordinates with Code 8

$$\begin{bmatrix} \Delta X_{1n} \\ \Delta Y_{1n} \\ \Delta Z_{1n} \end{bmatrix} = \begin{bmatrix} X_n - X_1 \\ Y_n - Y_1 \\ Z_n - Z_1 \end{bmatrix}$$

– Creation of the matrix $\sum_{(XYZ)_{1n}}$ with the Code 9

$$\sum_{(XYZ)_{1n}} = \begin{bmatrix} \sigma_{X_1}^2 & \sigma_{X_iY_1} & \sigma_{X_1Z_1} & 0 & 0 & 0 \\ \sigma_{X_1Y_1} & \sigma_{Y_1}^2 & \sigma_{Y_1Z_1} & 0 & 0 & 0 \\ \sigma_{X_1Z_1} & \sigma_{Y_1Z_1} & \sigma_{Z_1}^2 & 0 & 0 & 0 \\ 0 & 0 & 0 & \sigma_{X_n}^2 & \sigma_{X_nY_n} & \sigma_{X_nZ_n} \\ 0 & 0 & 0 & \sigma_{X_nY_n} & \sigma_{Y_n}^2 & \sigma_{Y_nZ_n} \\ 0 & 0 & 0 & \sigma_{X_nZ_n} & \sigma_{Y_nZ_n} & \sigma_{X_n}^2 \end{bmatrix}$$

– Calculation of the covariance matrix $\sum_{(\Delta X \Delta Y \Delta Z)_{1n}}$ with the Code 10

$$\sum_{(\Delta X \Delta Y \Delta Z)_i} = \begin{bmatrix} \sigma_{\Delta X_{1n}}^2 & \sigma_{\Delta X_{1n}\Delta Y_{1n}} & \sigma_{\Delta X_{1n}\Delta Z_{1n}} \\ \sigma_{\Delta X_{1n}\Delta Y_{1n}} & \sigma_{\Delta Y_{1n}}^2 & \sigma_{\Delta Y_{1n}\Delta Z_{1n}} \\ \sigma_{\Delta X_{1n}\Delta Z_{1n}} & \sigma_{\Delta Y_{1n}\Delta Z_{1n}} & \sigma_{\Delta Z_{1n}}^2 \end{bmatrix}$$

$$= \begin{bmatrix} -1 & 0 & 0 & +1 & 0 & 0 \\ 0 & -1 & 0 & 0 & +1 & 0 \\ 0 & 0 & -1 & 0 & 0 & +1 \end{bmatrix} \begin{bmatrix} \sigma_{X_1}^2 & \sigma_{X_iY_1} & \sigma_{X_1Z_1} & 0 & 0 & 0 \\ \sigma_{X_1Y_1} & \sigma_{Y_1}^2 & \sigma_{Y_1Z_1} & 0 & 0 & 0 \\ \sigma_{X_1Z_1} & \sigma_{Y_1Z_1} & \sigma_{Z_1}^2 & 0 & 0 & 0 \\ 0 & 0 & 0 & \sigma_{X_n}^2 & \sigma_{X_nY_n} & \sigma_{X_nZ_n} \\ 0 & 0 & 0 & \sigma_{X_nY_n} & \sigma_{Y_n}^2 & \sigma_{Y_nZ_n} \\ 0 & 0 & 0 & \sigma_{X_nZ_n} & \sigma_{Y_nZ_n} & \sigma_{X_n}^2 \end{bmatrix} \begin{bmatrix} -1 & 0 & 0 \\ 0 & -1 & 0 \\ 0 & 0 & -1 \\ +1 & 0 & 0 \\ 0 & +1 & 0 \\ 0 & 0 & +1 \end{bmatrix}$$

6.3.4. Transformation of the coordinates XYZ to NEU

To obtain the coordinates NEU (fig.6.9) the following equation should be resolved:

$$\begin{bmatrix} N_n \\ E_n \\ U_n \end{bmatrix} = \begin{bmatrix} -sin\varphi_1 \cdot cos\lambda_1 & -sin\varphi_1 \cdot sin\lambda_1 & cos\varphi_1 \\ -sin\lambda_1 & cos\lambda_1 & 0 \\ cos\varphi_1 \cdot cos\lambda_1 & cos\varphi_1 \cdot sin\lambda_1 & sin\varphi_1 \end{bmatrix} \begin{bmatrix} \Delta X_{1n} \\ \Delta Y_{1n} \\ \Delta Z_{1n} \end{bmatrix}$$

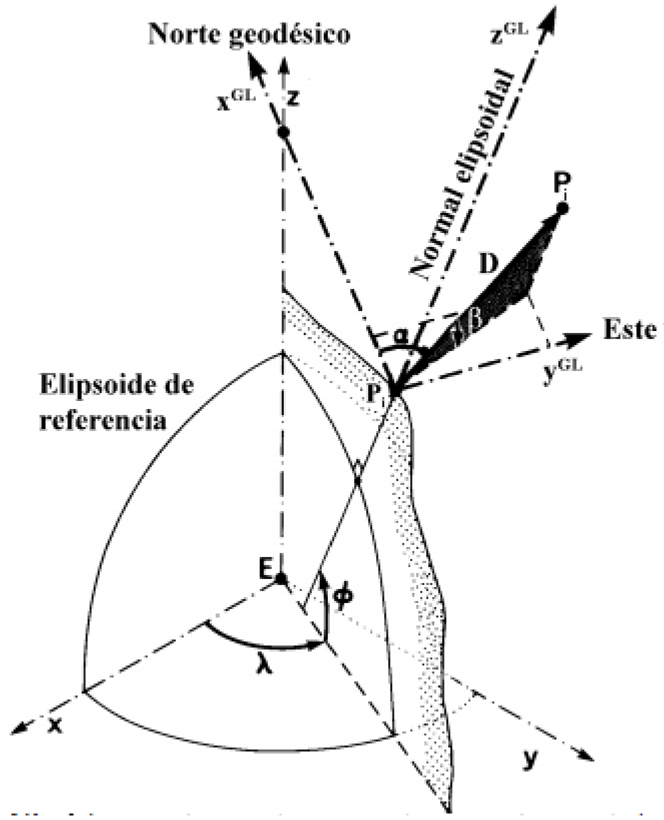

Fig. 6.9 – Connection between Cartesian system XYZ and Local system NEU

- Calculation of the trigonometric matrix with the Code 11

The latitude y longitude of the stations were transformed with the program PAG (fig 6.10).

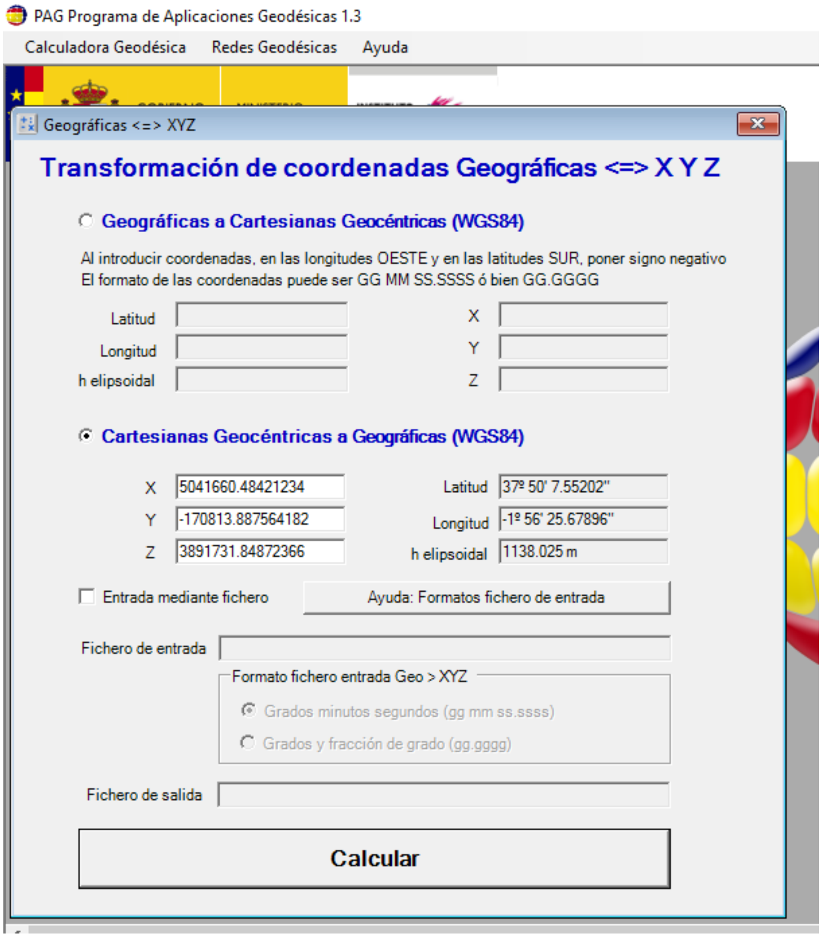

Fig. 6.10 – Transformation of the Cartesian coordinates to the Geographical ones (station AREZ)

– Calculation of the coordinates NEU with the Code 12

The obtained coordinates are gathered in the Supplement 1.

– Calculation of covariance matrix NEU to get out the deviations with the Code 13

$$\Sigma_{NEU} = \begin{bmatrix} \sigma_N^2 & \sigma_{NE} & \sigma_{NU} \\ \sigma_{NE} & \sigma_E^2 & \sigma_{EU} \\ \sigma_{NU} & \sigma_{EU} & \sigma_U^2 \end{bmatrix} =$$

$$= \begin{bmatrix} -sin\varphi_1 \cdot cos\lambda_1 & -sin\varphi_1 \cdot sin\lambda_1 & cos\varphi_1 \\ -sin\lambda_1 & cos\lambda_1 & 0 \\ cos\varphi_1 \cdot cos\lambda_1 & cos\varphi_1 \cdot sin\lambda_1 & sin\varphi_1 \end{bmatrix} \begin{bmatrix} \sigma_{\Delta X_{1n}}^2 & \sigma_{\Delta X_{1n}\Delta Y_{1n}} & \sigma_{\Delta X_{1n}\Delta Z_{1n}} \\ \sigma_{\Delta X_{1n}\Delta Y_{1n}} & \sigma_{\Delta Y_{1n}}^2 & \sigma_{\Delta Y_{1n}\Delta Z_{1n}} \\ \sigma_{\Delta X_{1n}\Delta Z_{1n}} & \sigma_{\Delta Y_{1n}\Delta Z_{1n}} & \sigma_{\Delta Z_{1n}}^2 \end{bmatrix}$$

$$\cdot \begin{bmatrix} -sin\varphi_1 \cdot cos\lambda_1 & -sin\varphi_1 & cos\varphi_1 cos\lambda_1 \\ -sin\varphi_1 \cdot sin\lambda_1 & cos\lambda_1 & cos\varphi_1 sin\lambda_1 \\ cos\varphi_1 & 0 & sin\varphi_1 \end{bmatrix}$$

– Creating of the file with NEU coordinates and deviations

The last step in transformation of the coordinates to NEU is to create the .txt file, which will be used for further work in SARI. For this we use Code 14, which will save the coordinates NEU, σ_N, σ_E, σ_U to the file .txt (fig 6.10).

t	N	E	U	sigmaN	sigmaE	sigmaU
2009.4671	0	0	0	1.677492e-03	1.429734e-03	6.236714e-03
2009.4699	6.913510e-04	-1.634573e-03	2.816955e-03	1.654906e-03	1.419403e-03	6.165528e-03
2009.4726	-1.732046e-03	-1.558044e-03	-3.379356e-03	1.655820e-03	1.419476e-03	6.167733e-03
2009.4753	-3.528291e-04	-3.521281e-03	1.131012e-02	1.659332e-03	1.425049e-03	6.188287e-03
2009.4781	-6.640125e-04	-3.391484e-03	-6.722887e-03	1.663275e-03	1.419335e-03	6.183940e-03
2009.4808	-3.092131e-03	-1.963102e-03	3.114532e-03	1.662983e-03	1.419885e-03	6.185581e-03
2010.4671	1.614912e-02	1.623485e-02	-3.257451e-03	1.657731e-03	1.443533e-03	6.188088e-03
2010.4699	1.670025e-02	1.645905e-02	-6.973202e-03	1.656647e-03	1.441771e-03	6.182532e-03
2010.4726	1.676440e-02	1.684559e-02	-1.274977e-02	1.661817e-03	1.445782e-03	6.222770e-03
2010.4753	1.622588e-02	1.565677e-02	-6.210853e-03	1.648478e-03	1.431574e-03	6.128691e-03
2010.4781	1.748591e-02	1.630789e-02	-4.947852e-03	1.690893e-03	1.443471e-03	6.261298e-03

Fig. 6.10 – The part of created file (station AREZ)

7. ABSOLUTE AND RESIDUAL VELOCITIES ANALYSIS

7.1. Introduction

Absolute velocity is the velocity of a body that can be measured only in a frame of reference that is at absolute rest. That is to say, this is origin velocity when the system is stationary. Velocity of light is an example for this.

Relative velocity is the vector difference between the velocities of two bodies: the velocity of a body with respect to another regarded as being at rest. In this work, the residual velocity field were calculated with respect to stable Eurasia.

To estimate the absolute velocity the online program SARI (Señales y Análisis de Ruido Interactivo (Interactive Signal and Noise Analysis)) was used.

The app was originally developed in early 2017 to estimate tectonic velocities from GPS position time series from the RESIF/RENAG network (RESIF 2017) and other network partners in France.

SARI, a new interactive time series analysis toolbox, is proposed focusing on the series visualization and signal processing using weighted least-squares, Kalman filtering, Vondrák band-pass smoother, and MLE stochastic noise analysis. The software is developed in the R programming language and can be run on a local machine or remotely via a public web server accessible at https://alvarosg.shinyapps.io/sari. [4]

7.2. Absolute velocity estimation

To find out the absolute velocity values and create the regression line, the program SARI was used. First, the file with NEU coordinates should be uploaded. Using the coordinates in the file, the points are drown with respect to the year of measurements. In order to create regression line the method (LS-least squares) and model components (lineal) for fit controls were selected (fig. 7.1-7.2). The reference epoch rate is the first day of observations in 2009. These parameters are the same for all stations.

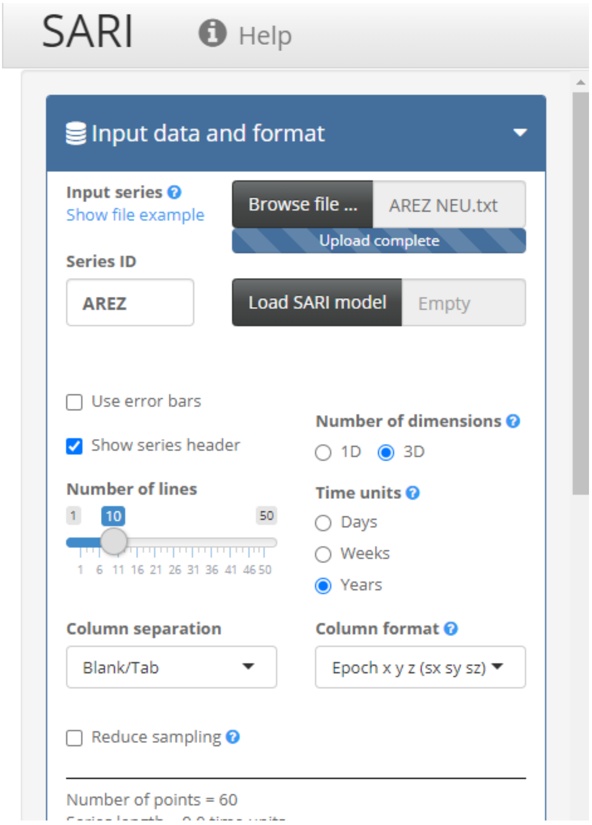

Fig. 7.1 – Parameters of SARI program

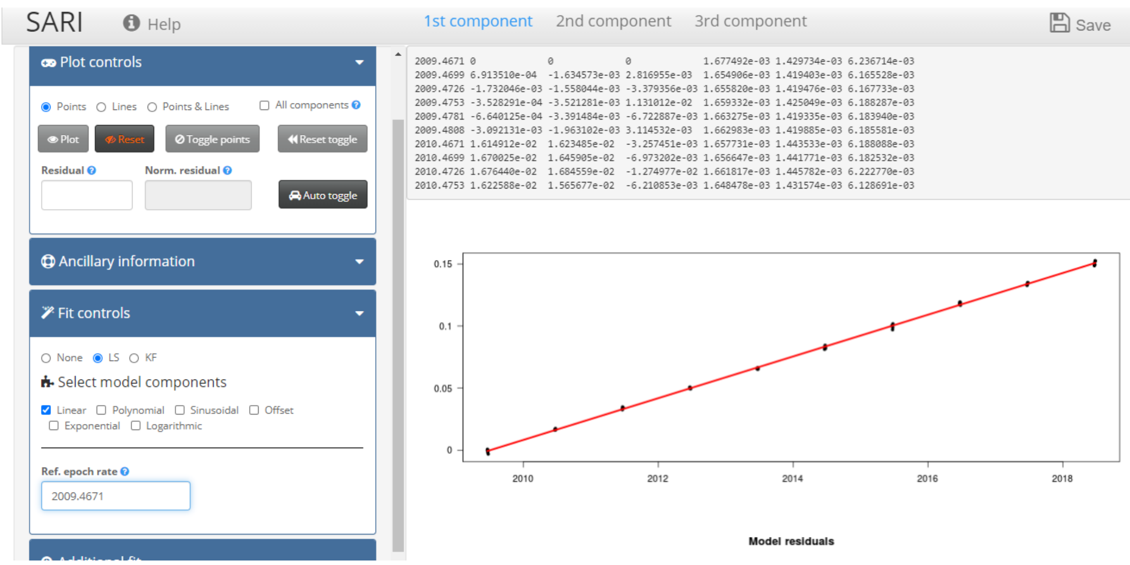

Fig. 7.2 – Parameters of SARI program

As the result, we obtain the lines of recreation of each station for three components North, East and Up (fig 7.4-7.18) and the values of the absolute velocities (table 7.3).

```
LS estimate

Formula: "y ~ Intercept + Rate*(x-2009.47)"

Parameters:
              Estimate     Std. Error    t value   Pr(>|t|)
Intercept -0.00270478483  0.00022851323 -11.83645 < 2.22e-16 ***
Rate       0.01909825137  0.00004277763 446.45415 < 2.22e-16 ***
---
Signif. codes:  0 ‘***’ 0.001 ‘**’ 0.01 ‘*’ 0.05 ‘.’ 0.1 ‘ ’ 1

Residual standard error: 0.0009517436 on 58 degrees of freedom

Correlation of Parameter Estimates:
     Intercept
Rate -0.84

Number of iterations to convergence: 1
Achieved convergence tolerance: 0.00000002773501
```

Fig. 7.3 – Example of SARI results of absolute velocities values, AREZ East

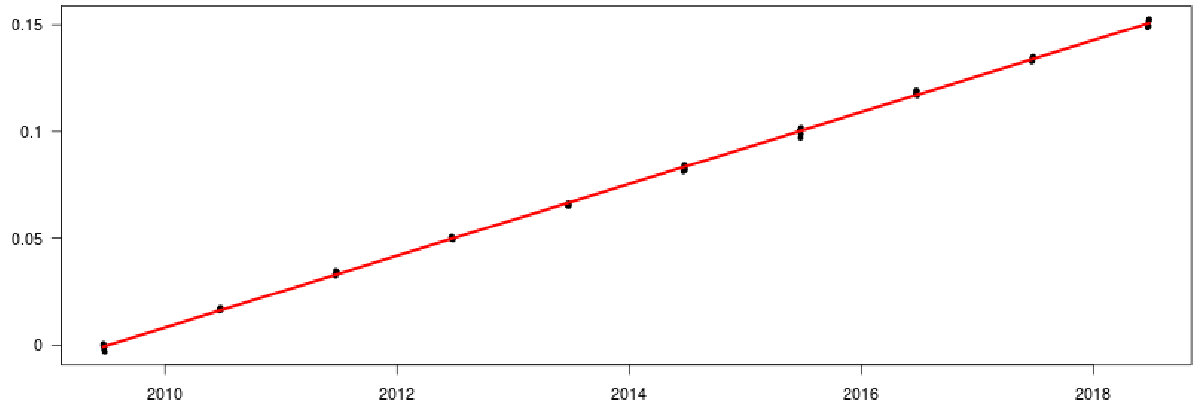

Fig. 7.4 – North component regression line, AREZ

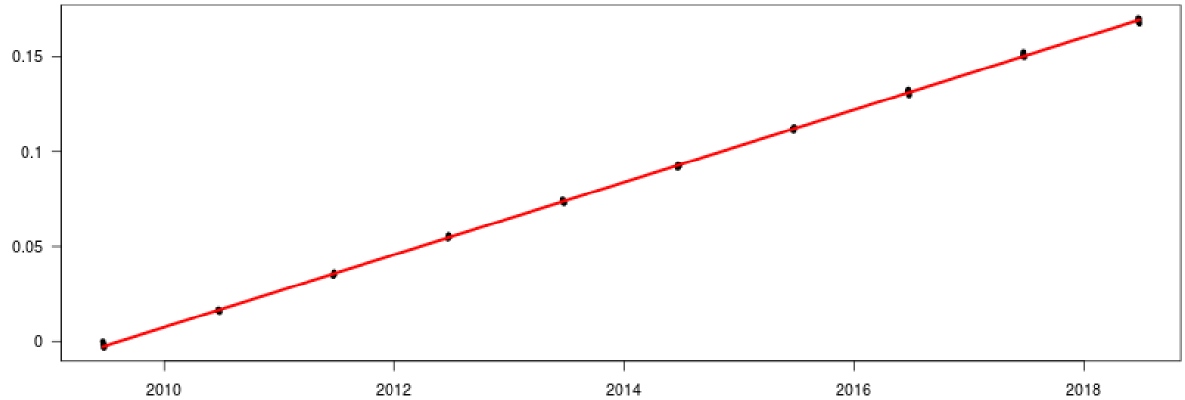

Fig. 7.5 – East component regression line, AREZ

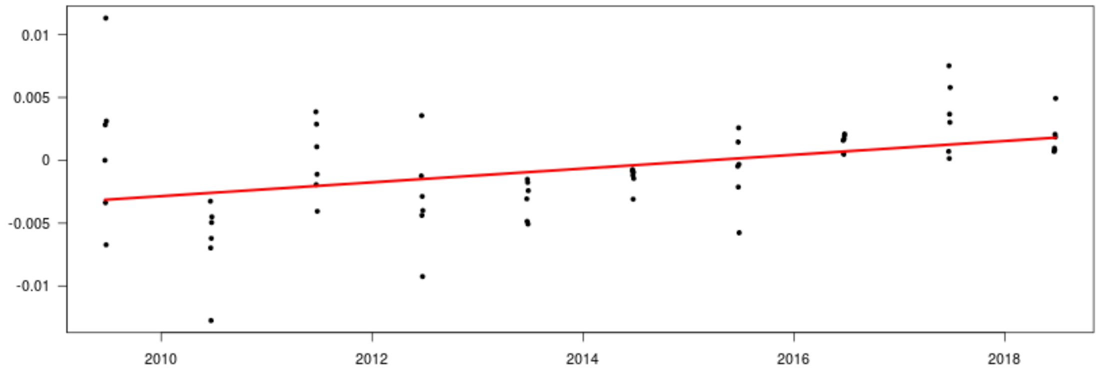

Fig. 7.6 – Up component regression line, AREZ

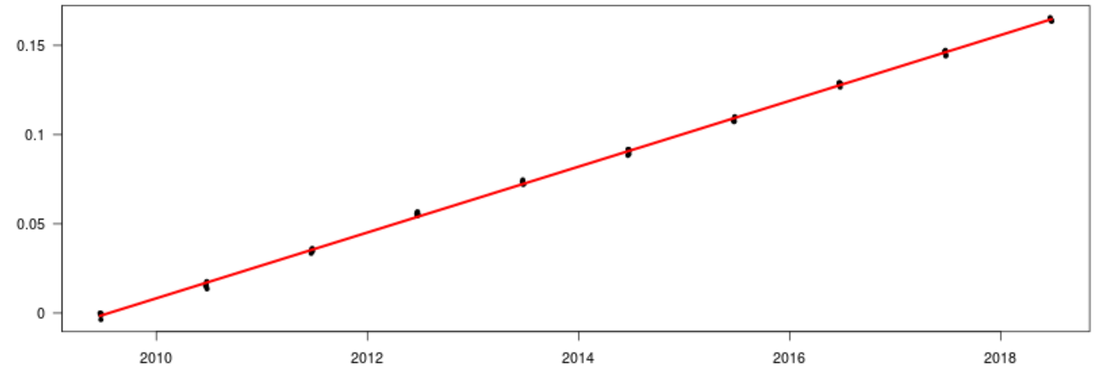

Fig. 7.7 – North component regression line, NEVA

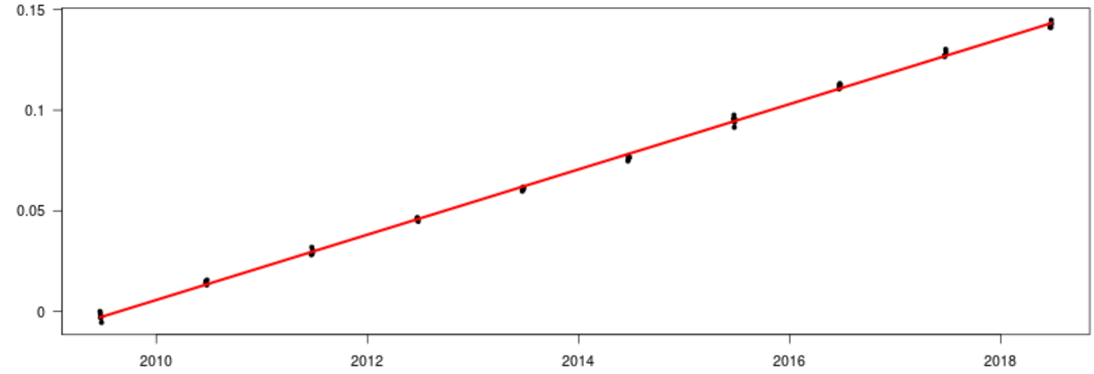

Fig. 7.8 – East component regression line, NEVA

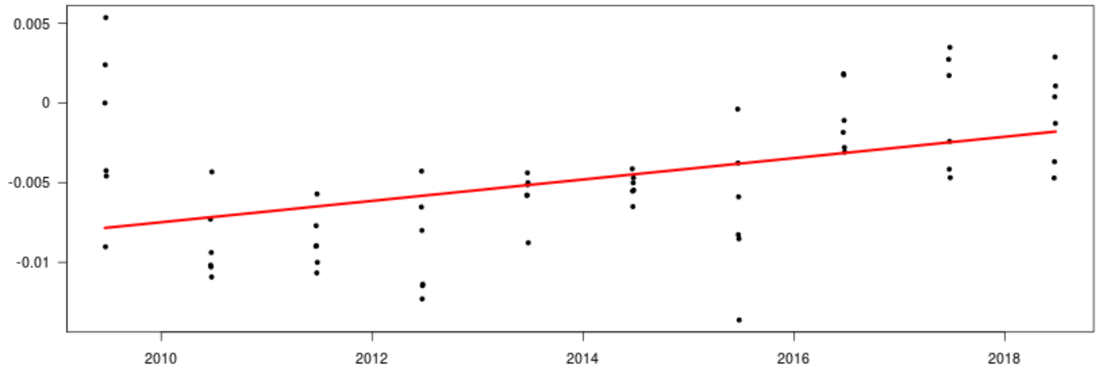

Fig. 7.9 – Up component regression line, NEVA

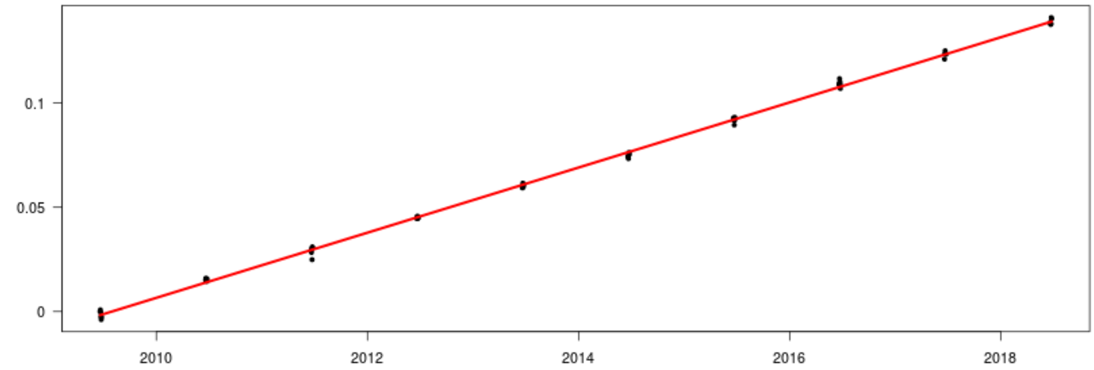

Fig. 7.10 – North component regression line, PALM

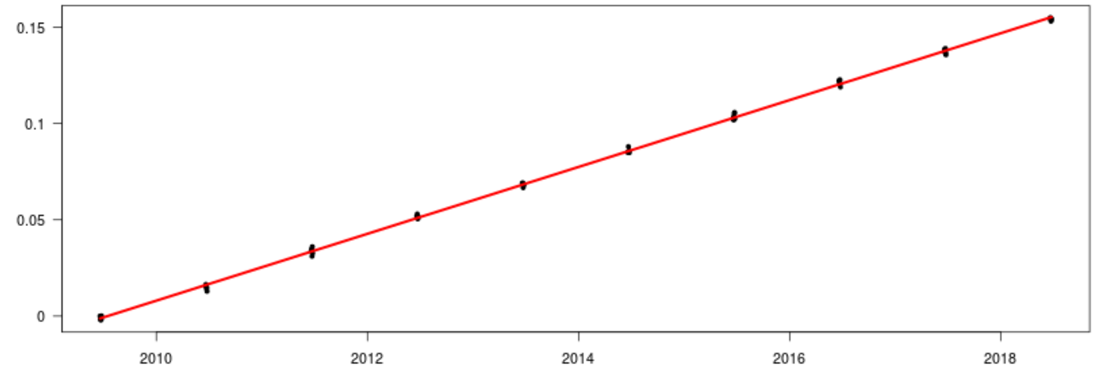

Fig. 7.11 – East component regression line, PALM

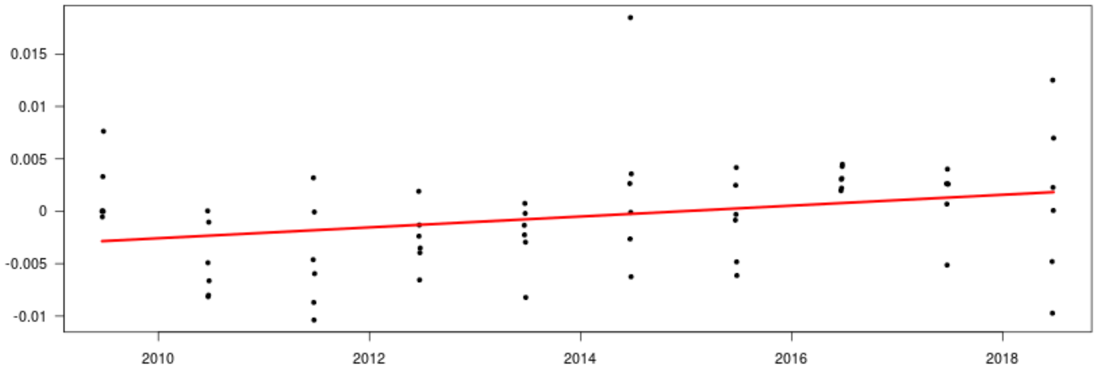

Fig. 7.12 – Up component regression line, PALM

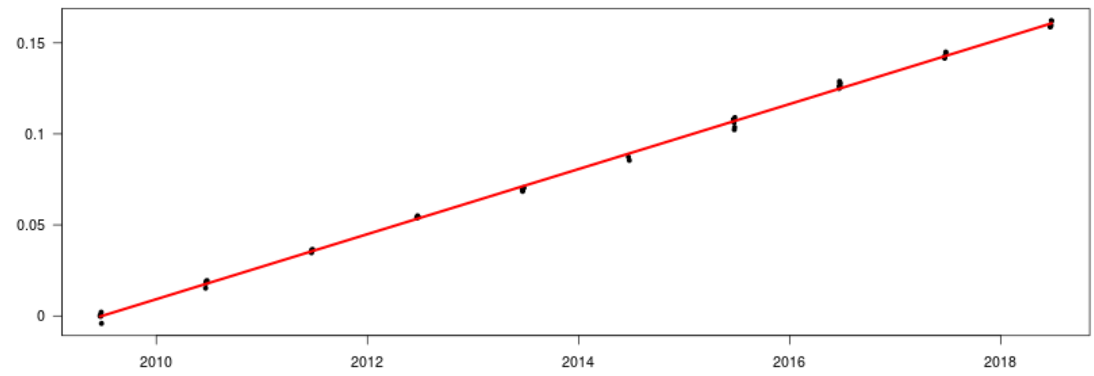

Fig. 7.13 – North component regression line, PILA

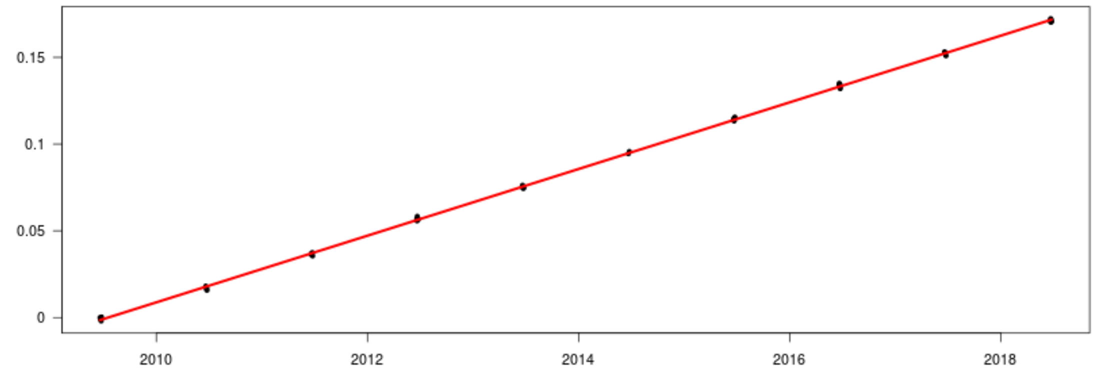

Fig. 7.14 – East component regression line, PILA

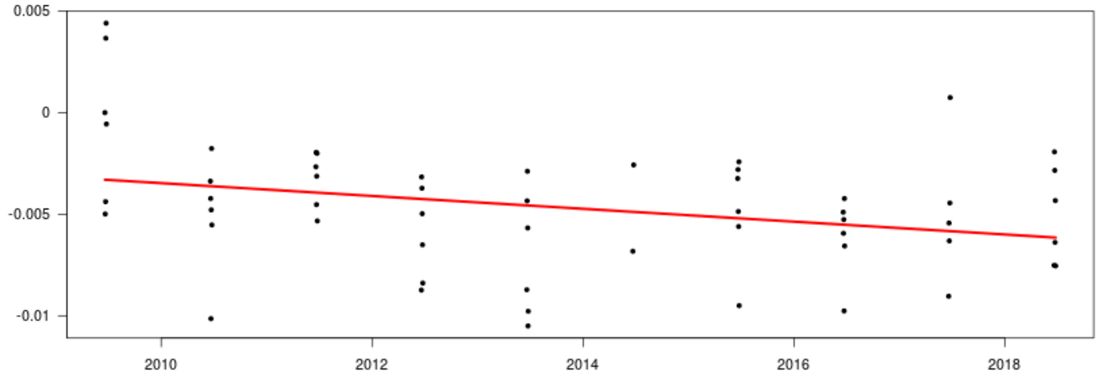

Fig. 7.15 – Up component regression line, PILA

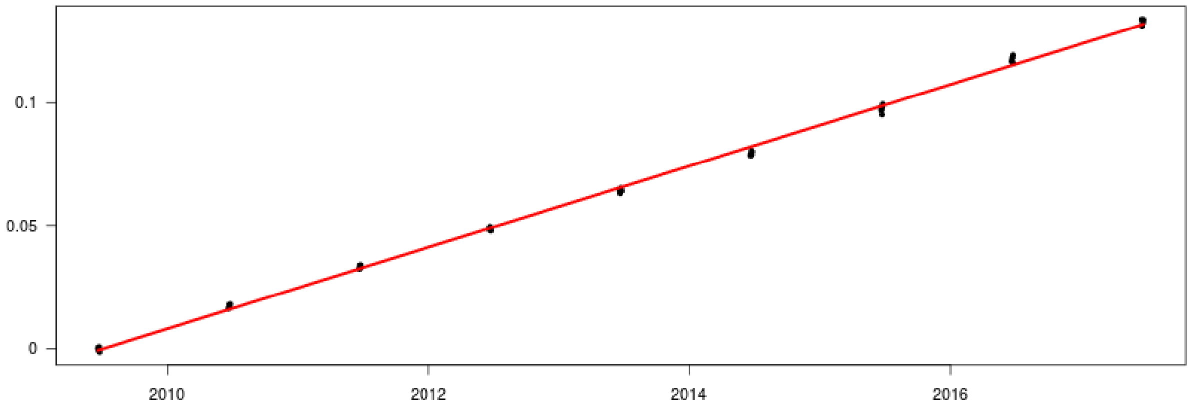

Fig. 7.16 – North component regression line, TGIL

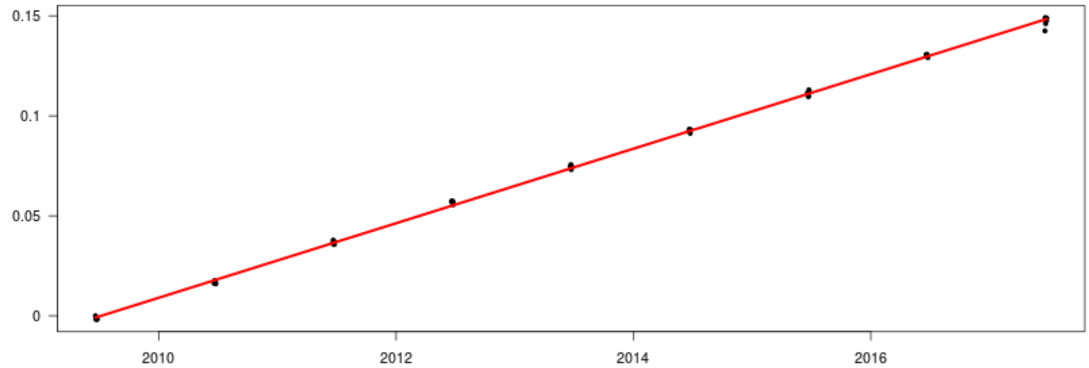

Fig. 7.17 – East component regression line, TGIL

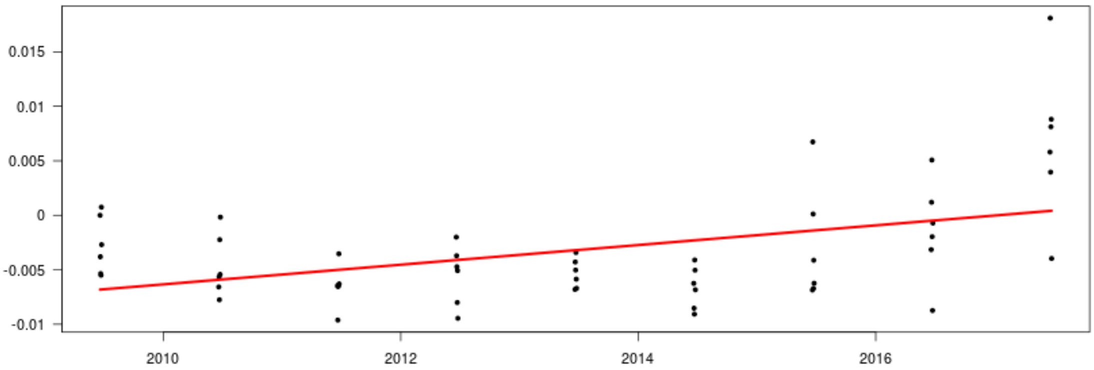

Fig. 7.18 – Up component regression line, TGIL

Table 7.1 – Absolute velocities

	Absolute velocity (mm/yr)								
Site	VE	σE	VN	σN	length	tg(VN/VE)	angle degrees	VUp	σUp
AREZ	19.10	±0.04	16.81	±0.05	25.44378	0.88010	41.35116	0.55	±0.17
NEVA	18.44	±0.06	16.22	±0.07	24.55854	0.87961	41.33517	0.67	±0.18
PALM	17.37	±0.06	15.63	±0.07	23.36694	0.89983	41.98174	0.52	±0.23
PILA	19.21	±0.05	17.87	±0.08	26.23663	0.93024	42.93034	-0.32	±0.14
TGIL	18.64	±0.07	16.55	±0.09	24.92694	0.88788	41.60109	0.90	±0.25

We have obtained absolute velocities (table 7.1) in agreement with the general movement of the area: mean of 18, 55 mm/year in East direction and 16, 62 mm/year in North direction.

In addition, we have calculated the length and the angle of the arrow for the further velocity map (fig.7.19).

$$V = \sqrt{{V_N}^2 + {V_E}^2}$$

$$\tan \alpha = \frac{V_N}{V_E}$$

$$Angle\ in\ degrees = ((\text{atan}(\tan \alpha)) \cdot 180°)/Pi$$

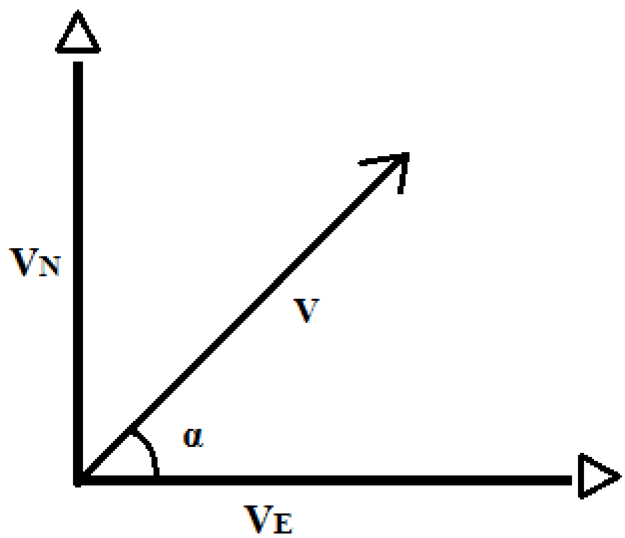

Fig. 7.19 – The directions of the vectors

7.2.1. Creation of absolute velocity map

To draw the arrows we need to convert the ITRF2014 coordinates to UTM. For his we need to transform coordinates XYZ (ITRF2014) to XYZ (ETRF2014). Than XYZ (ETRF2014) transform to Phi, Lambda, h (geographical) and finally to UTM:

1) XYZ (ITRF2014) to XYZ (ETRF2014)

On the page http://www.epncb.eu/_productsservices/coord_trans/ we convert the initial observation coordinates of the first epoch (2009.4671) (fig.7.20).

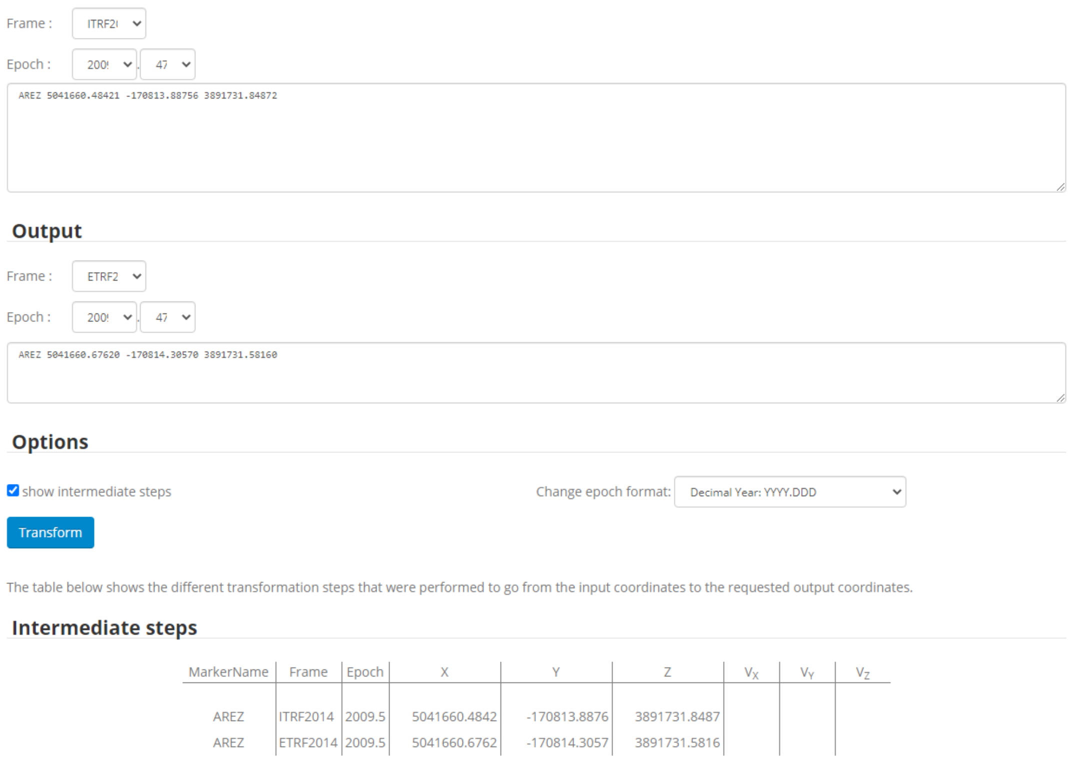

Fig. 7.20 – Transformation of the XYZ (ITRF2014) to XYZ (ETRF2014), AREZ

2) XYZ (ETRF2014) to Phi, Lambda, h (geodetic)

On the page http://earg.fcaglp.unlp.edu.ar/calc/xyz2fila.htm we convert the geocentric Cartesian coordinates to geodetic coordinates with the GRS80 ellipsoid (fig 7.21).

On the page https://www.calculadoraconversor.com/grados-a-grados-minutos-y-segundos/ we convert from fraction format to degrees.

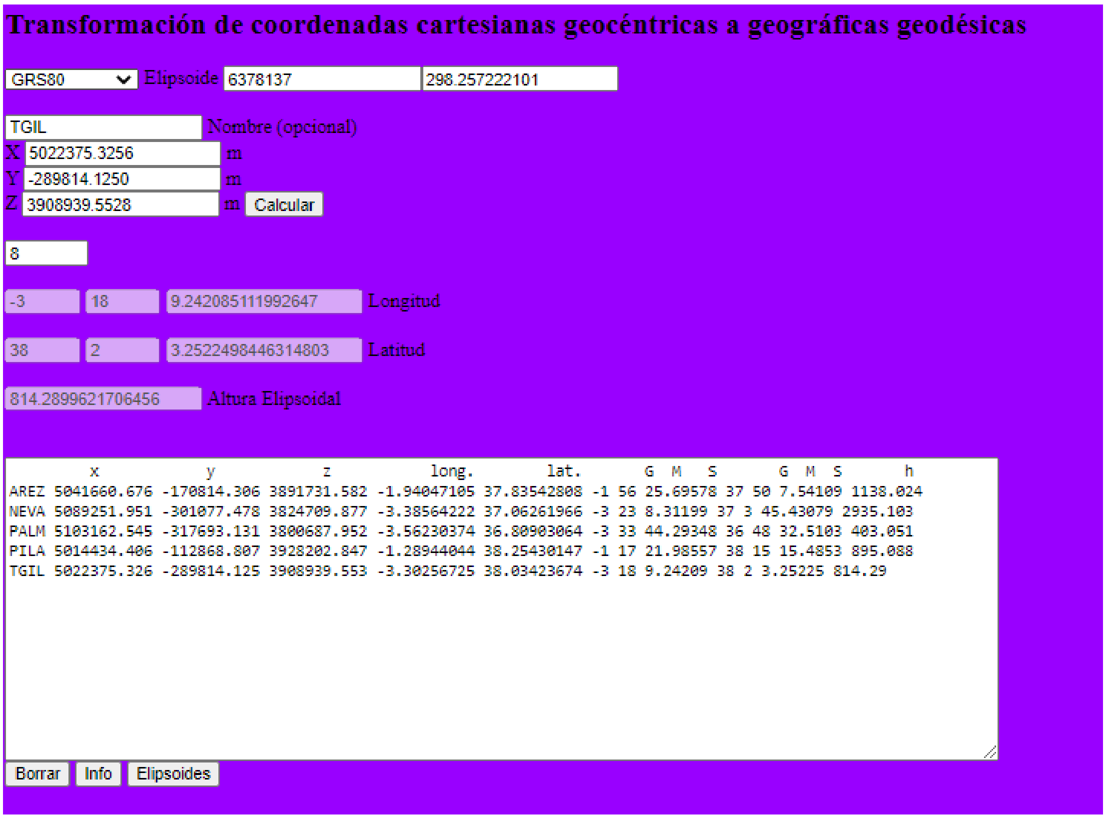

Fig. 7.21 – Transformation of the XYZ (ETRF2014) to Phi, Lambda, h (geodetic)

3) Phi, Lambda, h (geodetic) a UTM

On the page https://awsm-tools.com/geo/geographic-to-utm we convert geodetic coordinates to UTM (fig.7.22).

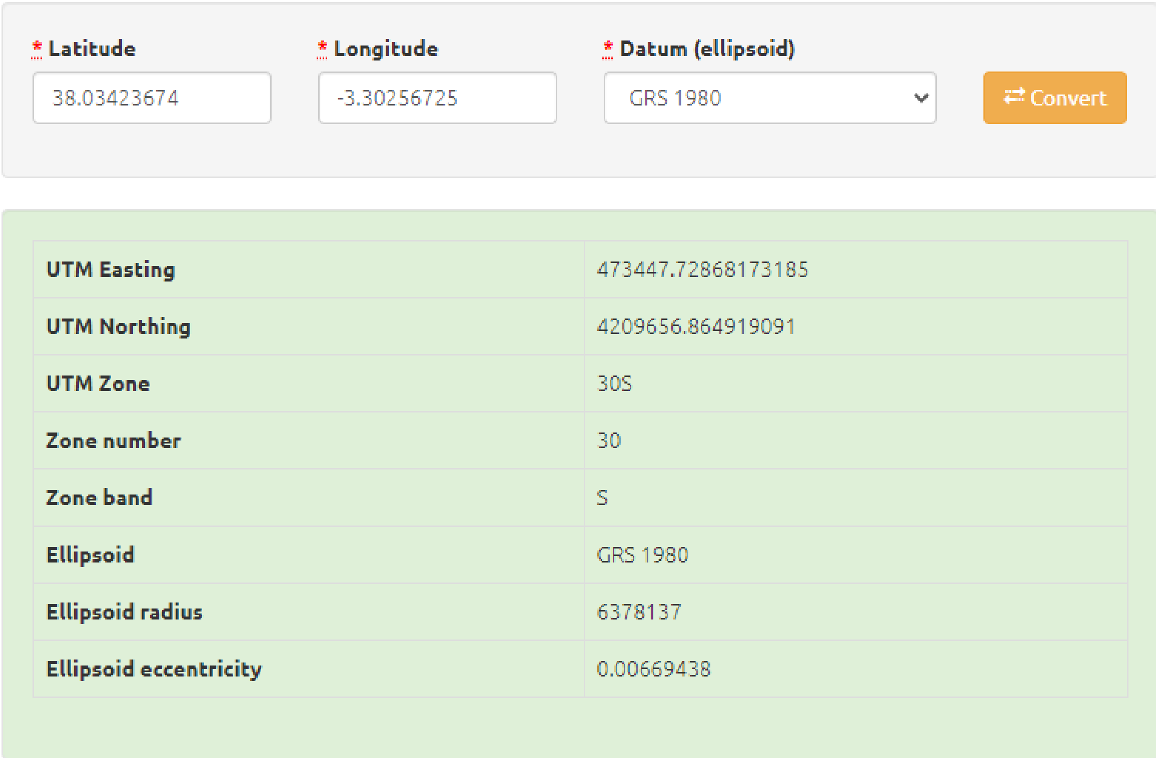

Fig. 7.22 – Transformation of Phi, Lambda (geodetic) to UTM, AREZ

The letter of the zone band is latitude band letter and shows the horizontal band, which consists the points of interest. It is used in Military Grid Reference System (MGRS).

As the result, we create the table with the transformed coordinates (table 7.2). The coordinates UTM serve as a starting point of the arrow. Using these data, length and angle calculated in the previous step we can create the velocity map (fig 7.23 and supplement 3).

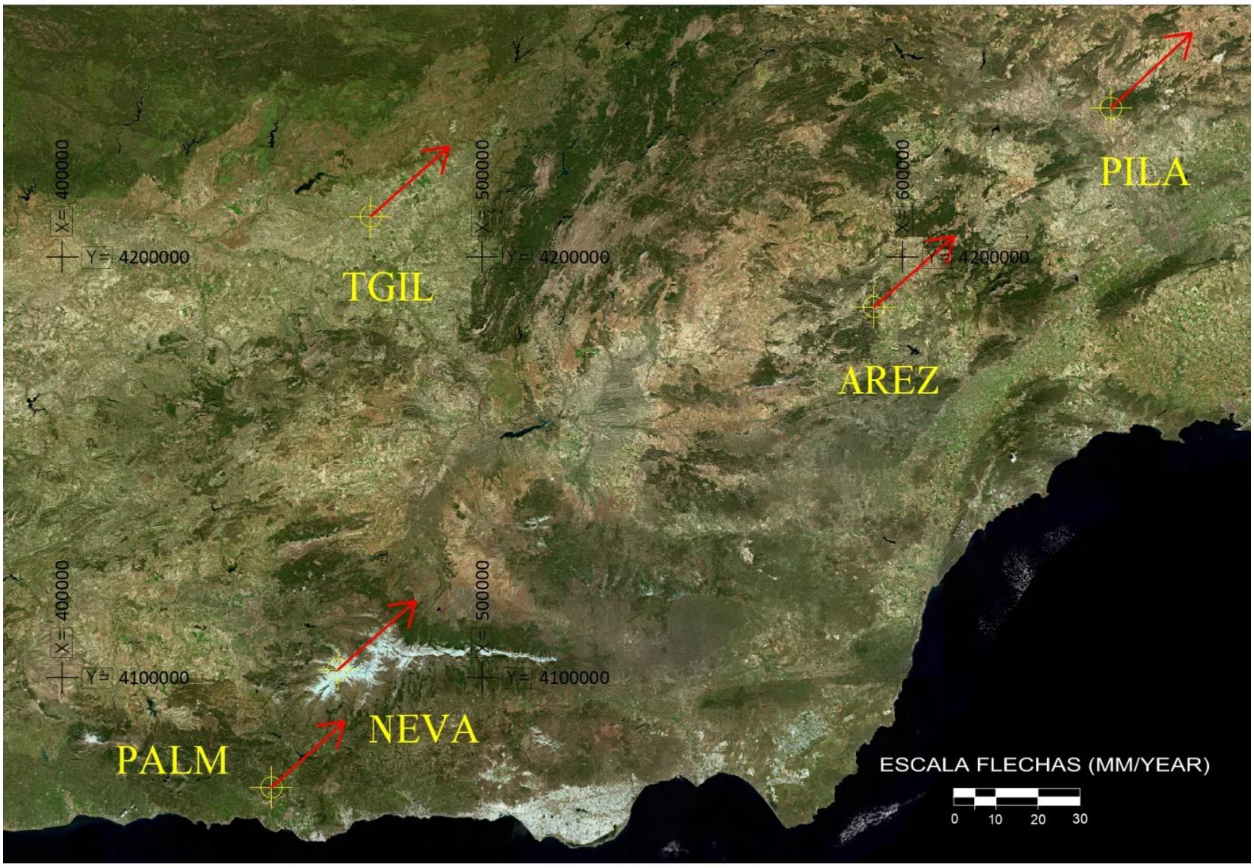

Fig. 7.23 – Absolute velocity map

Table 7.2 – Transformed coordinates

	AREZ			NEVA		
	X	Y	Z	X	Y	Z
ITRF2014	5041660.48421	-170813.88756	3891731.84872	5089251.77272	-301077.05631	3824710.14725
ETRF2014	5041660.67620	-170814.30570	3891731.58160	5089251.95130	-301077.47750	3824709.87650
	Longitude	Latitude	h	Longitude	Latitude	h
Geographical	-1.94047105	37.83542808	1138.024	-3.38564222	37.06261966	2935.103
	-1° 56' 25.69578"	37° 50' 7.54109"		-3° 23' 8.31199"	37° 3' 45.43078"	
	UTM X (Easting)	UTM Y (Northing)		UTM X (Easting)	UTM Y (Northing)	
UTM	593232.6394	4188084.4861		465715.1593	4101888.5490	

PALM			PILA			TGIL		
X	Y	Z	X	Y	Z	X	Y	Z
5103162.36926	-317692.70864	3800688.22309	5014434.20798	-112868.39112	3928203.11191	5022375.14173	-289813.70824	3908939.81991
5103162.54530	-317693.13070	3800687.95150	5014434.40640	-112868.80740	3928202.84670	5022375.32560	-289814.12500	3908939.55280
Longitude	Latitude	h	Longitude	Latitude	h	Longitude	Latitude	h
-3.56230374	36.80903064	403.051	-1.28944044	38.25430147	895.088	-3.30256725	38.03423674	814.29
-3° 33' 44.29346"	36° 48' 32.51030"		-1° 17' 21.98558"	38° 15' 15.48529"		-3° 18' 9.24210"	38° 2' 3.25226"	
UTM X (Easting)	UTM Y (Northing)		UTM X (Easting)	UTM Y (Northing)		UTM X (Easting)	JTM Y (Northing)	
449843.3515	4073835.3254		649667.7063	4235414.4248		473447.7287	4209656.8649	

7.2.2. Comparison of the calculated absolute velocity with ROA

In order to estimate the results of the calculations of the absolute velocities we compare them with the values obtained by the observations of ROA (San Fernando Naval Observatory).

During this work ROA used the program GIPSY-OASIS. The main advantage of this tool is that it uses more options of the processing, such as satellite clock corrections, atmospheric and ocean loadings and others. Moreover, the Observatory used the data of four years of the observations continues.

The comparing velocities are taken from the supplement file of the article «Topo-Iberia project: CGPS crustal velocity field in the Iberian Peninsula and Morocco» [7] (table 7.3).

Table 7.3 – Initial values of the absolute velocities

	Absolute velocity (mm/yr) ITRF 2014						ROA (GIPSY) ITRF 2008			
Site	VE	σE	VN	σN	Vup	σUp	VE	σE	VN	σN
AREZ	19.10	±0.04	16.81	±0.05	0.55	±0.17	18.45	± 0.44	16.59	± 0.33
NEVA	18.44	±0.06	16.22	±0.07	0.67	±0.18	17.98	± 0.63	15.37	± 0.79
PALM	17.37	±0.06	15.63	±0.07	0.52	±0.23	16.82	± 0.39	15.41	± 0.34
PILA	19.21	±0.05	17.87	±0.08	0.32	±0.14	18.57	± 0.39	17.37	± 0.47
TGIL	18.64	±0.07	16.55	±0.09	0.90	±0.25	18.07	± 0.40	16.10	± 0.32

The analysis of the absolute velocities is possible if bring values to a common form. Therefore, to compare velocities calculated in this thesis with the ones of ROA, we need to transform them from ITRF2014 to ITRF2008 using the formula:

$$\begin{bmatrix}\dot{X}\\ \dot{Y}\\ \dot{Z}\end{bmatrix}_{ITRFzz} = \begin{bmatrix}\dot{X}\\ \dot{Y}\\ \dot{Z}\end{bmatrix}_{ITRFyy} + \begin{bmatrix}\dot{T}_x\\ \dot{T}_y\\ \dot{T}_z\end{bmatrix} + \dot{D}\begin{bmatrix}X\\ Y\\ Z\end{bmatrix}_{ITRFyy(t)} + \begin{bmatrix}0 & -\dot{R}_z & \dot{R}_y\\ \dot{R}_z & 0 & -\dot{R}_x\\ -\dot{R}_y & \dot{R}_x & 0\end{bmatrix}\begin{bmatrix}X\\ Y\\ Z\end{bmatrix}_{ITRFyy(t)}$$

The formula above consists Cartesian component, which is necessary to obtain. To do this, we should pass from absolute velocities in local system (ENU) to the Cartesian ones (table 7.4):

$$\begin{bmatrix} V_X \\ V_Y \\ V_Z \end{bmatrix} = \begin{bmatrix} -sin\lambda & cos\lambda & 0 \\ -sin\varphi \cdot cos\lambda & -sin\varphi \cdot sin\lambda & cos\varphi \\ cos\varphi \cdot cos\lambda & cos\varphi \cdot sin\lambda & sin\varphi \end{bmatrix}^{-1} \cdot \begin{bmatrix} V_E \\ V_N \\ V_U \end{bmatrix}$$

To implement this formula, the Matlab program functionality was used by the following code:

```
Ve=18.64;
Vn=16.55;
Vu=0.90;
Venu=[Ve; Vn; Vu];
Lambda=-3.30256263;%grad
Phi=38.03423978; %grad
tregonometr=[-sind(Lambda) cosd(Lambda) 0; -sind(Phi)*cosd(Lambda) -
sind(Phi)*sind(Lambda) cosd(Phi); cosd(Phi)*cosd(Lambda)
cosd(Phi)*sind(Lambda) sind(Phi)];
Vxyz=(tregonometr^-1)*Venu
```

Table 7.4 – The result of the transformation of the ENU component to the XYZ

Absolute velocity (mm/yr) ITRF 2014			
Site	VX	VY	VZ
AREZ	-9.2244	19.4235	13.6135
NEVA	-8.1365	18.9536	13.3465
PALM	-7.8518	17.8924	12.8255
PILA	-10.3780	19.4485	14.2309
TGIL	-8.3985	19.1556	13.5900

Using the obtained Cartesian component the principal formula can be implemented. The other parameters are taken from the official page of ITRF (https://itrf.ign.fr/doc_ITRF/Transfo-ITRF2014_ITRFs.txt). In case of transforming from ITRF2014 to ITRF2008 the parameters shown in the fig. 7.24 were used.

```
Transformation parameters from ITRF2014 to past ITRFs.
-----------------------------------------------------------------------------------------
SOLUTION          Tx        Ty        Tz        D         Rx        Ry        Rz        EPOCH
UNITS----------> mm        mm        mm        ppb       .001"     .001"     .001"
                  .         .         .         .         .         .         .
        RATES     Tx        Ty        Tz        D         Rx        Ry        Rz
UNITS----------> mm/y      mm/y      mm/y      ppb/y     .001"/y   .001"/y   .001"/y
-----------------------------------------------------------------------------------------
  ITRF2008        1.6       1.9       2.4      -0.02      0.00      0.00      0.00    2010.0
       rates      0.0       0.0      -0.1       0.03      0.00      0.00      0.00
```

Fig. 7.24 – Parametres of the transformation

To simplify the calculations the following code was used:

```
vel2014=[-8.3985; 19.1556; 13.5900]; %mm/year
T=[0.0; 0.0; -0.1]; %mm/year
D=0.03*(10^-9); %ppb/y
XYZ=[5022375141.73; -289813708.24; 3908939819.91]; %mm
matriz=[0 -0.00 0.00; 0.00 0 -0.00; -0.00 0.00 0]; % rad/y
vel2008=vel2014+T+D*XYZ+matriz*XYZ
```

Table 7.5 – The result of the transformation from ITRF2014 to ITRF2008 (Cartesian component)

Absolute velocity (mm/yr) ITRF 2008			
Site	VX	VY	VZ
AREZ	-9.0732	19.4184	13.6303
NEVA	-7.9838	18.9446	13.3612
PALM	-7.6987	17.8829	12.8395
PILA	-10.2276	19.4451	14.2487
TGIL	-8.2478	19.1469	13.6073

Now, having the result, it is important to return to the local coordinate component, using the following formula and Matlab code:

$$\begin{bmatrix} V_E \\ V_N \\ V_U \end{bmatrix} = \begin{bmatrix} -sin\lambda & cos\lambda & 0 \\ -sin\varphi \cdot cos\lambda & -sin\varphi \cdot sin\lambda & cos\varphi \\ cos\varphi \cdot cos\lambda & cos\varphi \cdot sin\lambda & sin\varphi \end{bmatrix} \cdot \begin{bmatrix} V_X \\ V_Y \\ V_Z \end{bmatrix}$$

```
Vx=-8.3983;
Vy=19.1556;
Vz=13.4901;
Vxyz=[Vx; Vy; Vz];
Lambda=-3.30256263;%grad
Phi=38.03423978; %grad
tregonometr=[-sind(Lambda) cosd(Lambda) 0; -sind(Phi)*cosd(Lambda) -
sind(Phi)*sind(Lambda)       cosd(Phi);       cosd(Phi)*cosd(Lambda)
cosd(Phi)*sind(Lambda) sind(Phi)];
Venu=tregonometr*Vxyz
```

Table 7.6 – The result of the transformation from ITRF2014 to ITRF2008 (ENU component)

Absolute velocity (mm/yr) ITRF 2008			
Site	VE	VN	Vup
AREZ	19.1000	16.7305	0.6798
NEVA	18.4400	16.1395	0.8009
PALM	17.3700	15.5493	0.6512
PILA	19.2100	17.7909	0.4491
TGIL	18.6400	16.4706	1.0296

After the steps of transformations and calculations, we obtain the table 7.7 with the comparable absolute velocities.

As we can see, the values are vary within one millimeter per year in the component East and North. The parameter of the altitude is not included to the observations. Therefore, the result of the nine years of the observations (thesis) and the four-year observations (ROA) do not vary significantly. That could mean that the absolute velocity of the movement of the basis is stable and has persistent direction.

In order to represent the similarity of the results, the absolute velocity map which compare the vectors obtained in this thesis and in ROA was prepared (fig. 7.25 and supplement 3)

Table 7.7 – The table of the comparison

ROA (GIPSY) ITRF 2008							
Site	VE	σE	VN	σN	length	tg(VN/VE)	angle degrees
AREZ	18.45	± 0.44	16.59	± 0.33	24.81190	0.89919	41.96147
NEVA	17.98	± 0.63	15.37	± 0.79	23.65412	0.85484	40.52510
PALM	16.82	± 0.39	15.41	± 0.34	22.81185	0.91617	42.49502
PILA	18.57	± 0.39	17.37	± 0.47	25.42758	0.93538	43.08766
TGIL	18.07	± 0.40	16.10	± 0.32	24.20196	0.89098	41.70038

Absolute velocity (mm/yr) ITRF 2008						
Site	VE	VN	Vup	length	tg(VN/VE)	angle degrees
AREZ	19.1000	16.7305	0.6798	25.39133	0.87594	41.21649
NEVA	18.4400	16.1395	0.8009	24.50545	0.87524	41.19384
PALM	17.3700	15.5493	0.6512	23.31304	0.89518	41.83431
PILA	19.2100	17.7909	0.4491	26.18282	0.92613	42.80360
TGIL	18.6400	16.4706	1.0296	24.87429	0.88362	41.46433

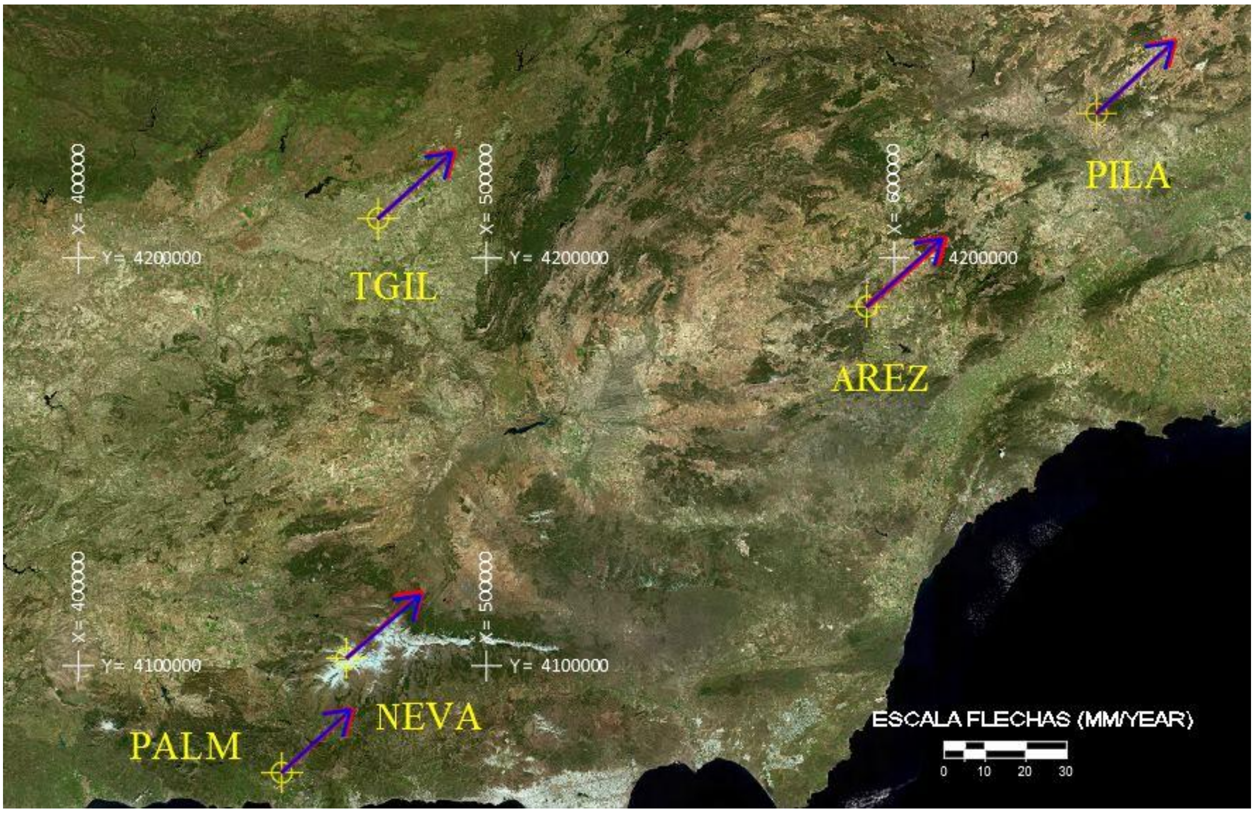

Fig. 7.25 – Comparison of the absolute velocity vectors

(red – thesis, blue – ROA)

7.3. Residual velocity estimation

Residual velocity is calculated using absolute velocity vector in Local system, which do not consist movement of Eurasia. That is to say, the Eurasian plate is fixed relatively to our field of study.

The formula to calculate this is following:

$$\begin{bmatrix} V_{Er} \\ V_{Nr} \\ V_{Nr} \end{bmatrix} = \begin{bmatrix} V_{Ea} \\ V_{Na} \\ V_{Na} \end{bmatrix} - \begin{bmatrix} -sin\lambda & -cos\lambda & 0 \\ -sin\varphi \cdot cos\lambda & -sin\varphi \cdot sin\lambda & cos\varphi \\ cos\varphi \cdot cos\lambda & cos\varphi \cdot sin\lambda & sin\varphi \end{bmatrix} \begin{bmatrix} 0 & Z & -Y \\ -Z & 0 & X \\ Y & -X & 0 \end{bmatrix} \begin{bmatrix} \omega_X \\ \omega_Y \\ \omega_Z \end{bmatrix}$$

$\begin{bmatrix} V_{Ea} \\ V_{Na} \\ V_{Na} \end{bmatrix}$ – Absolute velocities vector;

$\begin{bmatrix} 0 & Z & -Y \\ -Z & 0 & X \\ Y & -X & 0 \end{bmatrix}$ – Coordinates of the corresponding station;

$\begin{bmatrix} \omega_X \\ \omega_Y \\ \omega_Z \end{bmatrix}$ – Vector angular velocity of the Eurasian plate (ITRF2014 materialization);

ω_X =-4.12091628E-10 (rad/yr);

ω_Y =-2.5743606408E-9 (rad/yr);

ω_Z =3.733065336E-9 (rad/yr);

φ, λ – Longitude and latitude of the corresponding station (geographical coordinates).

To realize this formula, the Code 15 was written. The results of calculation are represented in the table 7.7.

Table 7.7 – Residual velocities

	Residual velocity (mm/yr)						
Site	VrE	VrN	VrUp	length (mm/yr)	tg	angle degrees	angle degrees+180
AREZ	-1.00	0.33	0.50	1.0480	-0.3302	-18.27244	161.72756
NEVA	-1.58	-0.31	0.62	1.6144	0.1981	11.20483	191.20483
PALM	-2.67	-0.90	0.47	2.8208	0.3376	18.65719	198.65719
PILA	-0.90	1.41	-0.37	1.6789	-1.5630	-57.38904	122.61096
TGIL	-1.17	0.03	0.85	1.1688	-0.0215	-1.23055	178.76945

We have obtained residual velocity field with values ranging from 1,05 to 2,82 mm/year according to the formula:

$$V = \sqrt{{V_{rN}}^2 + {V_{rE}}^2}$$

In addition, we have calculated the angle of the arrow for the further velocity map.

$$\tan \alpha = \frac{V_{rN}}{V_{rE}}$$

$$Angle\ in\ degrees = ((\mathrm{atan}(\tan \alpha)) \cdot 180°)/Pi$$

The coordinates UTM serve as a starting point of the arrow. Using these data, length and angle calculated in the previous step we can create the velocity map (fig 7.26 and supplement 3).

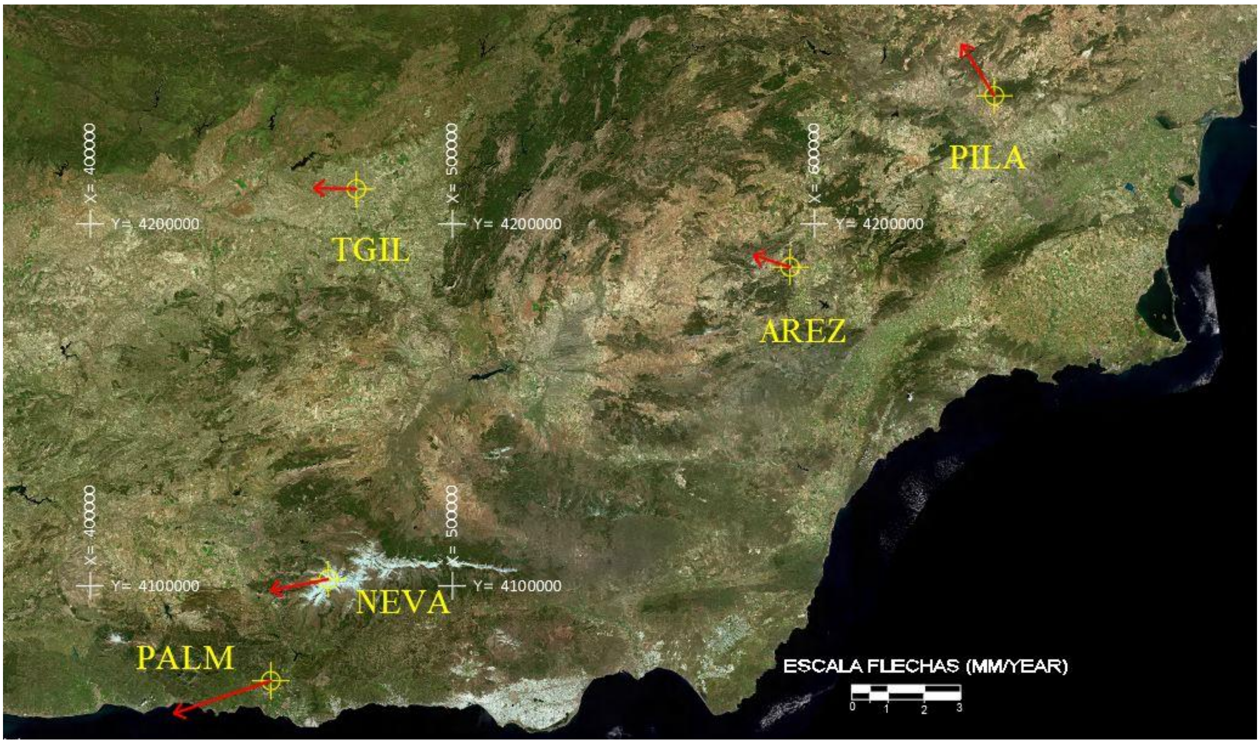

Fig. 7.26 – Residual velocity map

8. CONCLUSIONS

In the course of the master's thesis, in order to achieve the main goal, certain calculations were made for information processing, questions of geography, geology and terrain were studied. The similarities and differences between distinct reference systems, coordinate systems and reference frames were also analyzed and described.

First, an analysis of the terrain, its geology and relief was carried out. The reasons for the study in this area were identified and its significance was indicated.

In this work, various reference and reference systems were used. Therefore, part of the diploma is devoted to the analysis of the features of such reference systems, ITRS, ETRS89, GRS80, WGS84. We also paid attention to such reference frames as ITRF and ETRF, learned the difference between geodetic and Cartesian coordinate systems.

Since the satellite method was used to obtain the data, most of the work is devoted to the study of GNSS methods, the difference between the absolute and differential methods of obtaining data, code and phase methods, static and kinematic. A separate chapter talks about the PPP method that was used to process the data.

Data processing was performed on the online platform APPS (Automatic Precise Positioning Service). The obtained coordinates were transformed into local ones for further velocity analysis.

Thus, having the necessary coordinates, the analysis of the absolute and residual velocities was performed. The results were presented in the form of maps and tables. The velocity fields were compared with the results of the research of the past years.

The main aim of the work was to make the analysis and the estimation of the velocity field. The steps briefly described above gained it. In order to figure out if the obtained results were satisfactory, they were compared with the data of ROA

(San Fernando Naval Observatory). ROA possess the values of velocity field, which was calculated on the base of four-years continuous observations, while the data analyzed in this thesis is discontinues during ten years.

First, to accomplish the comparison with ROA, the results were transformed to the common format, ITRF2008. The same level of the data make possible their matching.

It was figured out that the values of the velocity field calculated by ROA are very similar to the meaning of the ones in this thesis. It could signify that the computation was held correctly and the movement of the stations and its speed are stable.

It can be seen that the vectors both of ROA and thesis are almost merge by analyzing the cartographic material. The direction of the vectors is correct according to the sign of the East and North values of the velocity fields.

Thus, we can make a conclusion that the final results are passable and indicate on the continues movement of the fixed bases.

BIBLIOGRAPHY

1. ITRF2014 [Electronic resource]. – Access mode: http://itrf.ensg.ign.fr/ITRF_solutions/2014/ITRF2014.php

2. Geology and tectonics of the Baetic System [Electronic resource]. – Access mode: https://www.ign.es/web/resources/sismologia/tproximos/sismotectonica/pag_sismotectonicas/beticas_en.html

3. Cordillera Bética [Electronic resource]. – Access mode: http://www.geodiversidad.es/geologia-de-iberia/alpino/cordillera-betica

4. Alvaro Santamaría-Gómez «SARI: interactive GNSS position time series analysis software» [Electronic resource]. – Access mode: https://doi.org/10.1007/s10291-019-0846-y

5. A.J. Gil, A. Sánchez-Alzola, J. Galindo-Zaldívar, M.J. Borque, M.C. Lacy, M. Avilés, P. Alfaro, A.C. López Garrido, C. Sanz de Galdeano, A. Herrera, F. Chacón, M. Madrigal, S. Blanca, J.C. Moreno, V. Tendero: Estimation of the crustal velocity field in the Balanegra fault from GPS position time series in 2006 – 2018

6. GipsyX [Electronic resource]. – Access mode: https://gipsy-oasis.jpl.nasa.gov/

7. J. Garate, J. Martin-Davila, G. Khazaradze, A. Echeverria, E. Asensio, A. J. Gil, M. C. de Lacy, J. A. Armenteros, A. M. Ruiz, J. Gallastegui, F. Alvarez-Lobato, C. Ayala, G. Rodrı´guez-Caderot, J. Galindo-Zaldı´var, A. Rimi, M. Harnafi: Topo-Iberia project: CGPS crustal velocity field in the Iberian Peninsula and Morocco

Online platforms used:

1. APPS server: https://apps.gdgps.net/
2. SARI program: https://alvarosg.shinyapps.io/sari/

SUPPLEMENT 1

PROCESSED COORDINATES XYZ AND NEU

Station AREZ

Year, month	Day	X, m	Y, m	Z, m	North, m	East, m	Height, m	Year fraction
2009, June	20	5041660.48421	-170813.88756	3891731.84872	0.00000	0.00000	0.00000	2009.4671
	21	5041660.48596	-170813.88926	3891731.85100	0.00069	-0.00163	0.00282	2009.4699
	22	5041660.48255	-170813.88907	3891731.84528	-0.00173	-0.00156	-3.37936	2009.4726
	23	5041660.49324	-170813.89139	3891731.85538	-0.00035	-0.00352	0.01131	2009.4753
	24	5041660.47920	-170813.89079	3891731.84408	-0.00066	-0.00339	-6.72289	2009.4781
	25	5041660.48850	-170813.88967	3891731.84819	-0.00309	-0.00196	0.00311	2009.4808
2010, June	20	5041660.47229	-170813.87092	3891731.85948	0.01615	0.01623	-3.25745	2010.4671
	21	5041660.46903	-170813.87058	3891731.85764	0.01670	0.01646	-6.97320	2010.4699
	22	5041660.46444	-170813.87004	3891731.85414	0.01676	0.01685	-1.27498	2010.4726
	23	5041660.46989	-170813.87141	3891731.85773	0.01623	0.01566	-6.21085	2010.4753
	24	5041660.47014	-170813.87077	3891731.85950	0.01749	0.01631	-4.94785	2010.4781
	25	5041660.47099	-170813.87175	3891731.85909	0.01662	0.01536	-4.50249	2010.4808
2011, June	20	5041660.46810	-170813.85242	3891731.87727	0.03315	0.03458	0.00386	2011.4671
	21	5041660.46390	-170813.85195	3891731.87326	0.03257	0.03491	-1.93985	2011.4699
	22	5041660.46631	-170813.85224	3891731.87799	0.03482	0.03469	0.00288	2011.4726
	23	5041660.46545	-170813.85160	3891731.87619	0.03395	0.03531	0.00108	2011.4753
	24	5041660.46358	-170813.85045	3891731.87507	0.03423	0.03639	-1.11448	2011.4781
	25	5041660.46126	-170813.85184	3891731.87321	0.03415	0.03492	-4.05743	2011.4808

Year, month	Day	X, m	Y, m	Z, m	North, m	East, m	Height, m	Year fraction
2012, June	20	5041660.45406	-170813.83249	3891731.88788	0.05056	0.05402	-1.24936	2012.4671
	21	5041660.45845	-170813.83200	3891731.89009	0.04962	0.05465	0.00355	2012.4699
	22	5041660.45153	-170813.83043	3891731.88614	0.05077	0.05599	-4.37694	2012.4726
	23	5041660.45328	-170813.83091	3891731.88631	0.04982	0.05557	-2.87612	2012.4753
	24	5041660.44830	-170813.83068	3891731.88233	0.04974	0.05563	-9.24825	2012.4781
	25	5041660.45263	-170813.83168	3891731.88528	0.04939	0.05479	-3.99827	2012.4808
2013, June	20	5041660.44406	-170813.81144	3891731.89870	0.06567	0.07472	-3.07014	2013.4671
	21	5041660.44272	-170813.81268	3891731.89746	0.06548	0.07343	-4.86167	2013.4699
	22	5041660.44512	-170813.81215	3891731.89985	0.06591	0.07405	-1.51436	2013.4726
	23	5041660.44451	-170813.81321	3891731.90018	0.06652	0.07296	-1.76164	2013.4753
	24	5041660.44277	-170813.81305	3891731.89704	0.06512	0.07306	-5.07078	2013.4781
	25	5041660.44448	-170813.81342	3891731.89915	0.06572	0.07275	-2.41902	2013.4808
2014, June	20	5041660.43682	-170813.79465	3891731.91238	0.08126	0.09126	-8.41692	2014.4671
	21	5041660.43618	-170813.79280	3891731.91346	0.08254	0.09308	-7.34820	2014.4699
	22	5041660.43518	-170813.79358	3891731.91397	0.08354	0.09227	-1.19111	2014.4726
	23	5041660.43311	-170813.79300	3891731.91355	0.08449	0.09278	-3.09696	2014.4753
	24	5041660.43645	-170813.79383	3891731.91271	0.08176	0.09206	-9.58181	2014.4781
	25	5041660.43560	-170813.79308	3891731.91304	0.08256	0.09278	-1.44617	2014.4808
2015, June	20	5041660.42600	-170813.77358	3891731.92783	0.10053	0.11195	-4.71947	2015.4671
	21	5041660.42773	-170813.77415	3891731.92870	0.10015	0.11144	0.00145	2015.4699
	22	5041660.42491	-170813.77427	3891731.92651	0.10014	0.11122	-2.12913	2015.4726
	23	5041660.43054	-170813.77481	3891731.92691	0.09700	0.11088	0.00258	2015.4753
	24	5041660.42719	-170813.77266	3891731.92659	0.09884	0.11291	-3.22019	2015.4781
	25	5041660.42107	-170813.77280	3891731.92557	0.10179	0.11256	-5.76840	2015.4808

Year, month	Day	X, m	Y, m	Z, m	North, m	East, m	Height, m	Year fraction
2016, June	20	5041660.41783	-170813.75331	3891731.94257	0.11760	0.13193	0.00158	2016.4671
	21	5041660.41673	-170813.75381	3891731.94231	0.11806	0.13139	0.00056	2016.4699
	22	5041660.41602	-170813.75246	3891731.94315	0.11919	0.13272	0.00048	2016.4726
	23	5041660.41688	-170813.75375	3891731.94398	0.11929	0.13146	0.00171	2016.4753
	24	5041660.41726	-170813.75574	3891731.94383	0.11890	0.12948	0.00196	2016.4781
	25	5041660.41873	-170813.75460	3891731.94219	0.11672	0.13067	0.00209	2016.4808
2017, June	20	5041660.40830	-170813.73483	3891731.95421	0.13302	0.15007	0.00070	2017.4671
	21	5041660.41386	-170813.73364	3891731.95822	0.13281	0.15145	0.00752	2017.4699
	22	5041660.40721	-170813.73245	3891731.95480	0.13421	0.15242	0.00014	2017.4726
	23	5041660.41029	-170813.73421	3891731.95652	0.13364	0.15076	0.00367	2017.4753
	24	5041660.40902	-170813.73442	3891731.95708	0.13486	0.15051	0.00302	2017.4781
	25	5041660.41107	-170813.73533	3891731.95892	0.13504	0.14967	0.00579	2017.4808
2018, June	20	5041660.39937	-170813.71569	3891731.96653	0.14863	0.16890	0.00070	2018.4671
	21	5041660.39882	-170813.71433	3891731.96773	0.14993	0.17024	0.00096	2018.4699
	22	5041660.39781	-170813.71568	3891731.96874	0.15133	0.16886	0.00082	2018.4726
	23	5041660.39998	-170813.71615	3891731.96796	0.14937	0.16847	0.00206	2018.4753
	24	5041660.39789	-170813.71461	3891731.97036	0.15258	0.16993	0.00185	2018.4781
	25	5041660.40032	-170813.71722	3891731.97213	0.15243	0.16740	0.00492	2018.4808

Station NEVA

Year, month	Day	X, m	Y, m	Z, m	North, m	East, m	Height, m	Year fraction
2009, June	20	5089251.77272	-301077.05631	3824710.14725	0.00000	0.00000	0.00000	2009.4671
	21	5089251.77528	-301077.05736	3824710.14775	-0.00118	-0.00089	0.00239	2009.4699
	22	5089251.76741	-301077.05631	3824710.13929	-0.00315	-0.00032	-0.00903	2009.4726
	23	5089251.77839	-301077.06032	3824710.14833	-0.00269	-0.00367	0.00536	2009.4753
	24	5089251.77099	-301077.05652	3824710.14248	-0.00277	-0.00031	-0.00425	2009.4781
	25	5089251.77232	-301077.05718	3824710.14010	-0.00550	-0.00090	-0.00459	2009.4808
2010, June	20	5089251.75923	-301077.04026	3824710.15423	0.01426	0.01522	-0.00730	2010.4671
	21	5089251.75651	-301077.03951	3824710.15309	0.01502	0.01582	-0.01018	2010.4699
	22	5089251.75645	-301077.03868	3824710.15305	0.01504	0.01664	-0.01029	2010.4726
	23	5089251.75778	-301077.04069	3824710.15264	0.01384	0.01471	-0.00939	2010.4753
	24	5089251.75719	-301077.03774	3824710.15111	0.01309	0.01762	-0.01092	2010.4781
	25	5089251.76067	-301077.04206	3824710.15711	0.01563	0.01351	-0.00433	2010.4808
2011, June	20	5089251.75044	-301077.02151	3824710.16449	0.02840	0.03342	-0.00900	2011.4671
	21	5089251.75167	-301077.02009	3824710.16512	0.02822	0.03491	-0.00770	2011.4699
	22	5089251.74848	-301077.01940	3824710.16729	0.03189	0.03541	-0.00897	2011.4726
	23	5089251.74899	-301077.01898	3824710.16383	0.02884	0.03587	-0.01067	2011.4753
	24	5089251.75295	-301077.01891	3824710.16682	0.02884	0.03616	-0.00572	2011.4781
	25	5089251.74846	-301077.02010	3824710.16554	0.03049	0.03471	-0.01001	2011.4808

Year, month	Day	X, m	Y, m	Z, m	North, m	East, m	Height, m	Year fraction
2012, June	20	5089251.74321	-301076.99888	3824710.17991	0.04586	0.05559	-0.00654	2012.4671
	21	5089251.74520	-301077.00011	3824710.18092	0.04543	0.05448	-0.00428	2012.4699
	22	5089251.74159	-301076.99785	3824710.17968	0.04669	0.05652	-0.00800	2012.4726
	23	5089251.73837	-301076.99749	3824710.17684	0.04637	0.05668	-0.01230	2012.4753
	24	5089251.73912	-301076.99951	3824710.17708	0.04605	0.05472	-0.01147	2012.4781
	25	5089251.73999	-301076.99919	3824710.17609	0.04474	0.05509	-0.01138	2012.4808
2013, June	20	5089251.73649	-301076.98033	3824710.19146	0.05978	0.07370	-0.00579	2013.4671
	21	5089251.73605	-301076.98144	3824710.19194	0.06039	0.07257	-0.00580	2013.4699
	22	5089251.73649	-301076.97943	3824710.19387	0.06174	0.07461	-0.00439	2013.4726
	23	5089251.73612	-301076.98197	3824710.19292	0.06112	0.07205	-0.00513	2013.4753
	24	5089251.73650	-301076.98169	3824710.19265	0.06068	0.07235	-0.00501	2013.4781
	25	5089251.73279	-301076.98137	3824710.19132	0.06186	0.07245	-0.00878	2013.4808
2014, June	20	5089251.72969	-301076.96529	3824710.20439	0.07473	0.08832	-0.00413	2014.4671
	21	5089251.72836	-301076.96183	3824710.20409	0.07541	0.09170	-0.00554	2014.4699
	22	5089251.72677	-301076.96174	3824710.20459	0.07677	0.09169	-0.00651	2014.4726
	23	5089251.72755	-301076.96286	3824710.20594	0.07734	0.09062	-0.00501	2014.4753
	24	5089251.72831	-301076.96443	3824710.20532	0.07633	0.08909	-0.00470	2014.4781
	25	5089251.72774	-301076.96222	3824710.20497	0.07647	0.09127	-0.00548	2014.4808
2015, June	20	5089251.72125	-301076.94514	3824710.22333	0.09564	0.10794	-0.00039	2015.4671
	21	5089251.71847	-301076.94497	3824710.22139	0.09577	0.10795	-0.00377	2015.4699
	22	5089251.71373	-301076.94541	3824710.22017	0.09763	0.10722	-0.00827	2015.4726
	23	5089251.71933	-301076.94554	3824710.21670	0.09149	0.10742	-0.00589	2015.4753
	24	5089251.71587	-301076.94312	3824710.21709	0.09397	0.10963	-0.00853	2015.4781
	25	5089251.71080	-301076.94244	3824710.21539	0.09568	0.11002	-0.01363	2015.4808

Year, month	Day	X, m	Y, m	Z, m	North, m	East, m	Height, m	Year fraction
2016, June	20	5089251.71233	-301076.92413	3824710.23435	0.11054	0.12838	-0.00184	2016.4671
	21	5089251.71448	-301076.92357	3824710.23763	0.11189	0.12907	0.00182	2016.4699
	22	5089251.71388	-301076.92358	3824710.23832	0.11280	0.12903	0.00176	2016.4726
	23	5089251.71131	-301076.92353	3824710.23698	0.11328	0.12892	-0.00110	2016.4753
	24	5089251.71017	-301076.92585	3824710.23549	0.11270	0.12653	-0.00280	2016.4781
	25	5089251.71089	-301076.92387	3824710.23422	0.11131	0.12855	-0.00308	2016.4808
2017, June	20	5089251.70738	-301076.90584	3824710.24991	0.12659	0.14635	0.00273	2017.4671
	21	5089251.70615	-301076.90615	3824710.24984	0.12726	0.14596	0.00172	2017.4699
	22	5089251.70146	-301076.90524	3824710.24634	0.12733	0.14659	-0.00416	2017.4726
	23	5089251.70280	-301076.90474	3824710.24753	0.12749	0.14718	-0.00241	2017.4753
	24	5089251.70560	-301076.90806	3824710.25335	0.13033	0.14403	0.00349	2017.4781
	25	5089251.69998	-301076.90717	3824710.24727	0.12889	0.14458	-0.00469	2017.4808
2018, June	20	5089251.69380	-301076.88583	3824710.25706	0.14118	0.16552	-0.00471	2018.4671
	21	5089251.69371	-301076.88674	3824710.25882	0.14260	0.16461	-0.00369	2018.4699
	22	5089251.69669	-301076.88689	3824710.26163	0.14304	0.16464	0.00039	2018.4726
	23	5089251.69979	-301076.88755	3824710.26163	0.14116	0.16416	0.00288	2018.4753
	24	5089251.69428	-301076.88744	3824710.26201	0.14478	0.16395	-0.00128	2018.4781
	25	5089251.69719	-301076.88812	3824710.26199	0.14299	0.16343	0.00106	2018.4808

Station PALM

Year, month	Day	X, m	Y, m	Z, m	North, m	East, m	Height, m	Year fraction
2009, June	20	5103162.36926	-317692.70864	3800688.22309	0.00000	0.00000	0.00000	2009.4671
	21	5103162.36825	-317692.71024	3800688.22341	0.00081	-0.00166	-0.00054	2009.4699
	22	5103162.36946	-317692.70877	3800688.22289	-0.00028	-0.00012	0.00005	2009.4726
	23	5103162.37327	-317692.71094	3800688.22306	-0.00250	-0.00205	0.00330	2009.4753
	24	5103162.37146	-317692.71042	3800688.21997	-0.00388	-0.00164	-0.00002	2009.4781
	25	5103162.37703	-317692.70901	3800688.22543	-0.00278	0.00011	0.00763	2009.4808
2010, June	20	5103162.36121	-317692.69231	3800688.23524	0.01515	0.01580	0.00004	2010.4671
	21	5103162.35681	-317692.69139	3800688.23293	0.01597	0.01644	-0.00491	2010.4699
	22	5103162.35459	-317692.69200	3800688.23043	0.01527	0.01570	-0.00815	2010.4726
	23	5103162.35472	-317692.69344	3800688.23037	0.01509	0.01426	-0.00801	2010.4753
	24	5103162.36072	-317692.69324	3800688.23403	0.01444	0.01484	-0.00104	2010.4781
	25	5103162.35540	-317692.69485	3800688.23165	0.01566	0.01290	-0.00664	2010.4808
2011, June	20	5103162.35008	-317692.67361	3800688.24386	0.02941	0.03377	-0.00462	2011.4671
	21	5103162.35700	-317692.67309	3800688.24772	0.02838	0.03472	0.00319	2011.4699
	22	5103162.34639	-317692.67263	3800688.24207	0.03021	0.03452	-0.00870	2011.4726
	23	5103162.34801	-317692.67618	3800688.23680	0.02489	0.03108	-0.01038	2011.4753
	24	5103162.35292	-317692.67153	3800688.24785	0.03098	0.03602	-0.00007	2011.4781
	25	5103162.34821	-317692.67464	3800688.24406	0.03065	0.03263	-0.00595	2011.4808

Year, month	Day	X, m	Y, m	Z, m	North, m	East, m	Height, m	Year fraction
2012, June	20	5103162.34730	-317692.65522	3800688.25999	0.04466	0.05196	0.00190	2012.4671
	21	5103162.34335	-317692.65605	3800688.25805	0.04544	0.05088	-0.00238	2012.4699
	22	5103162.34487	-317692.65400	3800688.25797	0.04455	0.05302	-0.00131	2012.4726
	23	5103162.33991	-317692.65487	3800688.25576	0.04572	0.05184	-0.00655	2012.4753
	24	5103162.34244	-317692.65633	3800688.25660	0.04482	0.05054	-0.00396	2012.4781
	25	5103162.34277	-317692.65541	3800688.25699	0.04496	0.05148	-0.00350	2012.4808
2013, June	20	5103162.33688	-317692.63745	3800688.26995	0.05954	0.06904	-0.00134	2013.4671
	21	5103162.33625	-317692.63756	3800688.26924	0.05933	0.06890	-0.00226	2013.4699
	22	5103162.33732	-317692.63738	3800688.27285	0.06160	0.06914	0.00075	2013.4726
	23	5103162.33696	-317692.63979	3800688.27153	0.06067	0.06671	-0.00021	2013.4753
	24	5103162.33531	-317692.63838	3800688.26928	0.05990	0.06802	-0.00295	2013.4781
	25	5103162.33038	-317692.63812	3800688.26708	0.06110	0.06797	-0.00822	2013.4808
2014, June	20	5103162.33215	-317692.62124	3800688.28425	0.07442	0.08493	0.00264	2014.4671
	21	5103162.32812	-317692.62064	3800688.28084	0.07412	0.08528	-0.00265	2014.4699
	22	5103162.34561	-317692.61896	3800688.29291	0.07338	0.08803	0.01847	2014.4726
	23	5103162.32958	-317692.62060	3800688.28314	0.07509	0.08540	-0.00011	2014.4753
	24	5103162.32395	-317692.61987	3800688.28046	0.07634	0.08578	-0.00625	2014.4781
	25	5103162.33222	-317692.62129	3800688.28570	0.07553	0.08488	0.00357	2014.4808

Year, month	Day	X, m	Y, m	Z, m	North, m	East, m	Height, m	Year fraction
2015, June	20	5103162.31935	-317692.60332	3800688.29699	0.09294	0.10202	-0.00084	2015.4671
	21	5103162.32258	-317692.60187	3800688.29835	0.09215	0.10367	0.00248	2015.4699
	22	5103162.32047	-317692.60342	3800688.29638	0.09177	0.10198	-0.00030	2015.4726
	23	5103162.32561	-317692.60047	3800688.29724	0.08950	0.10525	0.00417	2015.4753
	24	5103162.31711	-317692.59944	3800688.29365	0.09175	0.10575	-0.00483	2015.4781
	25	5103162.31502	-317692.60248	3800688.29401	0.09317	0.10258	-0.00614	2015.4808
2016, June	20	5103162.31319	-317692.58277	3800688.31159	0.10907	0.12214	0.00196	2016.4671
	21	5103162.31392	-317692.58302	3800688.31240	0.10928	0.12194	0.00304	2016.4699
	22	5103162.31178	-317692.58251	3800688.31389	0.11177	0.12231	0.00220	2016.4726
	23	5103162.31342	-317692.58216	3800688.31330	0.11033	0.12276	0.00313	2016.4753
	24	5103162.31489	-317692.58419	3800688.31307	0.10919	0.12083	0.00427	2016.4781
	25	5103162.31623	-317692.58612	3800688.31146	0.10703	0.11899	0.00448	2016.4808
2017, June	20	5103162.30754	-317692.56605	3800688.32164	0.12112	0.13848	0.00263	2017.4671
	21	5103162.30433	-317692.56740	3800688.32256	0.12373	0.13694	0.00069	2017.4699
	22	5103162.29888	-317692.56622	3800688.32022	0.12516	0.13777	-0.00513	2017.4726
	23	5103162.30720	-317692.56547	3800688.32446	0.12360	0.13904	0.00402	2017.4753
	24	5103162.30576	-317692.56770	3800688.32380	0.12386	0.13673	0.00259	2017.4781
	25	5103162.30595	-317692.56875	3800688.32348	0.12345	0.13569	0.00260	2017.4808
2018, June	20	5103162.29217	-317692.54910	3800688.33115	0.13856	0.15444	-0.00480	2018.4671
	21	5103162.28816	-317692.54828	3800688.32834	0.13873	0.15501	-0.00972	2018.4699
	22	5103162.30649	-317692.54973	3800688.34087	0.13775	0.15470	0.01251	2018.4726
	23	5103162.29800	-317692.55073	3800688.33504	0.13812	0.15318	0.00228	2018.4753
	24	5103162.29456	-317692.54925	3800688.33606	0.14106	0.15444	0.00007	2018.4781
	25	5103162.30039	-317692.55011	3800688.33976	0.14050	0.15395	0.00698	2018.4808

Station PILA

Year, month	Day	X, m	Y, m	Z, m	North, m	East, m	Height, m	Year fraction
2009, June	20	5014434.20798	-112868.39112	3928203.11191	0.00000	0.00000	0.00000	2009.4671
	21	5014434.20365	-112868.39209	3928203.10930	0.00061	-0.00107	-0.00499	2009.4699
	22	5014434.20465	-112868.39164	3928203.10904	-0.00020	-0.00059	-0.00438	2009.4726
	23	5014434.21066	-112868.39176	3928203.11441	0.00029	-0.00058	0.00366	2009.4753
	24	5014434.21011	-112868.39316	3928203.11625	0.00206	-0.00199	0.00440	2009.4781
	25	5014434.21010	-112868.39085	3928203.10832	-0.00413	0.00032	-0.00056	2009.4808
2010, June	20	5014434.19627	-112868.37310	3928203.12181	0.01528	0.01775	-0.00337	2010.4671
	21	5014434.19377	-112868.37269	3928203.12362	0.01825	0.01811	-0.00423	2010.4699
	22	5014434.18865	-112868.37322	3928203.12054	0.01899	0.01746	-0.01014	2010.4726
	23	5014434.19314	-112868.37450	3928203.12347	0.01850	0.01628	-0.00479	2010.4753
	24	5014434.19560	-112868.37375	3928203.12524	0.01837	0.01709	-0.00177	2010.4781
	25	5014434.19196	-112868.37505	3928203.12375	0.01944	0.01571	-0.00553	2010.4808
2011, June	20	5014434.18492	-112868.35427	3928203.13789	0.03519	0.03632	-0.00267	2011.4671
	21	5014434.18579	-112868.35394	3928203.13795	0.03470	0.03667	-0.00196	2011.4699
	22	5014434.18281	-112868.35350	3928203.13758	0.03626	0.03704	-0.00453	2011.4726
	23	5014434.18410	-112868.35430	3928203.13817	0.03592	0.03627	-0.00313	2011.4753
	24	5014434.18499	-112868.35314	3928203.13890	0.03596	0.03745	-0.00200	2011.4781
	25	5014434.18198	-112868.35502	3928203.13729	0.03652	0.03551	-0.00533	2011.4808

Year, month	Day	X, m	Y, m	Z, m	North, m	East, m	Height, m	Year fraction
2012, June	20	5014434.16891	-112868.33326	3928203.14898	0.05410	0.05697	-0.00874	2012.4671
	21	5014434.17339	-112868.33463	3928203.15225	0.05388	0.05570	-0.00317	2012.4699
	22	5014434.17288	-112868.33194	3928203.15209	0.05410	0.05838	-0.00372	2012.4726
	23	5014434.17132	-112868.33268	3928203.15202	0.05500	0.05760	-0.00498	2012.4753
	24	5014434.17052	-112868.33363	3928203.15054	0.05432	0.05663	-0.00651	2012.4781
	25	5014434.16906	-112868.33377	3928203.14934	0.05428	0.05647	-0.00839	2012.4808
2013, June	20	5014434.15978	-112868.31427	3928203.16113	0.06955	0.07575	-0.00872	2013.4671
	21	5014434.16393	-112868.31383	3928203.16294	0.06842	0.07628	-0.00435	2013.4699
	22	5014434.16434	-112868.31526	3928203.16474	0.06956	0.07486	-0.00289	2013.4726
	23	5014434.16167	-112868.31540	3928203.16362	0.07033	0.07466	-0.00568	2013.4753
	24	5014434.15788	-112868.31552	3928203.16062	0.07032	0.07446	-0.01050	2013.4781
	25	5014434.15844	-112868.31500	3928203.16110	0.07035	0.07498	-0.00978	2013.4808
2014, June	22	5014434.15068	-112868.29539	3928203.17627	0.08734	0.09442	-0.00682	2014.4726
	25	5014434.15522	-112868.29416	3928203.17741	0.08545	0.09574	-0.00257	2014.4808
2015, June	20	5014434.14116	-112868.27597	3928203.19468	0.10796	0.11362	-0.00324	2015.4671
	21	5014434.14188	-112868.27493	3928203.19451	0.10740	0.11468	-0.00280	2015.4699
	22	5014434.14094	-112868.27555	3928203.19235	0.10627	0.11403	-0.00487	2015.4726
	23	5014434.14281	-112868.27626	3928203.18876	0.10229	0.11337	-0.00561	2015.4753
	24	5014434.14450	-112868.27452	3928203.19181	0.10366	0.11515	-0.00242	2015.4781
	25	5014434.13566	-112868.27393	3928203.19160	0.10898	0.11553	-0.00950	2015.4808

Year, month	Day	X, m	Y, m	Z, m	North, m	East, m	Height, m	Year fraction
2016, June	20	5014434.12982	-112868.25541	3928203.20697	0.12492	0.13392	-0.00490	2016.4671
	21	5014434.12819	-112868.25426	3928203.20739	0.12627	0.13503	-0.00594	2016.4699
	22	5014434.12707	-112868.25465	3928203.20989	0.12893	0.13462	-0.00527	2016.4726
	23	5014434.12408	-112868.25475	3928203.20640	0.12804	0.13445	-0.00977	2016.4753
	24	5014434.12857	-112868.25739	3928203.20957	0.12771	0.13191	-0.00423	2016.4781
	25	5014434.12797	-112868.25662	3928203.20659	0.12575	0.13267	-0.00657	2016.4808
2017, June	20	5014434.11664	-112868.23591	3928203.21754	0.14165	0.15312	-0.00904	2017.4671
	21	5014434.11929	-112868.23621	3928203.22000	0.14194	0.15288	-0.00544	2017.4699
	22	5014434.11783	-112868.23640	3928203.22043	0.14318	0.15266	-0.00632	2017.4726
	24	5014434.11814	-112868.23777	3928203.22301	0.14499	0.15129	-0.00445	2017.4781
	25	5014434.12247	-112868.23828	3928203.22589	0.14456	0.15088	0.00074	2017.4808
2018, June	20	5014434.10763	-112868.21730	3928203.23197	0.15882	0.17152	-0.00752	2018.4671
	21	5014434.11188	-112868.21832	3928203.23557	0.15900	0.17060	-0.00193	2018.4699
	22	5014434.11112	-112868.21660	3928203.23510	0.15912	0.17229	-0.00285	2018.4726
	23	5014434.10783	-112868.21857	3928203.23349	0.15987	0.17025	-0.00639	2018.4753
	24	5014434.10803	-112868.21726	3928203.23661	0.16221	0.17156	-0.00433	2018.4781
	25	5014434.10559	-112868.21815	3928203.23448	0.16205	0.17062	-0.00755	2018.4808

Station TGIL

Year, month	Day	X, m	Y, m	Z, m	North, m	East, m	Height, m	Year fraction
2009, June	20	5022375.14173	-289813.70824	3908939.81991	0.00000	0.00000	0.00000	2009.4671
	21	5022375.13843	-289813.70946	3908939.81786	0.00038	-0.00141	-0.00381	2009.4699
	22	5022375.13798	-289813.70935	3908939.81592	-0.00087	-0.00133	-0.00535	2009.4726
	23	5022375.13776	-289813.70990	3908939.81593	-0.00074	-0.00188	-0.00550	2009.4753
	24	5022375.14186	-289813.70994	3908939.82082	0.00058	-0.00169	0.00075	2009.4781
	25	5022375.14044	-289813.70973	3908939.81707	-0.00149	-0.00156	-0.00269	2009.4808
2010, June	20	5022375.12745	-289813.69116	3908939.82871	0.01633	0.01623	-0.00658	2010.4671
	21	5022375.12826	-289813.69096	3908939.82920	0.01622	0.01648	-0.00565	2010.4699
	22	5022375.12572	-289813.68957	3908939.82914	0.01778	0.01771	-0.00775	2010.4726
	23	5022375.13003	-289813.69039	3908939.83252	0.01777	0.01715	-0.00224	2010.4753
	24	5022375.12794	-289813.69053	3908939.83000	0.01707	0.01688	-0.00543	2010.4781
	25	5022375.13143	-289813.69161	3908939.83400	0.01803	0.01601	-0.00017	2010.4808
2011, June	20	5022375.11888	-289813.67034	3908939.84136	0.03230	0.03652	-0.00647	2011.4671
	21	5022375.11632	-289813.66889	3908939.83962	0.03256	0.03782	-0.00962	2011.4699
	22	5022375.11791	-289813.67051	3908939.84248	0.03378	0.03629	-0.00654	2011.4726
	23	5022375.11865	-289813.67120	3908939.84165	0.03264	0.03565	-0.00644	2011.4753
	24	5022375.12098	-289813.66981	3908939.84349	0.03270	0.03717	-0.00353	2011.4781
	25	5022375.11804	-289813.67090	3908939.84266	0.03382	0.03592	-0.00630	2011.4808

Year, month	Day	X, m	Y, m	Z, m	North, m	East, m	Height, m	Year fraction
2012, June	20	5022375.11377	-289813.64946	3908939.85667	0.04825	0.05707	-0.00200	2012.4671
	21	5022375.11199	-289813.64907	3908939.85619	0.04898	0.05736	-0.00372	2012.4699
	22	5022375.11087	-289813.64899	3908939.85599	0.04951	0.05738	-0.00472	2012.4726
	23	5022375.10871	-289813.64953	3908939.85338	0.04877	0.05670	-0.00801	2012.4753
	24	5022375.11069	-289813.64924	3908939.85563	0.04932	0.05712	-0.00508	2012.4781
	25	5022375.10809	-289813.65070	3908939.85173	0.04780	0.05550	-0.00945	2012.4808
2013, June	20	5022375.10120	-289813.63108	3908939.86627	0.06419	0.07470	-0.00681	2013.4671
	21	5022375.10391	-289813.63143	3908939.86689	0.06300	0.07451	-0.00428	2013.4699
	22	5022375.10277	-289813.63023	3908939.86722	0.06400	0.07563	-0.00503	2013.4726
	23	5022375.10309	-289813.63276	3908939.86923	0.06530	0.07312	-0.00342	2013.4753
	24	5022375.10210	-289813.63146	3908939.86663	0.06391	0.07437	-0.00586	2013.4781
	25	5022375.10130	-289813.63126	3908939.86629	0.06414	0.07452	-0.00670	2013.4808
2014, June	20	5022375.09391	-289813.61299	3908939.87780	0.07840	0.09233	-0.00625	2014.4671
	21	5022375.09169	-289813.61191	3908939.87702	0.07919	0.09329	-0.00853	2014.4699
	22	5022375.09165	-289813.61225	3908939.87617	0.07853	0.09295	-0.00907	2014.4726
	23	5022375.09433	-289813.61284	3908939.88076	0.08047	0.09251	-0.00411	2014.4753
	24	5022375.09458	-289813.61407	3908939.87885	0.07877	0.09129	-0.00504	2014.4781
	25	5022375.09250	-289813.61213	3908939.87871	0.08001	0.09311	-0.00684	2014.4808

Year, month	Day	X, m	Y, m	Z, m	North, m	East, m	Height, m	Year fraction
2015, June	20	5022375.08241	-289813.59317	3908939.89296	0.09811	0.11146	-0.00686	2015.4671
	21	5022375.09396	-289813.59387	3908939.90023	0.09671	0.11143	0.00674	2015.4699
	22	5022375.08840	-289813.59532	3908939.89646	0.09711	0.10966	0.00011	2015.4726
	23	5022375.08429	-289813.59488	3908939.89067	0.09509	0.10986	-0.00671	2015.4753
	24	5022375.08470	-289813.59175	3908939.89457	0.09802	0.11301	-0.00413	2015.4781
	25	5022375.08211	-289813.59251	3908939.89440	0.09946	0.11210	-0.00624	2015.4808
2016, June	20	5022375.07483	-289813.57355	3908939.91009	0.11696	0.13062	-0.00315	2016.4671
	21	5022375.07851	-289813.57374	3908939.91245	0.11656	0.13064	0.00120	2016.4699
	22	5022375.08060	-289813.57372	3908939.91607	0.11813	0.13078	0.00507	2016.4726
	23	5022375.07491	-289813.57436	3908939.91186	0.11828	0.12981	-0.00196	2016.4753
	24	5022375.06890	-289813.57437	3908939.90853	0.11935	0.12945	-0.00874	2016.4781
	25	5022375.07725	-289813.57510	3908939.91084	0.11601	0.12920	-0.00072	2016.4808
2017, June	20	5022375.07219	-289813.56148	3908939.92888	0.13382	0.14251	0.00580	2017.4671
	21	5022375.08396	-289813.55551	3908939.93427	0.13104	0.14915	0.01810	2017.4699
	22	5022375.07117	-289813.55779	3908939.92747	0.13347	0.14613	0.00396	2017.4726
	23	5022375.07524	-289813.55678	3908939.92911	0.13230	0.14738	0.00813	2017.4753
	24	5022375.07549	-289813.55655	3908939.92993	0.13279	0.14762	0.00882	2017.4781
	25	5022375.06492	-289813.55463	3908939.92282	0.13376	0.14893	-0.00396	2017.4808

SUPPLEMENT 2

MATLAB CODES

Code 1

```
function[]=escribir(a)
id = fopen(a);
%open the file
line = fgetl(id);
%line 1
line = fgetl(id);
%line 2
X=line(26:47);
dx=line(54:74);

line = fgetl(id); %line 3
Y=line(26:47);
dy=line(54:74);

line = fgetl(id); %line 4
Z=line(26:47);
dz=line(54:74);

line = fgetl(id); %line 5
dxy=line(14:35);

line = fgetl(id); %line 6
dzx=line(14:35);

line = fgetl(id); %line 7
dzy=line(14:35);

fclose(id);

fileID = fopen('TGIL.txt','a');
fprintf(fileID,'\n'); % to save by the lines

fprintf(fileID,'%c',X);
fprintf(fileID,'%c',' ');
fprintf(fileID,'%c',Y);
fprintf(fileID,'%c',' ');
fprintf(fileID,'%c',Z);
fprintf(fileID,'%c',' ');
fprintf(fileID,'%c',dx);
fprintf(fileID,'%c',' ');
```

```
fprintf(fileID,'%c',dy);
fprintf(fileID,'%c',' ');
fprintf(fileID,'%c',dz);
fprintf(fileID,'%c',' ');
fprintf(fileID,'%c',dxy);
fprintf(fileID,'%c',' ');
fprintf(fileID,'%c',dzx);
fprintf(fileID,'%c',' ');
fprintf(fileID,'%c',dzy);
fprintf(fileID,'%c',' ');

fclose(fileID);
```

Code 2

```
function[Ro_yx,Ro_zx,Ro_zy,Sigm_x,Sigm_y,Sigm_z]=LectorStacov(id)
line = fgetl(id);
Ro_yx=str2num(line(145:166));
Ro_zx=str2num(line(168:188));
Ro_zy=str2num(line(190:211));
Sigm_x=str2num(line(79:99));
Sigm_y=str2num(line(101:121));
Sigm_z=str2num(line(123:143));
```

Code 3

```
function[Sigm_x2,Sigm_y2,Sigm_z2,Sigm_yx,Sigm_zx,Sigm_zy]=calcular(Ro_y
x,Ro_zx,Ro_zy,Sigm_x,Sigm_y,Sigm_z)
% This function performs the conversion from Ro_yx to Sigm_yx
% Conversion equations
Sigm_yx=Ro_yx*Sigm_y*Sigm_x;
Sigm_zx=Ro_zx*Sigm_z*Sigm_x;
Sigm_zy=Ro_zy*Sigm_z*Sigm_y;
Sigm_x2=Sigm_x*Sigm_x;
Sigm_y2=Sigm_y*Sigm_y;
Sigm_z2=Sigm_z*Sigm_z;

fileID = fopen('TGIL con sigmas.txt','a');
fprintf(fileID,'\n'); % to graguar by the lines

fprintf(fileID,'%c',Sigm_x2);
fprintf(fileID,'%c',' ');
```

```
fprintf(fileID,'%c',Sigm_y2);
fprintf(fileID,'%c',' ');
fprintf(fileID,'%c',Sigm_z2);
fprintf(fileID,'%c',' ');
fprintf(fileID,'%c',Sigm_yx);
fprintf(fileID,'%c',' ');
fprintf(fileID,'%c',Sigm_zx);
fprintf(fileID,'%c',' ');
fprintf(fileID,'%c',Sigm_zy);

fclose(fileID);
```

Code 4

```
function[a]=Sigmas()
id=fopen('TGIL con sigmas.txt');
a=[];
line = fgetl(id);
j=1;
while 1
line = fgetl(id);
    if j==55
        break
    end
i=1;
a(j,i)=str2num(line(11:22));
i=i+1;
a(j,i)=str2num(line(24:35));
i=i+1;
a(j,i)=str2num(line(37:48));
i=i+1;
a(j,i)=str2num(line(50:61));
i=i+1;
a(j,i)=str2num(line(63:74));
i=i+1;
a(j,i)=str2num(line(76:87));
j=j+1;
end
end
```

Code 5

```
function[b]=XYZ()
id=fopen('TGIL.txt');
b=[];
j=1;
while 1
line = fgetl(id);
   if j==55
      break
   end
i=1;
b(j,i)=str2num(line(12:32));
i=i+1;
b(j,i)=str2num(line(34:55));
i=i+1;
b(j,i)=str2num(line(57:77));
j=j+1;
end
end
```

Code 6

```
function [ c ] = matrix( j,a )
%UNTITLED4 Summary of this function goes here
%   Detailed explanation goes here
c(1,1)=a(j,1);
c(2,2)=a(j,2);
c(3,3)=a(j,3);
c(1,2)=a(j,4);
c(1,3)=a(j,5);
c(2,3)=a(j,6);
c(2,1)=a(j,4);
c(3,1)=a(j,5);
c(3,2)=a(j,6);
end
```

Code 7

```
function [ d ] = matrixcoord( j,b )
%UNTITLED4 Summary of this function goes here
%   Detailed explanation goes here
```

```
d(1,1)=b(j,1);
d(2,1)=b(j,2);
d(3,1)=b(j,3);
end
```

Code 8

```
delta_coord11=mcoord1-mcoord1;
delta_coord12=mcoord2-mcoord1;
delta_coord13=mcoord3-mcoord1;
delta_coord14=mcoord4-mcoord1;
delta_coord15=mcoord5-mcoord1;
delta_coord16=mcoord6-mcoord1;
delta_coord17=mcoord7-mcoord1;
delta_coord18=mcoord8-mcoord1;
delta_coord19=mcoord9-mcoord1;
delta_coord110=mcoord10-mcoord1;
delta_coord111=mcoord11-mcoord1;
delta_coord112=mcoord12-mcoord1;
delta_coord113=mcoord13-mcoord1;
delta_coord114=mcoord14-mcoord1;
delta_coord115=mcoord15-mcoord1;
delta_coord116=mcoord16-mcoord1;
delta_coord117=mcoord17-mcoord1;
delta_coord118=mcoord18-mcoord1;
delta_coord119=mcoord19-mcoord1;
delta_coord120=mcoord20-mcoord1;
delta_coord121=mcoord21-mcoord1;
delta_coord122=mcoord22-mcoord1;
delta_coord123=mcoord23-mcoord1;
delta_coord124=mcoord24-mcoord1;
delta_coord125=mcoord25-mcoord1;
delta_coord126=mcoord26-mcoord1;
delta_coord127=mcoord27-mcoord1;
delta_coord128=mcoord28-mcoord1;
delta_coord129=mcoord29-mcoord1;
delta_coord130=mcoord30-mcoord1;
delta_coord131=mcoord31-mcoord1;
delta_coord132=mcoord32-mcoord1;
delta_coord133=mcoord33-mcoord1;
delta_coord134=mcoord34-mcoord1;
delta_coord135=mcoord35-mcoord1;
```

```
delta_coord136=mcoord36-mcoord1;
delta_coord137=mcoord37-mcoord1;
delta_coord138=mcoord38-mcoord1;
delta_coord139=mcoord39-mcoord1;
delta_coord140=mcoord40-mcoord1;
delta_coord141=mcoord41-mcoord1;
delta_coord142=mcoord42-mcoord1;
delta_coord143=mcoord43-mcoord1;
delta_coord144=mcoord44-mcoord1;
delta_coord145=mcoord45-mcoord1;
delta_coord146=mcoord46-mcoord1;
delta_coord147=mcoord47-mcoord1;
delta_coord148=mcoord48-mcoord1;
delta_coord149=mcoord49-mcoord1;
delta_coord150=mcoord50-mcoord1;
delta_coord151=mcoord51-mcoord1;
delta_coord152=mcoord52-mcoord1;
delta_coord153=mcoord53-mcoord1;
delta_coord154=mcoord54-mcoord1;
delta_coord155=mcoord55-mcoord1;
delta_coord156=mcoord56-mcoord1;
delta_coord157=mcoord57-mcoord1;
delta_coord158=mcoord58-mcoord1;
delta_coord159=mcoord59-mcoord1;
delta_coord160=mcoord60-mcoord1;
```

Code 9

```
m_11=[m1 m_de0; m_de0 m1];
m_12=[m1 m_de0; m_de0 m2];
m_13=[m1 m_de0; m_de0 m3];
m_14=[m1 m_de0; m_de0 m4];
m_15=[m1 m_de0; m_de0 m5];
m_16=[m1 m_de0; m_de0 m6];
m_17=[m1 m_de0; m_de0 m7];
m_18=[m1 m_de0; m_de0 m8];
m_19=[m1 m_de0; m_de0 m9];
m_110=[m1 m_de0; m_de0 m10];
m_111=[m1 m_de0; m_de0 m11];
m_112=[m1 m_de0; m_de0 m12];
m_113=[m1 m_de0; m_de0 m13];
m_114=[m1 m_de0; m_de0 m14];
```

```
m_115=[m1 m_de0; m_de0 m15]; *
m_116=[m1 m_de0; m_de0 m16];
m_117=[m1 m_de0; m_de0 m17];
m_118=[m1 m_de0; m_de0 m18];
m_119=[m1 m_de0; m_de0 m19];
m_120=[m1 m_de0; m_de0 m20];
m_121=[m1 m_de0; m_de0 m21];
m_122=[m1 m_de0; m_de0 m22];
m_123=[m1 m_de0; m_de0 m23];
m_124=[m1 m_de0; m_de0 m24];
m_125=[m1 m_de0; m_de0 m25];
m_126=[m1 m_de0; m_de0 m26];
m_127=[m1 m_de0; m_de0 m27];
m_128=[m1 m_de0; m_de0 m28];
m_129=[m1 m_de0; m_de0 m29];
m_130=[m1 m_de0; m_de0 m30];
m_131=[m1 m_de0; m_de0 m31];
m_132=[m1 m_de0; m_de0 m32];
m_133=[m1 m_de0; m_de0 m33];
m_134=[m1 m_de0; m_de0 m34];
m_135=[m1 m_de0; m_de0 m35];
m_136=[m1 m_de0; m_de0 m36];
m_137=[m1 m_de0; m_de0 m37];
m_138=[m1 m_de0; m_de0 m38];
m_139=[m1 m_de0; m_de0 m39];
m_140=[m1 m_de0; m_de0 m40];
m_141=[m1 m_de0; m_de0 m41];
m_142=[m1 m_de0; m_de0 m42];
m_143=[m1 m_de0; m_de0 m43];
m_144=[m1 m_de0; m_de0 m44];
m_145=[m1 m_de0; m_de0 m45];
m_146=[m1 m_de0; m_de0 m46];
m_147=[m1 m_de0; m_de0 m47];
m_148=[m1 m_de0; m_de0 m48];
m_149=[m1 m_de0; m_de0 m49];
m_150=[m1 m_de0; m_de0 m50];
m_151=[m1 m_de0; m_de0 m51];
m_152=[m1 m_de0; m_de0 m52];
m_153=[m1 m_de0; m_de0 m53];
m_154=[m1 m_de0; m_de0 m54];
m_155=[m1 m_de0; m_de0 m55];
m_156=[m1 m_de0; m_de0 m56];
```

m_157=[m1 m_de0; m_de0 m57];
m_158=[m1 m_de0; m_de0 m58];
m_159=[m1 m_de0; m_de0 m59];
m_160=[m1 m_de0; m_de0 m60];

$$* \ m\_de0 = \begin{bmatrix} 0 & 0 & 0 \\ 0 & 0 & 0 \\ 0 & 0 & 0 \end{bmatrix}$$

Code 10

m_deltacovar_11=G*m_11*Gtrans; *
m_deltacovar_12=G*m_12*Gtrans;
m_deltacovar_13=G*m_13*Gtrans;
m_deltacovar_14=G*m_14*Gtrans;
m_deltacovar_15=G*m_15*Gtrans;
m_deltacovar_16=G*m_16*Gtrans;
m_deltacovar_17=G*m_17*Gtrans;
m_deltacovar_18=G*m_18*Gtrans;
m_deltacovar_19=G*m_19*Gtrans;
m_deltacovar_110=G*m_110*Gtrans;
m_deltacovar_111=G*m_111*Gtrans;
m_deltacovar_112=G*m_112*Gtrans;
m_deltacovar_113=G*m_113*Gtrans;
m_deltacovar_114=G*m_114*Gtrans;
m_deltacovar_115=G*m_115*Gtrans;
m_deltacovar_116=G*m_116*Gtrans;
m_deltacovar_117=G*m_117*Gtrans;
m_deltacovar_118=G*m_118*Gtrans;
m_deltacovar_119=G*m_119*Gtrans;
m_deltacovar_120=G*m_120*Gtrans;
m_deltacovar_121=G*m_121*Gtrans;
m_deltacovar_122=G*m_122*Gtrans;
m_deltacovar_123=G*m_123*Gtrans;
m_deltacovar_124=G*m_124*Gtrans;
m_deltacovar_125=G*m_125*Gtrans;
m_deltacovar_126=G*m_126*Gtrans;
m_deltacovar_127=G*m_127*Gtrans;
m_deltacovar_128=G*m_128*Gtrans;
m_deltacovar_129=G*m_129*Gtrans;
m_deltacovar_130=G*m_130*Gtrans;
m_deltacovar_131=G*m_131*Gtrans;

```
m_deltacovar_132=G*m_132*Gtrans;
m_deltacovar_133=G*m_133*Gtrans;
m_deltacovar_134=G*m_134*Gtrans;
m_deltacovar_135=G*m_135*Gtrans;
m_deltacovar_136=G*m_136*Gtrans;
m_deltacovar_137=G*m_137*Gtrans;
m_deltacovar_138=G*m_138*Gtrans;
m_deltacovar_139=G*m_139*Gtrans;
m_deltacovar_140=G*m_140*Gtrans;
m_deltacovar_141=G*m_141*Gtrans;
m_deltacovar_142=G*m_142*Gtrans;
m_deltacovar_143=G*m_143*Gtrans;
m_deltacovar_144=G*m_144*Gtrans;
m_deltacovar_145=G*m_145*Gtrans;
m_deltacovar_146=G*m_146*Gtrans;
m_deltacovar_147=G*m_147*Gtrans;
m_deltacovar_148=G*m_148*Gtrans;
m_deltacovar_149=G*m_149*Gtrans;
m_deltacovar_150=G*m_150*Gtrans;
m_deltacovar_151=G*m_151*Gtrans;
m_deltacovar_152=G*m_152*Gtrans;
m_deltacovar_153=G*m_153*Gtrans;
m_deltacovar_154=G*m_154*Gtrans;
m_deltacovar_155=G*m_155*Gtrans;
m_deltacovar_156=G*m_156*Gtrans;
m_deltacovar_157=G*m_157*Gtrans;
m_deltacovar_158=G*m_158*Gtrans;
m_deltacovar_159=G*m_159*Gtrans;
m_deltacovar_160=G*m_160*Gtrans;
```

$$* \; G = \begin{bmatrix} -1 & 0 & 0 & +1 & 0 & 0 \\ 0 & -1 & 0 & 0 & +1 & 0 \\ 0 & 0 & -1 & 0 & 0 & +1 \end{bmatrix}; \; Gtrans = \begin{bmatrix} -1 & 0 & 0 \\ 0 & -1 & 0 \\ 0 & 0 & -1 \\ +1 & 0 & 0 \\ 0 & +1 & 0 \\ 0 & 0 & +1 \end{bmatrix}$$

Code 11

```
% Phi = '37? 50' 7.55202"';
% Lambda = '-1? 56' 25.67896"';
```

```
% Latitud y Longitud AREZ
% Phi = '37? 3' 45.44176"';
% Lambda = '-3? 23' 8.29541"';
% Latitud y Longitud NEVA
% Phi = '36? 48' 32.52128"';
% Lambda = '-3? 33' 44.27693"';
% Latitud y Longitud PALM
% Phi = '38? 15' 15.49622"';
% Lambda = '-1? 17' 21.96864"';
% Latitud y Longitud PILA
% Phi = '38? 2' 3.26322"';
% Lambda = '-3? 18' 9.22546"';
% Latitud y Longitud TGIL
Lambda = -3 -(18/60)-(9.22546/3600);
Phi = 38+(2/60)+(3.26322/3600);
m_trigonometr=[-sind(Phi)*cosd(Lambda) -sind(Phi)*sind(Lambda) cosd(Phi); -
sind(Lambda) cosd(Lambda) 0; cosd(Phi)*cosd(Lambda) cosd(Phi)*sind(Lambda)
sind(Phi)]
```

Code 12

```
NEU1=m_trigonometr*delta_coord11;
NEU2=m_trigonometr*delta_coord12;
NEU3=m_trigonometr*delta_coord13;
NEU4=m_trigonometr*delta_coord14;
NEU5=m_trigonometr*delta_coord15;
NEU6=m_trigonometr*delta_coord16;
NEU7=m_trigonometr*delta_coord17;
NEU8=m_trigonometr*delta_coord18;
NEU9=m_trigonometr*delta_coord19;
NEU10=m_trigonometr*delta_coord110;
NEU11=m_trigonometr*delta_coord111;
NEU12=m_trigonometr*delta_coord112;
NEU13=m_trigonometr*delta_coord113;
NEU14=m_trigonometr*delta_coord114;
NEU15=m_trigonometr*delta_coord115;
NEU16=m_trigonometr*delta_coord116;
NEU17=m_trigonometr*delta_coord117;
NEU18=m_trigonometr*delta_coord118;
NEU19=m_trigonometr*delta_coord119;
NEU20=m_trigonometr*delta_coord120;
NEU21=m_trigonometr*delta_coord121;
```

```
NEU22=m_trigonometr*delta_coord122;
NEU23=m_trigonometr*delta_coord123;
NEU24=m_trigonometr*delta_coord124;
NEU25=m_trigonometr*delta_coord125;
NEU26=m_trigonometr*delta_coord126;
NEU27=m_trigonometr*delta_coord127;
NEU28=m_trigonometr*delta_coord128;
NEU29=m_trigonometr*delta_coord129;
NEU30=m_trigonometr*delta_coord130;
NEU31=m_trigonometr*delta_coord131;
NEU32=m_trigonometr*delta_coord132;
NEU33=m_trigonometr*delta_coord133;
NEU34=m_trigonometr*delta_coord134;
NEU35=m_trigonometr*delta_coord135;
NEU36=m_trigonometr*delta_coord136;
NEU37=m_trigonometr*delta_coord137;
NEU38=m_trigonometr*delta_coord138;
NEU39=m_trigonometr*delta_coord139;
NEU40=m_trigonometr*delta_coord140;
NEU41=m_trigonometr*delta_coord141;
NEU42=m_trigonometr*delta_coord142;
NEU43=m_trigonometr*delta_coord143;
NEU44=m_trigonometr*delta_coord144;
NEU45=m_trigonometr*delta_coord145;
NEU46=m_trigonometr*delta_coord146;
NEU47=m_trigonometr*delta_coord147;
NEU48=m_trigonometr*delta_coord148;
NEU49=m_trigonometr*delta_coord149;
NEU50=m_trigonometr*delta_coord150;
NEU51=m_trigonometr*delta_coord151;
NEU52=m_trigonometr*delta_coord152;
NEU53=m_trigonometr*delta_coord153;
NEU54=m_trigonometr*delta_coord154;
NEU55=m_trigonometr*delta_coord155;
NEU56=m_trigonometr*delta_coord156;
NEU57=m_trigonometr*delta_coord157;
NEU58=m_trigonometr*delta_coord158;
NEU59=m_trigonometr*delta_coord159;
NEU60=m_trigonometr*delta_coord160;
```

Code 13

```
m_cov_NEU1=m_trigonometr*m_deltacovar_11*(m_trigonometr');
m_cov_NEU2=m_trigonometr*m_deltacovar_12*(m_trigonometr');
m_cov_NEU3=m_trigonometr*m_deltacovar_13*(m_trigonometr');
m_cov_NEU4=m_trigonometr*m_deltacovar_14*(m_trigonometr');
m_cov_NEU5=m_trigonometr*m_deltacovar_15*(m_trigonometr');
m_cov_NEU6=m_trigonometr*m_deltacovar_16*(m_trigonometr');
m_cov_NEU7=m_trigonometr*m_deltacovar_17*(m_trigonometr');
m_cov_NEU8=m_trigonometr*m_deltacovar_18*(m_trigonometr');
m_cov_NEU9=m_trigonometr*m_deltacovar_19*(m_trigonometr');
m_cov_NEU10=m_trigonometr*m_deltacovar_110*(m_trigonometr');
m_cov_NEU11=m_trigonometr*m_deltacovar_111*(m_trigonometr');
m_cov_NEU12=m_trigonometr*m_deltacovar_112*(m_trigonometr');
m_cov_NEU13=m_trigonometr*m_deltacovar_113*(m_trigonometr');
m_cov_NEU14=m_trigonometr*m_deltacovar_114*(m_trigonometr');
m_cov_NEU15=m_trigonometr*m_deltacovar_115*(m_trigonometr');
m_cov_NEU16=m_trigonometr*m_deltacovar_116*(m_trigonometr');
m_cov_NEU17=m_trigonometr*m_deltacovar_117*(m_trigonometr');
m_cov_NEU18=m_trigonometr*m_deltacovar_118*(m_trigonometr');
m_cov_NEU19=m_trigonometr*m_deltacovar_119*(m_trigonometr');
m_cov_NEU20=m_trigonometr*m_deltacovar_120*(m_trigonometr');
m_cov_NEU21=m_trigonometr*m_deltacovar_121*(m_trigonometr');
m_cov_NEU22=m_trigonometr*m_deltacovar_122*(m_trigonometr');
m_cov_NEU23=m_trigonometr*m_deltacovar_123*(m_trigonometr');
m_cov_NEU24=m_trigonometr*m_deltacovar_124*(m_trigonometr');
m_cov_NEU25=m_trigonometr*m_deltacovar_125*(m_trigonometr');
m_cov_NEU26=m_trigonometr*m_deltacovar_126*(m_trigonometr');
m_cov_NEU27=m_trigonometr*m_deltacovar_127*(m_trigonometr');
m_cov_NEU28=m_trigonometr*m_deltacovar_128*(m_trigonometr');
m_cov_NEU29=m_trigonometr*m_deltacovar_129*(m_trigonometr');
m_cov_NEU30=m_trigonometr*m_deltacovar_130*(m_trigonometr');
m_cov_NEU31=m_trigonometr*m_deltacovar_131*(m_trigonometr');
m_cov_NEU32=m_trigonometr*m_deltacovar_132*(m_trigonometr');
m_cov_NEU33=m_trigonometr*m_deltacovar_133*(m_trigonometr');
m_cov_NEU34=m_trigonometr*m_deltacovar_134*(m_trigonometr');
m_cov_NEU35=m_trigonometr*m_deltacovar_135*(m_trigonometr');
m_cov_NEU36=m_trigonometr*m_deltacovar_136*(m_trigonometr');
m_cov_NEU37=m_trigonometr*m_deltacovar_137*(m_trigonometr');
m_cov_NEU38=m_trigonometr*m_deltacovar_138*(m_trigonometr');
m_cov_NEU39=m_trigonometr*m_deltacovar_139*(m_trigonometr');
m_cov_NEU40=m_trigonometr*m_deltacovar_140*(m_trigonometr');
m_cov_NEU41=m_trigonometr*m_deltacovar_141*(m_trigonometr');
m_cov_NEU42=m_trigonometr*m_deltacovar_142*(m_trigonometr');
```

```
m_cov_NEU43=m_trigonometr*m_deltacovar_143*(m_trigonometr');
m_cov_NEU44=m_trigonometr*m_deltacovar_144*(m_trigonometr');
m_cov_NEU45=m_trigonometr*m_deltacovar_145*(m_trigonometr');
m_cov_NEU46=m_trigonometr*m_deltacovar_146*(m_trigonometr');
m_cov_NEU47=m_trigonometr*m_deltacovar_147*(m_trigonometr');
m_cov_NEU48=m_trigonometr*m_deltacovar_148*(m_trigonometr');
m_cov_NEU49=m_trigonometr*m_deltacovar_149*(m_trigonometr');
m_cov_NEU50=m_trigonometr*m_deltacovar_150*(m_trigonometr');
m_cov_NEU51=m_trigonometr*m_deltacovar_151*(m_trigonometr');
m_cov_NEU52=m_trigonometr*m_deltacovar_152*(m_trigonometr');
m_cov_NEU53=m_trigonometr*m_deltacovar_153*(m_trigonometr');
m_cov_NEU54=m_trigonometr*m_deltacovar_154*(m_trigonometr');
m_cov_NEU55=m_trigonometr*m_deltacovar_155*(m_trigonometr');
m_cov_NEU56=m_trigonometr*m_deltacovar_156*(m_trigonometr');
m_cov_NEU57=m_trigonometr*m_deltacovar_157*(m_trigonometr');
m_cov_NEU58=m_trigonometr*m_deltacovar_158*(m_trigonometr');
m_cov_NEU59=m_trigonometr*m_deltacovar_159*(m_trigonometr');
m_cov_NEU60=m_trigonometr*m_deltacovar_160*(m_trigonometr');
```

Code 14

```
fileID = fopen('TGIL NEU.txt','a');
fprintf(fileID,'\n');%para graguar por las lineas
c=0;
while c<54
    c=c+1;
    var1=eval(['NEU' num2str(c)]);
    var2=eval(['m_cov_NEU' num2str(c)]);
    fprintf(fileID,'%d',var1(1,1));
    fprintf(fileID,'%c',' ');
    fprintf(fileID,'%d',var1(2,1));
    fprintf(fileID,'%c',' ');
    fprintf(fileID,'%d',var1(3,1));
    fprintf(fileID,'%c',' ');
    fprintf(fileID,'%d',(var2(1,1))^(1/2));
    fprintf(fileID,'%c',' ');
    fprintf(fileID,'%d',(var2(2,2))^(1/2));
    fprintf(fileID,'%c',' ');
    fprintf(fileID,'%d',(var2(3,3))^(1/2));
    fprintf(fileID,'%c',' ');
    fprintf(fileID,'\n');
```

```
end
fclose(fileID);
```

Code 15

```
%examle of TGIL station
Lambda=-3.30256725; %grad
Phi=38.03423674; %grad
tregonometr=[-sind(Lambda) cosd(Lambda) 0; -sind(Phi)*cosd(Lambda) -
sind(Phi)*sind(Lambda) cosd(Phi); cosd(Phi)*cosd(Lambda)
cosd(Phi)*sind(Lambda) sind(Phi)];
X=5022375325.60; %mm
Y=-289814125.00; %mm
Z=3908939552.80; %mm
cartesian=[0 Z -Y; -Z 0 X; Y -X 0];
Ve=18.64;
Vn=16.55;
Vu=0.90;
Venu=[Ve; Vn; Vu];
Wx=-4.12091628E-10 ; %rad/yr;
Wy=-2.5743606408E-9; %rad/yr;
Wz=3.733065336E-9; %rad/yr;
%Wx=-0.085; %mas/yr
%Wy=-0.531; %mas/yr
%Wz=0.770; %mas/yr
W=[Wx; Wy; Wz];
Vr=Venu-tregonometr*cartesian*W
```

SUPPLEMENT 3

ABSOLUTE AND RESIDUAL VELOCITY MAPS

Absolute velocity map

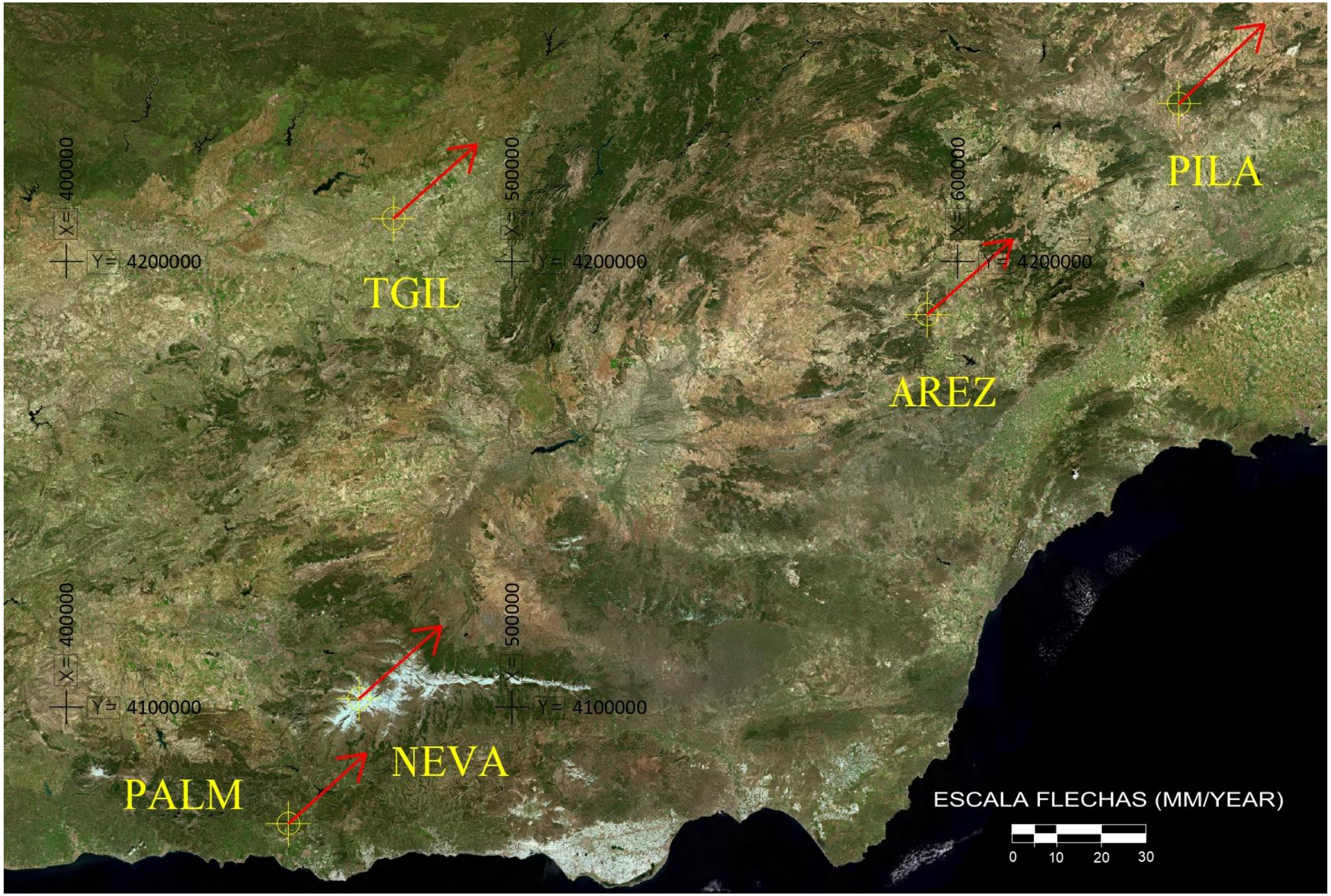

Residual velocity map

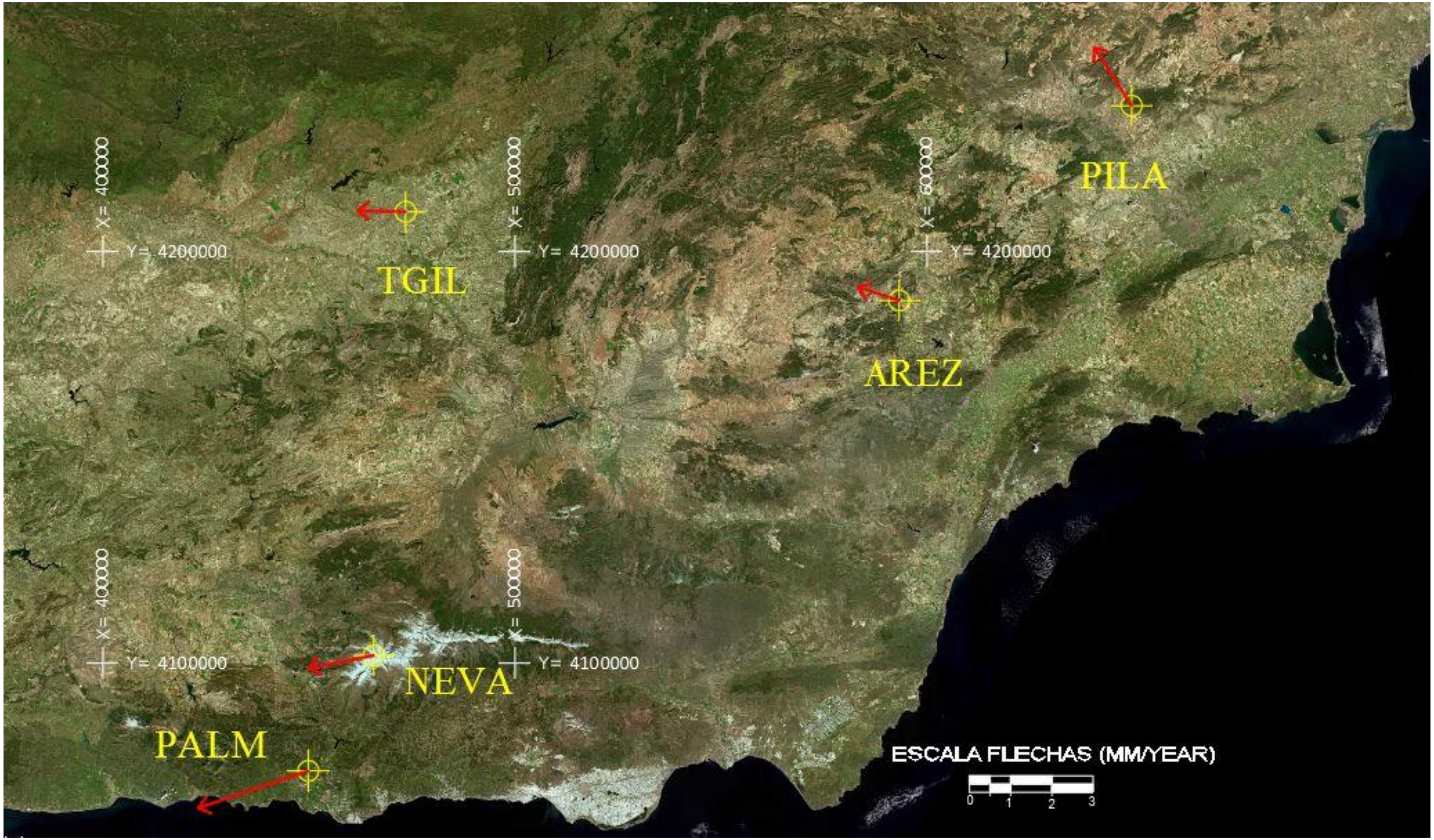

Absolute velocity comparison with ROA